

# **Exploring Fluid Flow in the Gulf of Cadiz: From Mud Volcanoes to Transform Faults**

Dissertation for the Doctoral Degree in Natural Sciences  
in the Faculty of Geosciences  
University of Bremen

Submitted by

**Shuhui Xu**

Bremen, October 2023



## **REVIEWERS / GUTACHTER**

**Prof. Dr. Achim Kopf**

University of Bremen

MARUM - Centre for Marine Environmental Sciences

Leobener Straße 8

28359 Bremen, Germany

**PD Dr. Florian Scholz**

GEOMAR Helmholtz Center for Ocean Research Kiel

Wischhofstraße 1-3

24148 Kiel, Germany

Date of the doctoral colloquium / Datum des Prüfungskolloquiums

24 January / Januar 2024



## **Versicherung an Eides Statt / *Affirmation in lieu of an oath***

**gem. § 5 Abs. 5 der Promotionsordnung vom 18.06.2018 /  
according to § 5 (5) of the Doctoral Degree Rules and Regulations of 18 June, 2018**

Ich / I, \_\_\_\_\_  
(Vorname / First Name, Name / Name, Anschrift / Address, ggf. Matr.-Nr. / student ID no., if applicable)

versichere an Eides Statt durch meine Unterschrift, dass ich die vorliegende Dissertation selbständig und ohne fremde Hilfe angefertigt und alle Stellen, die ich wörtlich dem Sinne nach aus Veröffentlichungen entnommen habe, als solche kenntlich gemacht habe, mich auch keiner anderen als der angegebenen Literatur oder sonstiger Hilfsmittel bedient habe und die zu Prüfungszwecken beigelegte elektronische Version (PDF) der Dissertation mit der abgegebenen gedruckten Version identisch ist. / *With my signature I affirm in lieu of an oath that I prepared the submitted dissertation independently and without illicit assistance from third parties, that I appropriately referenced any text or content from other sources, that I used only literature and resources listed in the dissertation, and that the electronic (PDF) and printed versions of the dissertation are identical.*

Ich versichere an Eides Statt, dass ich die vorgenannten Angaben nach bestem Wissen und Gewissen gemacht habe und dass die Angaben der Wahrheit entsprechen und ich nichts verschwiegen habe. / *I affirm in lieu of an oath that the information provided herein to the best of my knowledge is true and complete.*

Die Strafbarkeit einer falschen eidesstattlichen Versicherung ist mir bekannt, namentlich die Strafandrohung gemäß § 156 StGB bis zu drei Jahren Freiheitsstrafe oder Geldstrafe bei vorsätzlicher Begehung der Tat bzw. gemäß § 161 Abs. 1 StGB bis zu einem Jahr Freiheitsstrafe oder Geldstrafe bei fahrlässiger Begehung. / *I am aware that a false affidavit is a criminal offence which is punishable by law in accordance with § 156 of the German Criminal Code (StGB) with up to three years imprisonment or a fine in case of intention, or in accordance with § 161 (1) of the German Criminal Code with up to one year imprisonment or a fine in case of negligence.*

\_\_\_\_\_  
Ort / Place, Datum / Date

\_\_\_\_\_  
Unterschrift / Signature

\*The affirmation was signed in the submitted printed version.



## ABSTRACT

Cold seeps have been identified globally spanning diverse geologic settings and represent important seafloor manifestations of material transfer between geosphere and hydrosphere. The material extrusions give rise to seafloor topographic features that are indicative of focused release of overpressure, fluids, and, in the case of mud volcanoes, sediments. As emitted fluids have experienced various diagenetic processes at depth, their expulsion may play a significant role in global biogeochemical cycles. To gain insights into fluid circulation within cold seep systems, it is imperative to acquire a comprehensive understanding of the fluids' origin and the geochemical processes that exert an influence on their composition.

In this dissertation, the plate boundary region between Africa and Eurasia is studied to identify cold seeps of various origin. The sites investigated span from the Gulf of Cadiz in the west, geodynamically dominated by transform faulting, to the Hellenic subduction zone to the East, a mature subduction system with reverse faulting. Seeping features that can be directly observed at or near the seabed in these regions are manifold, and mud volcanoes (MVs) are the most prominent among them. The first and second manuscripts in this study investigate several MVs in the Gulf of Cadiz, aiming to enhance the understanding of MVs' morphological characteristics, deep-seated fluid migrations, and salinity patterns. A presentation of new discoveries about mud volcanism through the Gulf of Cadiz accretionary prisms is reported in the first manuscript, covering their morphologies, physical properties and lithological changes in mud breccias, and fluid compositions. The six MVs investigated (already known MVs Yuma, Ginsburg and Meknes and newly discovered MVs R2, D2 and Funky Monkey) are located along different strike-slip fault segments. While two of them are textbook examples of inactive mud domes, the other four MVs attest recent activity in different evolution stages. At active seepage sites, we traced back the origin of venting fluids to clay mineral dehydration and identified pronounced crustal influence and less intense pore water freshening present in the deeper MVs located close to major strike-slip faults (Funky Monkey MV). The second manuscript presents in turn a deeper understanding of fluid circulation within "the MV system" to investigate the relationship between evolving surface characteristics and dynamic subsurface conditions. Two MVs situated in the Gulf of Cadiz (Yuma, Ginsburg) and one MV in the Mediterranean Ridge (Milano) have been studied, which show striking differences in fluid composition between their summit and moat/rim. Through the utilization of fluid geochemistry, pore water modeling, and high-resolution seismic data, this study has identified not only the widely-known central conduits within the MV system, expelling freshening fluids due to clay mineral dehydration, but also the rim-related fluid pathways actively emitting saline fluids resulting from the leaching of evaporites. The chemical and fluid fluxes of 5 MVs have been analyzed and related to the MVs life-cycle (depletion and quiescence periods). The results indicate the involvement of additional (shallow) fluid sources during a later evolutionary stage, particularly when the moat is being developed. Based on the calculated flow rates at the moat area, in the case of the Ginsburg MV, this newly described rim-related fluid circulation

significantly contributes to fluid cycling in MVs, especially during long intervals of inactivity. Although this research is confined to the Gulf of Cadiz and the Mediterranean Ridge, the rim-related fluid circulation may have global implications. This enhances our understanding of the coverage and timespan of quiescent fluid seeping and its impact on the global fluid and methane budgets, which indicates the need for further efforts to improve the estimates including not only the summit areas of MVs but also the peripheric systems of these complexes.

To gain a more comprehensive insight into fluid seepage in the Gulf of Cadiz, the third manuscript shifts the focus from MVs to transform faults. Its objective is to define the contribution of oceanic transform faults as important settings for the circulation of deep-sourced fluid flow and their influence on global mass balances. The fault fluids are sampled from two different pull-apart basins on the dextral strike-slip faults, as known as the South West Iberian Margin (SWIM) faults defining the Africa-Eurasia plate boundary in the Gulf of Cadiz. Chemical and isotopic composition analysis has been conducted on fault fluids and compared with those from nearby tectonic-controlled cold seep sites including MVs and pockmarks. In contrast to the prevalent freshening signals (Cl depletion) observed in the MV fluids, the geochemical results show a missing signal from clay mineral dehydration in the fault fluids, suggesting an almost absent connection with terrigenous sediments. The geochemical composition of fault fluids is, instead, characterized by i) considerably high Na and Cl concentrations attributed to intensely interaction with Triassic evaporites at depth; and ii) strong enrichment of less radiogenic Sr, compared to present-day seawater values. When related to pure Triassic evaporitic fluids, the relatively radiogenic  $^{87}\text{Sr}/^{86}\text{Sr}$  ratios in the fault fluids hint a potential contribution from continental crustal fluids, with modeling indicating up to 22%. This provides insights into the impact of transform faults in focusing crustal signals from the depths, thereby advancing our understanding of the deep hydrologic cycle within transform-type plate boundaries.

This thesis offers insights into fluid flow dynamics at seep sites in the Gulf of Cadiz plus a comparison to analogue processes further east across the Mediterranean Ridge. Through the investigation of fluids in mud volcanoes and fault systems, this study reveals: i) their relationship and different mechanisms in upward-channeling deep fluids; ii) the signature of fluids and the potential origin from crustal basement; and iii) the significant role these fluid systems play in influencing fluid cycling and global element budgets.

## ZUSAMMENFASSUNG

Kaltwasserquellen wurden weltweit in vielfältigen geologischen Umgebungen identifiziert und stellen wichtige Erscheinungen auf dem Meeresboden dar, die den Materialaustausch zwischen der Geosphäre und der Hydrosphäre widerspiegeln. Die Materialextrusionen führen zu topografischen Merkmalen des Meeresbodens, die auf die gezielte Freisetzung von Überdruck, Flüssigkeiten und, im Fall von Schlammvulkanen, Sedimenten hinweisen. Da emittierte Fluide in der Tiefe verschiedene diagenetische Prozesse durchlaufen haben, könnte ihr Ausstoß eine wichtige Rolle in globalen biogeochemischen Kreisläufen spielen. Um Einblicke in die Fluidzirkulation in Kaltwasserquellensystemen zu gewinnen, ist es unerlässlich, ein umfassendes Verständnis der Herkunft der Fluiden und der geochemischen Prozesse zu erlangen, die einen Einfluss auf ihre Zusammensetzung haben.

In dieser Dissertation wird die Plattengrenzregion zwischen Afrika und Eurasien untersucht, um Kaltwasserquellen unterschiedlicher Herkunft zu identifizieren. Die untersuchten Standorte erstrecken sich von der Golf von Cadiz im Westen, geodynamisch dominiert von Transformstörungen, bis zur Hellenischen Subduktionszone im Osten, einem ausgereiften Subduktionssystem mit Überschiebungen. Die austretenden Merkmale, die in diesen Regionen direkt am oder in der Nähe des Meeresbodens beobachtet werden können, sind vielfältig, wobei Schlammvulkane (SV) die prominentesten unter ihnen sind. Das erste und das zweite Manuskript dieser Studie untersuchen mehrere SV im Golf von Cadiz mit dem Ziel, das Verständnis der morphologischen Eigenschaften von SV, tiefliegender Fluidwanderungen und Salzgehaltsmuster zu verbessern. Im ersten Manuskript wird über neue Entdeckungen zum Schlammvulkanismus durch die Akkretionsprismen des Golf von Cadiz berichtet, die sich mit deren Morphologie, physikalischen Eigenschaften und lithologischen Veränderungen in Schlammbrekzien sowie Fluidzusammensetzungen befassen. Die sechs untersuchten SV (bereits bekannte SV Yuma, Ginsburg und Meknes sowie die neu entdeckten SV R2, D2 und Funky Monkey) befinden sich entlang verschiedener Abschnitte von Blattverschiebung Störungen. Während zwei von ihnen Musterbeispiele für inaktive SV sind, belegen die anderen vier SV eine jüngste Aktivität in unterschiedlichen Entwicklungsstadien. An aktiven Kaltwasserquellen haben wir den Ursprung der Entlüftungsfluide auf die Dehydrierung von Tonmineralien zurückgeführt und einen ausgeprägten Krusteneinfluss und eine weniger intensive Porenwasserauffrischung in den tieferen SV festgestellt, die sich in der Nähe großer Blattverschiebung Störungszonen (Funky Monkey SV) befinden. Das zweite Manuskript präsentiert wiederum ein tieferes Verständnis der Fluidzirkulation innerhalb des „SV-Systems“, um die Beziehung zwischen sich entwickelnden Oberflächeneigenschaften und dynamischen Untergrundbedingungen zu untersuchen. Es wurden zwei SV im Golf von Cadiz (Yuma, Ginsburg) und ein SV im Mediterranen Rücken (Milano) untersucht, die auffällige Unterschiede in der Fluidzusammensetzung zwischen ihrem Gipfel und ihrem Graben/Rand aufweisen. Durch die Nutzung von Fluidgeochemie, Porenwassermodellierung und hochauflösenden seismischen Daten hat diese Studie nicht nur die weithin bekannten zentralen

Leitungen innerhalb des SV-Systems identifiziert, die erfrischende Fluide aufgrund der Dehydrierung von Tonmineralien ausstoßen, sondern auch die randbezogenen Leitungen Fluidwege, die aktiv salzhaltige Fluide abgeben, die aus der Auslaugung von Evaporiten resultieren. Die chemischen und flüssigen Strömungen von 5 SV wurden analysiert und mit dem Lebenszyklus der SV (Erschöpfungs- und Ruheperioden) in Beziehung gesetzt. Die Ergebnisse deuten auf die Beteiligung zusätzlicher (flacher) Fluidquellen in einem späteren Evolutionsstadium hin, insbesondere bei der Entwicklung des SV Graben. Basierend auf den berechneten Durchflussraten im Bereich des Grabens trägt die in diesem Fall bei Ginsburg SV beschriebene, mit dem Rand verbundene Flüssigkeitszirkulation signifikant zum Flüssigkeitskreislauf in SV bei, insbesondere während langer Inaktivitätszeiträume. Obwohl diese Forschung auf den Golf von Cadiz und den mediterranen Rücken beschränkt ist, könnte die mit dem Rand verbundene Flüssigkeitszirkulation globale Auswirkungen haben. Dies vertieft unser Verständnis für die Ausdehnung und Dauer des ruhenden Flüssigkeitsaustritts und dessen Einfluss auf die globalen Flüssigkeits- und Methanhaushalte, was die Notwendigkeit weiterer Bemühungen zur Verbesserung der Schätzungen einschließt, die nicht nur die Gipfelbereiche von SV, sondern auch die peripheren Systeme dieser Komplexe berücksichtigen.

Um einen umfassenderen Einblick in die Kaltwasserquelle von Golf von Cadiz zu erhalten, verlagert das dritte Manuskript den Schwerpunkt von SV auf Transformstörungen. Das Ziel ist es, den Beitrag ozeanischer Transformstörungen als wichtige Rahmenbedingungen für die Zirkulation von Flüssigkeitsströmen aus der Tiefe und ihren Einfluss auf globale Massenbilanzen zu definieren. Die Verwerfungsfluide werden aus zwei verschiedenen Pull-Apart-Becken auf den dextralen Blattverschiebung Störungen entnommen, die als South West Iberian Margin (SWIM) bekannt sind und die Plattengrenze zwischen Afrika und Eurasien im Golf von Cadiz definieren. An Verwerfungsfluide wurden Analysen der chemischen und Isotopenzusammensetzung durchgeführt und mit denen von nahegelegenen tektonisch kontrollierten Kaltwasserquelle, einschließlich SV und Pockmarks, verglichen. Im Gegensatz zu den vorherrschenden Auffrischungssignalen (Cl-Abbau), die in den SV-Fluide beobachtet wurden, zeigen die geochemischen Ergebnisse ein fehlendes Signal der Tonmineral-Dehydrierung in den Verwerfungsfluide, was auf einen nahezu fehlenden Zusammenhang mit terrigenen Sedimenten schließen lässt. Die geochemische Zusammensetzung von Porenwasser ist stattdessen gekennzeichnet durch i) beträchtlich hohe Na- und Cl-Konzentrationen, die auf eine intensive Wechselwirkung mit triassischen Evaporiten in der Tiefe zurückzuführen sind; und ii) starke Anreicherung von weniger radiogenem Sr im Vergleich zu den heutigen Meerwasserwerten. Im Vergleich zu reinen evaporitischen Flüssigkeiten aus der Trias deuten die relativ radiogenen  $^{87}\text{Sr}/^{86}\text{Sr}$ -Verhältnisse in den Porenwassern auf einen möglichen Beitrag von kontinentalen Krustenflüssigkeiten hin, wobei Modellierungen bis zu 22 % vermuten lassen. Dies liefert Einblicke in die Auswirkungen von Transformstörungen auf die Fokussierung von Krustensignalen aus der Tiefe und erweitert so unser Verständnis des tiefen Wasserkreislaufs innerhalb der Plattengrenzen.

Diese Dissertation bietet Einblicke in die Fluidströmungsdynamik an Kaltwasserquellen im Golf von Cadiz und vergleicht sie mit analogen Prozessen weiter östlich am Mittelmeer-Rücken. Durch die Untersuchung von Fluiden in SV und Störungssystemen enthüllt diese Studie: i) ihre Beziehung und verschiedene Mechanismen bei der Aufwärtsleitung von Tiefenfluiden; ii) die charakteristischen Merkmale von Fluiden und deren potenzielle Herkunft aus dem Krustenuntergrund; und iii) die bedeutende Rolle, die diese Fluidsysteme bei der Beeinflussung der Fluidzirkulation und der globalen Elementhaushalte spielen.



# CONTENTS

<b>ABSTRACT</b> .....	<b>I</b>
<b>ZUSAMMENFASSUNG</b> .....	<b>III</b>
<b>Chapter 1: Introduction</b> .....	<b>1</b>
1.1 Seabed fluid flow: cold seeps .....	1
1.2 Mud volcanoes .....	4
1.3 Pore fluid geochemistry .....	11
1.4 Motivation.....	15
1.5 Outline of this cumulative dissertation .....	16
1.6 Contribution to the manuscripts.....	17
<b>Chapter 2</b>	
<b>Mud volcanoes in the Gulf of Cadiz as a manifestation of tectonic processes and deep-seated fluid mobilization</b> .....	<b>19</b>
2.1 Introduction.....	20
2.2 Study area.....	21
2.3 Methods.....	24
2.3.1 Hydroacoustics.....	24
2.3.2 Sampling .....	25
2.3.3 Physical properties .....	25
2.3.4 Mineralogy .....	25
2.3.5 Geochemistry .....	26
2.4 Results.....	26
2.4.1 Morphology.....	26
2.4.2 Sediment characteristics.....	28
2.4.3 Mineralogy .....	31
2.4.4 Geochemistry .....	31
2.5 Discussion .....	32
2.5.1 Morphology related to mud extrusion and degree of activity.....	32
2.5.2 Mud breccia composition.....	34
2.5.3 Diagenetic processes.....	36
2.5.4 Fluid sources .....	39
2.6 Conclusions.....	42
Supplementary material .....	44
<b>Chapter 3</b>	
<b>The rise and fall of mud volcano systems: new insights on fluid circulation unravel their complex structural evolution</b> .....	<b>45</b>
3.1 Introduction.....	46
3.2 Geological setting .....	47

3.3 Materials and methods .....	49
3.3.1 Hydroacoustics.....	49
3.3.2 Seismic acquisition/processing .....	49
3.3.3 Sediment and pore water sampling .....	50
3.3.4 Geochemical measurements.....	50
3.3.5 Pore water modeling .....	51
3.4 Results.....	52
3.4.1 Morphology and sedimentology .....	52
3.4.2 Mud volcano internal structure .....	55
3.4.3 Pore water geochemistry and modeling.....	56
3.5 Discussion.....	59
3.5.1 Fluid pathways: central conduit and rim system.....	59
3.5.2 Fluid sources .....	62
3.5.3 Role of rim-related fluid pathways during MV evolution .....	64
3.6 Conclusions.....	66
Supplementary material .....	68

## **Chapter 4**

### **Ascent of fluids through km-thick sedimentary cover links to active tectonics in the Gulf of Cadiz .....**

<b>69</b>	
4.1 Introduction.....	70
4.2 Materials and methods .....	72
4.2.1 Bathymetry.....	72
4.2.2 Heat flow.....	72
4.2.3 Sediment coring and pore water sampling.....	72
4.2.4 Chemical analyses.....	73
4.2.5 Isotopic analyses .....	73
4.2.6 Fluid mixing models .....	73
4.3 Results.....	74
4.4 Discussion .....	77
4.4.1 Elevated heat flow as an indicator for upward fluid flow.....	77
4.4.2 Fluid origins: evaporites dissolution versus clay dehydration.....	78
4.4.3 Continental crust fluids as a potential fluid origin.....	80
4.5 Implications.....	86
Supplementary material .....	87

### **Chapter 5: Conclusions and outlook..... 88**

5.1 Conclusions.....	88
5.2 Outlook .....	89

### **Acknowledgements .....**

### **References..... 92**

# Chapter 1: Introduction

## 1.1 Seabed fluid flow: cold seeps

The exchange of fluids, materials, and energy within and through the geosphere (including the lithosphere, hydrosphere, atmosphere, and biosphere) is a fundamental process that holds great significance for the evolution of the Earth's surface and interior (e.g., Judd and Hovland, 2007; Schlesinger and Bernhardt, 2013). Numerous biogeochemical cycles are active across a range of scales, primarily within the geologic settings of plate boundaries, volcanic arcs, and continental margins. In the marine environment, cold seeps are widespread and important seafloor manifestations of material transfer across the seabed-seawater interface. At these submarine cold seeps, gases, liquids, as well as sediments, migrate from the subsurface to the seabed floor and into the water column, and part of volatile elements and compounds such as methane may even reach the atmosphere (e.g., Milkov et al., 2003). As these emitted fluids have experienced various diagenetic processes at depth, their chemical and isotopic compositions generally differ significantly from seawater, and their expulsion may play a significant role in global biogeochemical cycles. For example, the release of volatile hydrocarbons creates a favorable environment that supports rich ecosystems, making it a hotspot of life on the seafloor (Levin, 2005; Levin et al., 2016), and methane, in particular, can further contribute to the global greenhouse gas budget (Etiopie and Milkov., 2004; Etiopie, 2005). Other elements that exhibit high concentrations in cold seep environments, like B, Li, Ba, and Sr, have a significant impact on the chemical composition of the ocean and are relevant to diverse geological topics such as the alteration of oceanic crust (Chan et al., 1992), the reconstruction of paleoproductivity (Dymond et al., 1992), and stratigraphic correlation (Banner, 2004). Moreover, during the long migration of deep fluids, the interactions between the fluids and surrounding materials can lead to chemical compositional changes, ultimately influencing the frictional properties of fluid pathways, such as faults (Lauer et al., 2017).

Since the first discovery of submarine seeps in 1970 (Judd and Hovland, 2007), numerous cold seep sites have been identified worldwide, spanning diverse geologic settings and encompassing water depths ranging from less than 100m to over 7000m (Sibuet and Olu, 1998; Fujikura et al., 1999; Treude et al., 2005) (Figure 1-1). By far, convergent margins hold the most frequent and well-studied cold seep systems. At convergent margins, a subduction zone is formed when a denser oceanic plate is subducting beneath another less dense continental or oceanic plate, descending into the mantle (Stern, 2002). The subduction's delivery makes the recycling of hydrated lithologies back into the mantle, called "subduction factory" (Tatsumi, 2005). When sediments are completely subducted beneath the overriding plate, a non-accretionary type margin is formed. Instead, a portion of sediment on the incoming plate accreted to the edge of the overriding plate, forming an accretionary wedge (von Huene and Scholl, 1991; Saffer and Tobin, 2011). At both subduction margins, overpressure is widely build-up in fluids and sediments, in response to lateral compression from plate movement and diagenesis-related processes of fluid production such as transformation of hydrous minerals

and thermal degradation of organic matter (Moore and Vrolijk, 1992; Ranero et al., 2008). The upward migration of these overpressure materials fuels the formation of various seepage structures in the overlying plate. While the occurrence of cold seeps on convergent margins is mainly associated with their compressional tectonics, there are also numerous seepages identified on passive margins, which are driven by rapid sediment loading and differential compaction (Berndt, 2005). Furthermore, transform plate boundaries are favorable geologic settings for seepage occurrence, but the reported findings are not as well-investigated as those in convergent and passive margins (Hensen et al., 2019). Along transform boundaries, the relative motion between two plates is horizontal, and the fault planes can cut across thick sedimentary sequences, extending to great depths (Bartolome et al., 2012; Gerya, 2016). The deep-reaching plate margins may contain a zone characterized by parallel faults and extensively fractured rock, providing pathways for the upward migration of fluids. In addition, transform boundaries at continental margins are the sites of high seismic activity, which can potentially trigger fluids ascending. Recently, there has been an increasing focus on studying gas and fluid seepage in transform-type plate boundaries (Shakirov et al. 2004; Prouty et al., 2020).

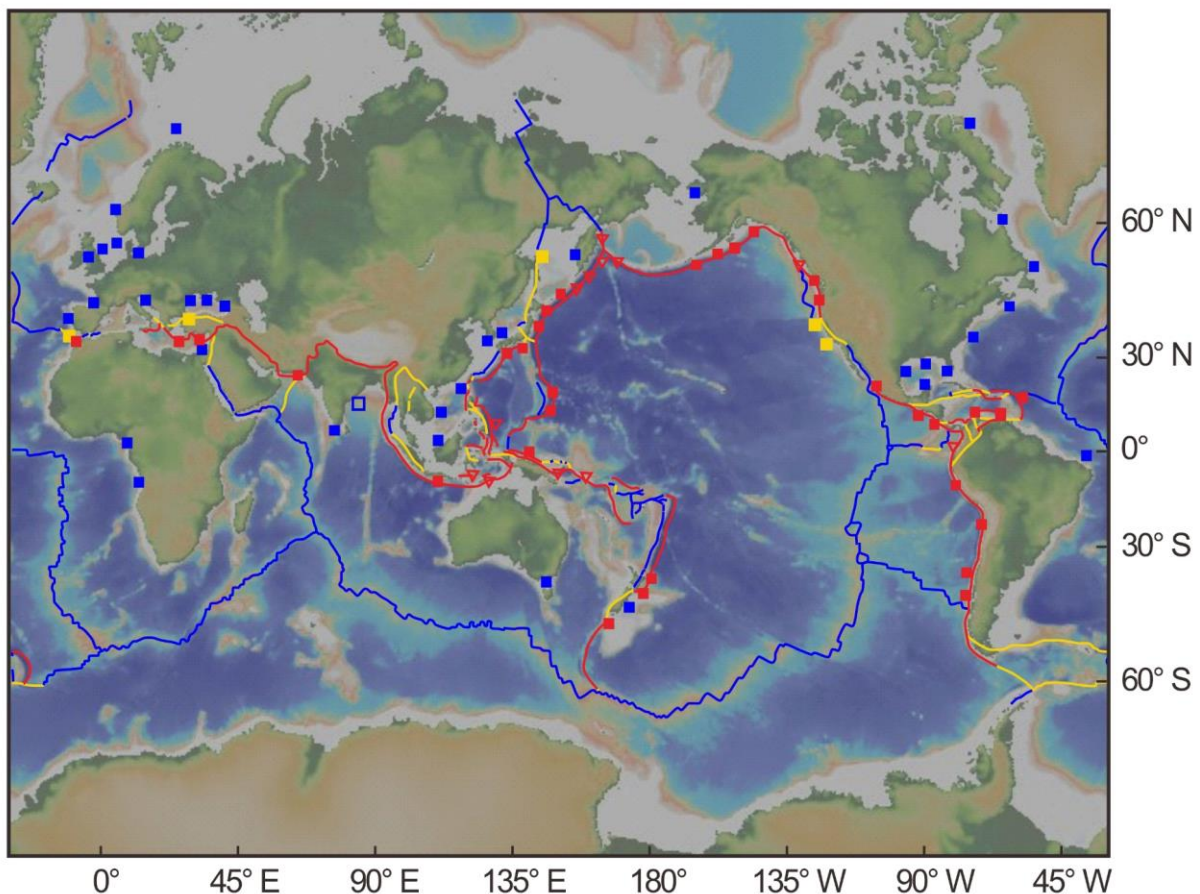


**Figure 1-1.** Global distribution of cold seeps (modified from Suess, 2014, and references therein). The active margin sites (red), passive margin sites (blue), and transform margin sites (yellow) are shown.

Cold seeps are extensively found in various geological settings, and the formation of related seafloor features serves as tangible evidence, clearly documenting the occurrence and historical activities of this phenomenon. The active expulsion of free gas into the hydrosphere is characterized by hydroacoustic image of gas flare in the water column, and many of chemosynthetic biological communities, like tube worms and bacterial mats, can be observed around the seepage sites (Sibuet and Olu, 1998; Greinert et al., 2006; Chand et al., 2012). In addition to the direct detection of fluid emission, the methane-derived authigenic carbonates (MDACs) are the product transformed from cold seep fluids. Near the seafloor, the symbiotic activity of sulphate-reducing bacteria and the methanogenic archaea leads to the formation of bicarbonate and reduced sulphur (anaerobic oxidation of methane, AOM), further precipitated to form carbonates and pyrite respectively (Judd and Hovland, 2007). The MDACs exhibit a wide variety of morphologies and sizes, such as tubular chimneys, pavements and slabs. When MDAC chimneys refer to the AOM process occurred within the subsurface plumbing system (Ceramicola et al., 2018), some scattered MDAC in the form of thin crusts and slabs can be observed in mud volcanoes (MVs) indicating an advanced evolutionary stage (León et al., 2006, 2007). As MDACs provide a substrate that is significantly harder than the surrounding seabed, they can be identified by higher acoustic backscatter intensity (Zitter et al., 2005). Moreover, there are some more obvious structures which alter the seabed in response to the material transfer across the seabed-seawater interface. While pockmarks are characterized by negative reliefs, MVs are positive topographical features. Pockmarks, most commonly shaped as conical and elliptical seabed depressions, were initially reported by King and McLean in 1970. They exhibit a wide range of sizes, spanning from a few meters to hundreds of meters, and can be found distributed in aligned strings or merged composites in soft, fine-grained and clay-rich sediments (Pilcher and Argent, 2007). As the pockmarks are formed through the expulsion of liquids and gases removing seabed sediments, they possess erosive characteristics that can be identified through seismic analysis and sediment coring (Judd and Hovland, 2007; Cathles et al., 2010). MVs, another prominent geomorphological indicator of cold seeps, are formed when sediments are transported together with fluids. Depending on whether the viscosity of the erupted mud is low (high fluid content) or high (low fluid content) either a shield-like structure or a conical structure builds up (Dimitrov, 2002; Kopf, 2002). In comparison to pockmarks, MVs are generally larger seafloor manifestations, with diameters reaching up to 4 km onshore and 12 km offshore (Orange et al., 2009). The extrusive edifice of MVs on the seafloor is composed of mud-flow erupted in multiple phases of activity, which can be traced back to overpressured formations on the order of several kilometers deep. Hence, the MVs offer a window to the depths, enabling us access to materials that would otherwise be challenging to obtain through current scientific drilling. By analyzing the emission products of MVs, we can gain valuable insights into deeper-seated processes.

In addition to seeping features that can be directly observed at or near the seabed, cold seep systems also comprise two internal elements, the overpressured sources (source of the fluids) and the plumbing system (Talukder, 2012). The development of cold seep is mainly driven by overpressure formed at depth, through mechanical (disequilibrium compaction) and

diagenesis-related chemical processes. Fluid production processes such as clay mineral dehydration and hydrocarbon formation are two of the major fluid supplies associated with cold seep, further contributing to overpressure by fluid expansion (Osborne and Swarbrick, 1997). Both of these chemical processes are driven by elevated p-T conditions with increasing burial depth. A large number of studies attested that hydrous minerals (e.g., smectite, opal) lose their interlayer water or change mineral phase during dehydration and form deep-seated aqueous fluids (Kastner et al., 2014). One of the prominent types of dehydration processes is the smectite to illite transformation, which primarily occurs between 60 and 150 °C with the initiation of the transformation at 67-81 °C through the loss of the 2nd water layer (Colten-Bradley, 1987). The transformation continues to 250 °C for the loss of the remaining water layer. In the gaseous phase, methane is the predominant component of seeping fluids documented in various cold seep sites. Due to sediment burial to several kilometers depth and tectonic processes such as underthrusting, organic matter are exposed to elevated p-T conditions and experience degradation. There are two main sources of methane, which include shallow-formed biogenic methane and thermogenic methane from thermocatalytic cracking of organic material (kerogen). By far, the majority of studies on hydrocarbons at cold seeps point to a thermogenic origin. The conversion of kerogen to light hydrocarbons within a closed system can produce a large volume increase of up to 25%, boosting the development of an overpressured source layer in the sedimentary column (Meissner, 1978; Osborne and Swarbrick, 1997). The transport pathway between the overpressured source and the seafloor manifestations is referred to as the plumbing system. There are several geological features associated with plumbing systems, including structural (faults and fractures), stratigraphical (e.g., higher permeability sedimentary layers), and intrusion-related (sand intrusions, salt and mud diapirs) (Cartwright et al., 2007; Talukder, 2012). Faults and fractures are the most ubiquitous plumbing systems, closely associated with and integrated into intrusion-related features, e.g., salt/mud diapirs. Besides, faulting and fracturing are one of the most important triggers in facilitating fluid flow ascent. A large number of studies have shown that the location and distribution of deep-rooted cold seeps on the seabed are controlled by faults in many places. In the eastern Nankai accretionary wedge, cold fluid venting linearly aligned, corresponding to a surface expression of the shallow detachment faults (Kobayashi, 2002). In the eastern Mediterranean, pockmarks most frequently occur near MVs and along fault lines (Dimitrov and Woodside, 2003). And most of the MVs in the Gulf of Cadiz follow the main trends of thrust-related diapiric ridges and strike-slip faults (Medialdea et al., 2009).

## **1.2 Mud volcanoes**

Among various cold seep features, mud volcanoes (MVs) are formed when sediments and fluids are transported together, piercing through the surface (Kopf, 2002; Suess, 2014). In response to localized and concentrated mud and fluid fluxes in multiple eruptive phases, cone-shaped to shield-like edifices are built up, making MVs an obvious positive structure on the seafloor (Kopf, 2002). They occur in a wide variety of geological environments, with convergent plate margins fueling the most abundant MVs confirmed and inferred to date

(Milkov, 2000; Mazzini and Etiope, 2017). The most affected areas can be found in the Mediterranean Sea and Tethyan Belt, which spans from south of Greece over the Black and Caspian Sea into Azerbaijan, the Crimea and Taman Peninsulas, Iran and Turkmenistan into the Makran coast (Kopf, 2002). With the Training-Through-Research Programme (TTR) extending the research area outside the Mediterranean and discovering large fields in the Gulf of Cadiz and in the Norwegian Sea, many other projects were prompted and followed, in particular, in the Gulf of Cadiz, Alboran Sea, Anaximander Mountains, and Nile Deep Sea Fan (Mazzini and Etiope, 2017).

MVs commonly refer to constructional edifices at the seafloor that are formed through a series of natural processes. To describe the set of structures associated with mud volcanism from source to extrusive, Stewart and Davis (2006) introduced the term “mud volcano system”, which comprises three main components: a source stratigraphic succession, mud volcano conduits (intrusive complexes), and mud volcanoes (outcropping or buried extrusive edifices) (Figure 1-2).

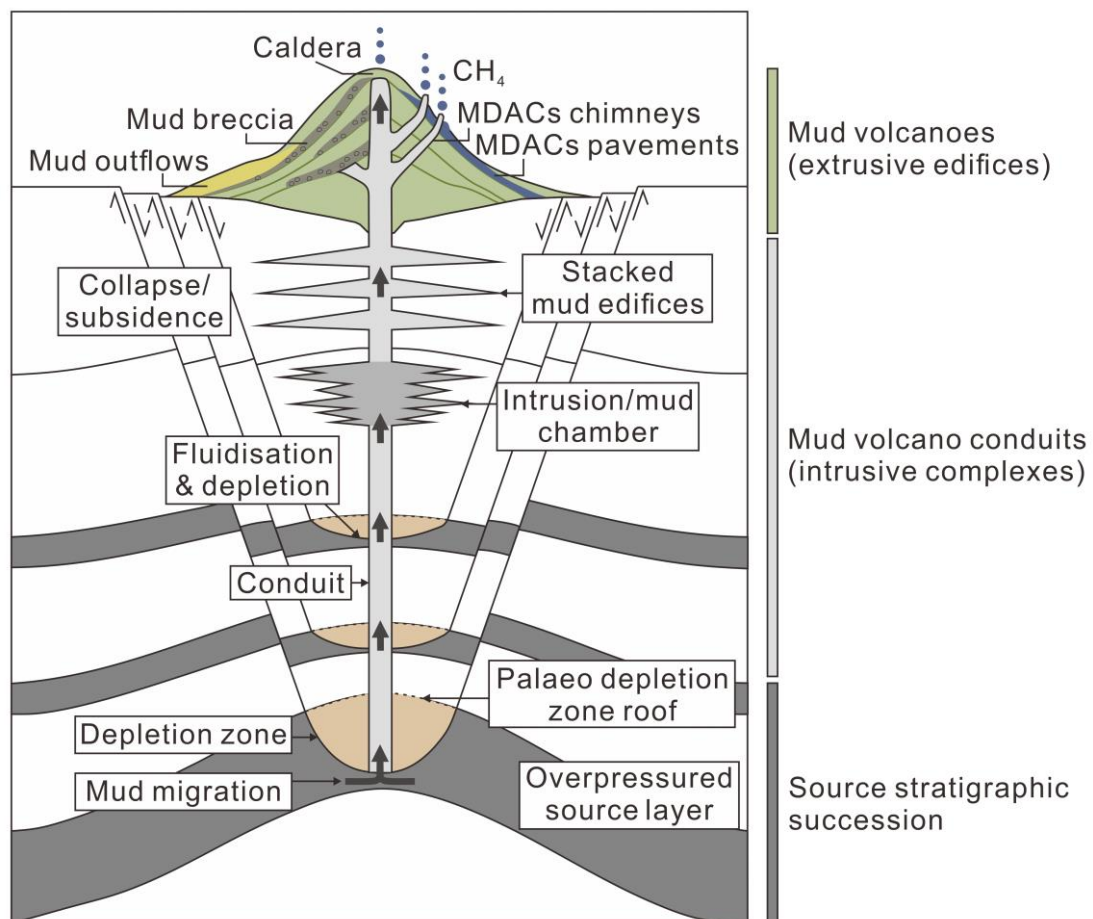


**Figure 1-2.** A schematic diagram illustrating basic structure and main elements of a conical mud volcano, and highlighting subdivisions of a mud volcano system (modified from Cartwright et al. 2023, Ceramicola et al., 2018, and references therein).

As the surface expression of mud mobilization, mud volcanoes (MVs) are the well-studied part of the whole system due to their easy accessibility, particularly in the case of terrestrial MVs (Yusifov and Rabinowitz, 2004; Mazzini et al., 2009). The size and geometry of MVs can vary significantly, with diameters and heights ranging from meters to tens of kilometers across and reaching heights of hundred meters (Orange et al., 2009). Based on the angle of edifice flanks, the morphologies of MVs range from classical conical shapes to laterally extensive shield-like shapes (Kopf, 2002). The resulting morphologies are controlled by numerous factors such as the nature, relative proportions and volume of extruded material, and the frequency and vigor of eruptions (Dimitrov, 2002; Kopf, 2002; Mazzini and Etiope, 2017). For example, gas-dominated and powerful short-lived eruptions typically result in a blocky morphology, whereas frequent eruptions of low (water dominated) and high viscous (sediments dominated) mud breccia give rise to flat mud pies and classical mud cones, respectively (Dimitrov, 2002; Kopf, 2002). In addition to a close link to the morphology, the products of emission possess preserve (part of) the original signature, serving as windows into deeper processes. The emission products of MVs are normally a mixture of gas, aqueous fluids, and sediments. These products may originate from different stratigraphic layers, ranging from shallow origins to considerable depths below the surface (Kopf, 2002). Extensive research has been conducted to investigate the chemical properties of the released gas and fluids, as well as the lithological and mineralogical characteristics of the sediments, aiming to elucidate their respective origins and relevance to elements cycles (e.g., Planke et al., 2003; Aloisi et al., 2004; Gennari et al., 2013).

The gases emitted by MVs typically consist of light hydrocarbons, with methane (both biogenic and thermogenic) usually accounting for over 80 vol% (Mazzini and Etiope, 2017), while in some cases associated with hydrothermal fluid circulation, the gas phase may be dominated by CO<sub>2</sub> due to magma degassing (Sheppard et al., 1992; Chiodini et al., 1996). Because methane is known as a powerful greenhouse gas, many studies (e.g., Kopf, 2003; Milkov et al., 2003; Vanneste et al., 2011; Etiope et al., 2019) have made an effort to estimate the methane flux rate from MVs, in order to investigate the role of MVs in the atmospheric methane budget (Figure 1-3). The aqueous fluids expelled from submarine MVs generally exhibit significant differences in composition compared to seawater. They represent a mixed result of chemically distinct formation water from various depths reacting with rocks and sediments during their migrations through vertical conduits spanning kilometers in size (Kastner et al., 1991; Kopf, 2002). The inherited signatures of aqueous fluids can serve as a proxy for tracing processes at depth, especially in cases where in situ samples may not be accessible (e.g., Hulme et al., 2010). Furthermore, the expelled aqueous fluids can be utilized to understand water-rock interactions. In deep sedimentary oil-bearing basins, they can provide important information for evaluating the petroleum potential (e.g., Milkov, 2005). In the case of marine MVs, the expelled fluids are intimately linked to many processes, including anaerobic oxidation of methane, gas hydrate formation, clay mineral dehydration, and hydrothermal activity, which will be discussed in Section 1.3.

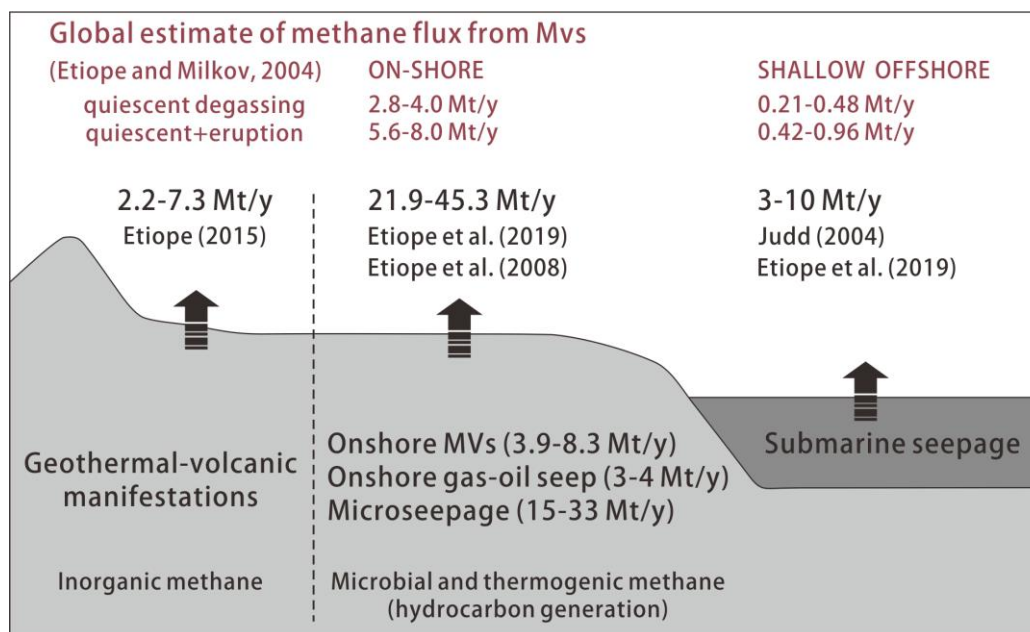


**Figure 1-3.** Geologic sources of methane and global output into the atmosphere by combining literature estimates and recent updates from Etiopie and Schwietzke (2019) and references therein. A global estimate of methane flux from MVs is based on data collected from Etiopie and Milkov (2004).

For the emitted sediments, Cita et al. (1989) introduced the term 'mud breccia' to describe specific sediments associated with mud volcanoes. Mud breccia refers to a clay mineral-rich mud matrix that contains clasts of varying sizes and lithologies. As the edifices are constructed through different mudflow generations, different phases of outflowing mud breccia can be traced on the flanks of the structures (Kopf et al., 1998). The source stratigraphic succession of MVs is typically a thick, under-compacted series of clays or shales (Yassir, 1989). Analyzing the erupted mud breccia can offer valuable insights into their origins and formation processes. The mud breccia clasts usually present high variability in size and lithology, reflecting the characteristics of the surrounding rocks and sediment layers encountered during the ascent of mud (Staffini et al., 1993; Kopf, 2002). The incorporation of these clasts into the mud breccia matrix results from the forceful expulsion of materials during the eruption process. In comparison with the difficult interpretation and attribution of mud breccia clasts, the mud breccia matrix provides a more comprehensive representation of the whole breccia framework and can shed light on the origin of the mud source stratigraphic succession. The micropaleontological studies carried out on the matrix can give assess to date the age of the source sediments involved in mud-breccia extrusion, which can further enable the identification and differentiation of elements from both the source layer and the overlying sedimentary sequence (Pinheiro et al., 2003; Gennari et al., 2013). Through mineralogical analysis, the clay mineral composition of the matrix can reflect the thermal maturation stage of clays, e.g., the degree of smectite-to-illite conversion, and thereby indicate a shallow or deep burial history (Martín-Puertas et al., 2007). Based on the analysis of total carbon contents, lipid biomarkers, and vitrinite reflectance, the depositional environment, thermal maturity, and

burial depth of the matrix can be constrained, defined, and estimated (Schulz et al., 1997; Kopf et al., 2000; Stadnitskaia et al., 2008). As MVs often serve as the surface expression of petroleum seepage, frequently linked to natural gas or oil reservoirs, they are generally considered a part of the petroleum system (Abrams, 2005; Etiope, 2015). The study of mud breccia matrix can further reveal the hydrocarbon potential of their source stratigraphic succession.

In order to gain deeper insights into the processes that facilitate the ascent of the source stratigraphic succession, the study of MVs' formation mechanisms receives increasing attention. The main engine driving the formation of MVs is the combination work of excess pore fluid pressure (overpressure) and buoyancy (e.g. Kopf, 2002; Revil, 2002). The source stratigraphic succession of MVs is typically a clay-bearing strata, which exhibits an overall lower density compared to surrounding sediments, leading to a density inversion. As asserted by Kopf (2002), such density inversion is the prerequisite for MV initiation, allowing the sediment body start to ascend. The build-up of overpressure within the strata can further support and accelerate the motion upwards. The principal cause of overpressure generation is disequilibrium compaction, occurring under the circumstances of rapid sedimentation and tectonic compression (Judd and Hovland, 2007). During burial, pore fluids become trapped in fine-grained sediments, preventing their drainage and leading to an increase in the pore fluid pressure. In addition to physical processes, a range of chemical mechanisms can also contribute to overpressure build-up (Maltman and Bolton, 2003). The most cited ones are associated with fluid production processes, including smectite-to-illite transformation (aqueous fluid) and hydrocarbon generation (gas). There are two potential outcomes and models have been considered. Driven by buoyancy contrasts, the underlying sediment will push through the cap sediment to flow as a coherent sediment mass (buoyancy model), while the excess pore fluids will induce the fluidization of sediment particles (hydraulic model) (Brown, 1990; Dimitrov, 2002; Jonk, 2010).

To identify and characterize the source regions for MVs is a challenging task, and the methods employed often rely on the analysis of extruded products (e.g., Deville et al., 2003; Praeg et al., 2009) or more direct seismic imaging techniques (e.g., Graue, 2000; Kirkham et al., 2017; Dupuis et al., 2019). Stewart and Davies (2006) introduced the term "depletion zone" to refer to the thinning areas at their parent stratigraphic unit where the depletion of parental fine-grained sediments has been mobilized and transported to the surface. Recently, Cartwright et al. (2023) documented 86 depletion zones associated with MVs in the western Nile Cone, offshore Egypt, characterized by circular to elliptical planforms with a bowl or conical geometry. However, sediments and the liquid-gaseous fraction of the fluid are often not syngenetic (Kopf, 2002). The depletion zone characterizes the source stratigraphic unit for sediments, while the identification of the root for fluids mainly relies on their geochemical fingerprint (e.g., Planke et al., 2003).

The MV conduits represent the transitory part from the source stratigraphic unit to the constructional edifices at the seabed, which is the most complex and the least known of the MV system (Kirkham et al., 2018). The understanding of MV conduits mainly rely on geophysical approaches i.e., seismic imaging. However, obtaining a clear image of MV conduits is challenging, due to their complex composition of brecciated and mixed lithologies resulting in high heterogeneity, and significant fluid presence attenuating the seismic signal (Mazzini and Etiope, 2017; Kirkham et al., 2018). With the recent advances and availability of 3D seismic data, MV conduits are primarily identified as pipe-like structures (Davies and Stewart, 2005; Kirkham et al., 2018; Oppo et al., 2021). But detailed analysis of the geometry and expression of MV conduits remains limited. Based on the crater formation study of recently erupted MVs offshore Egypt, Pryce et al. (2023) proposed that during the initial phase of mud volcanism, their genesis was characterized by highly vigorous eruptions of a predominantly gas (methane) and water mix, and the edifice construction was built by subsequent mud extrusion. This is consistent with the observations that there are similarities between the early stages of MV conduits and the fluid escape pipes (Kirkham et al., 2018; Figure 1-4). Through the progressive inclusion of larger quantities of fine-grained sediment into the migrating fluids, the MV conduit gradually assumes its final geometry, reflecting an evolutionary outcome of a fluid escape pipe (Cartwright, 2007; Huuse et al., 2010; Kirkham et al., 2018). The formation of MV conduits involves sediment deformation to accommodate fluid and particle influx (Jonk, 2010). Two major processes, hydrofracturing and migration along faults, play significant roles. Hydrofracturing occurs when fluid overpressure reaches the fracture pressure of an overlying layer, leading to the opening of impermeable barriers (Revil, 2002). This allows for the local fluidization and brecciation of sedimentary units. Faults, on the other hand, serve as the frequently encountered and effective pathways for the migration of fluids and fluidized sediments. One key issue is that faults exhibit dual behavior regarding fluid migration, functioning either as sealing or leaking structures (Smith, 1980; Sibson, 1995; Cartwright et al., 2007). Faults with damage zones exhibit higher permeability compared to their host sequences, frequently serving as major flow routes (Talukder, 2012). These pathways can persistently facilitate cross-strata migration and are particularly prone to acting as fluid valves during active rupture. However, in most cases, fault zone rocks exhibit lower permeability than their host rocks, with horizontal stress typically leading to fault closure, thus acting as barriers to fluid migration (Talukder, 2012). These faults need to be dilated to behave as conduits. For these faults to effectively act as conduits, they need a process of dilation, where high pore fluid pressure plays a critical role in opening a fault and sustaining fault permeability (Sibson, 1988, 1996; Clennell et al., 1998). Faults commonly extend beyond 5 km in length and can cross thick sealing sequences, endowing them with the capability to serve as extensive conduits for the vertical transport of significant fluid and sediment flux over long distances (Hooper, 1991).

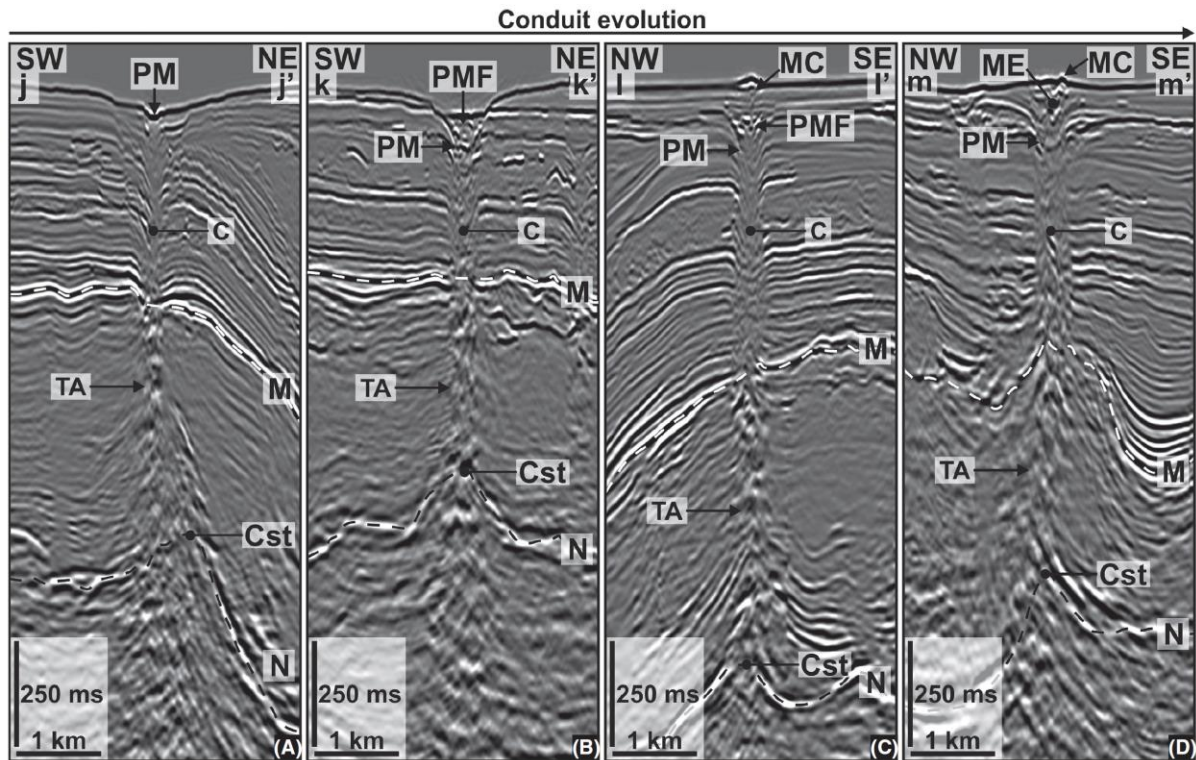


**Figure 1-4.** Conduit evolution from fluid escape pipe to mud volcano conduit (modified from Kirkham et al., 2018). (A) A fluid escape pipe with a seafloor pockmark at its upper terminus. (B) A fluid escape pipe with a pockmark at its upper terminus that exhibits a sedimentary fill that is possibly extrusive. (C) A pipe-like conduit overlain by a mud cone at the seafloor, potentially the formation of a juvenile mud volcano. (D) A mud volcano conduit feeding a relative small extruded mud edifice. *PM*, pockmark; *PMF*, pockmark fill; *MC*, mud cone; *ME*, mud edifice; *C*, conduit; *TA*, trail of amplitude; *Cst*, crest; *M*, horizon M (top-salt); *N*, horizon N (base-salt). The seismic profiles are sourced from Kirkham et al. (2018), and the locations of lines *j-j'*, *k-k'*, *l-l'*, and *m-m'* can be found therein.

Mud volcanism is characterized by its inherent episodic nature. The occurrence of eruption is primarily regulated by the local stress and pressure regime within the source stratigraphic succession (Deville and Guerlais, 2009). The dynamic changes in the fluid pressure govern the cyclic phases of activity, which are characterized by alternating periods of eruption and dormancy. In the evolutionary models of MVs (León et al., 2007; 2012; Menapace et al., 2019), the activity of MVs can be divided into four successive phases: i) eruption, violent eruptions of mud breccia and formation of the MV edifice (Figure 1-5A); ii) depletion, moderate to slow fluid seepage through cracks, gryphons and adjacent high permeable surroundings (Figure 1-5B); iii) quiescence and build-up, subsidence of the edifice forming the moat around MVs and accumulation of fluid pressure (Figure 1-5C); and iv) re-activation, breakout of an eventual “plug” and a new episode of active mud flow extrusion (Figure 1-5D). Multiple extrusive activities throughout the lifespan of a MV have been confirmed through drilling and seismic imaging, where mudflow deposits interfinger with hemiplagic background sediments giving rise to a typical “Christmas tree” geometry at shallow levels (Robertson and Kopf, 1998).

However, eruptions commonly last only a few days or less, standing as a remarkably brief period in a broader temporal framework of a MV's lifecycle (Mazzini and Etiope, 2017). It is during the short duration of eruptive phases that a considerable volume of materials, prominently encompassing mud breccia, is vigorously expelled to the surface and build the bulk of the MV edifice, embodying the intensity and efficiency of these eruptive events (Kopf, 2002). In contrast, interval phases of depletion and quiescence that separate different eruptive events account for a big part of the MVs' life cycles (over 95-97%; Kopf, 2002; Menapace et al., 2019). These long periods, despite their relatively subdued character, exhibit a significant influence on fluid budgets due to the continuous seepage of fluids, comparable to the effects observed during the violent eruptive phases (Etiope et al., 2007; Etiope et al., 2011; Hong et al., 2013).

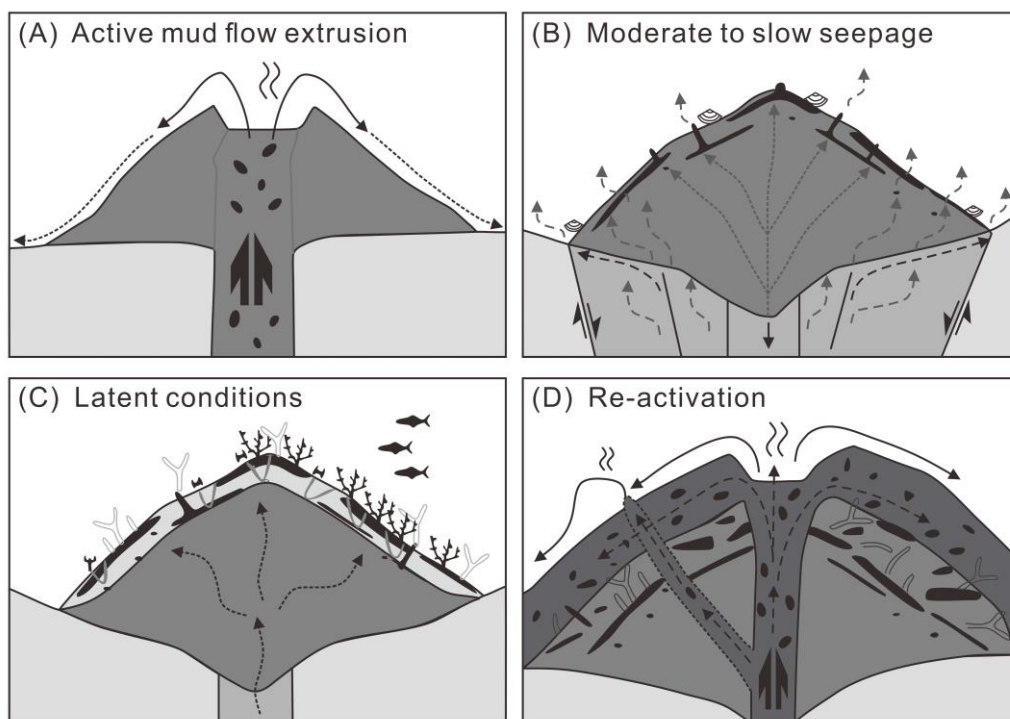


**Figure 1-5.** Four fundamental stages of MVs evolution (modified from León et al., 2007).

### 1.3 Pore fluid geochemistry

Pore waters are aqueous solutions present within the pore spaces between particles in sediments or rocks, generally originating as seawater trapped from the overlying water column (Chester and Jickells, 2012), and can be extracted from sediments with Rhizon samplers attached to syringes (Dickens et al., 2007) (Figure 1-6). During progressive burial, the sediment-pore water continuum has experienced a series of processes such as compaction, dissolution of detrital minerals and precipitation of authigenic minerals (Chester and Jickells, 2012). These alterations lead to changes in the composition of pore waters and thus make pore water composition a repository of crucial insights into fluid-rock interactions, geochemical cycles and microbial activities within cold seep systems.

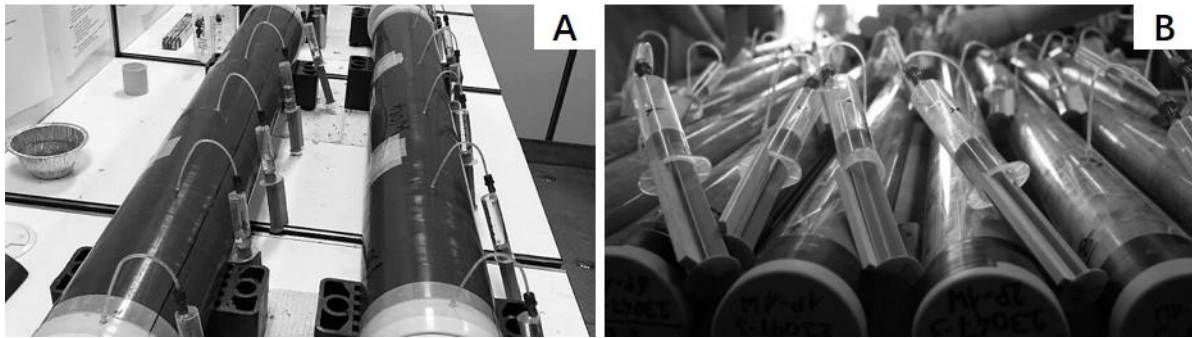


**Figure 1-6.** Pore water extraction with rhizons and syringes from gravity cores (A) and MeBo cores (B) (pictures taken from R/V Meteor cruises M149 and M167).

Early diagenesis occurs in sediments and rocks during their initial burial stages (Figure 1-7), typically within a burial depth up to a few hundred meters and under temperatures similar to those at the seafloor (Berner, 1980). It acts as a bridge between the initial sedimentation and more advanced diagenetic alterations that occur under deeper burial conditions and higher temperatures. During early diagenetic processes, organic matter undergoes alteration through a combination of microbial activity, chemical reactions, and physical processes (Berner, 1980). At cold seeps, anaerobic oxidation of methane (AOM) is the key process occurring in shallow subsurface sediments, regarded as a major sink for methane (Hinrichs and Boetius, 2002; Reeburgh, 2007). AOM is a microbial process mainly taking place in anoxic sediments, within the topmost layers affected by seawater sulfate penetration. Downward diffusing sulfate and upward migrating methane are utilized by a consortium of sulfate-reducing bacteria (SRBs) and methanogenic archaea (ANMEs) (Boetius et al., 2000).



The collaboration between these two microbial groups occurs within a zone known as the sulfate-methane transition zone (SMTZ), where sulfate becomes nearly depleted, and methane concentration exhibits a significant increase with depth (Borowski et al., 1996, 1999). The distinctive concentration distribution of methane and sulfate, exhibiting a concave-up shape for methane and a concave-down shape for sulfate, can be recognized at numerous cold seeps, signifying the occurrence of AOM processes (Boetius et al., 2000; Bohrmann et al., 2003; Werne et al., 2004). This process results in bicarbonate production, which in turn increases alkalinity, and also triggers the precipitation of different authigenic minerals such as carbonates, gypsum, and iron sulfides (e.g., Ritger et al., 1987; Luff and Wallmann, 2003; Schoonen, 2004). This fundamental contribution of AOM to the formation of methane-derived authigenic carbonates (MDACs) is evident through AOM-specific lipid biomarkers that exhibit  $^{13}C$ -depletion and are incorporated into the composition of MDACs (Hinrichs et al., 1999; Orphan et al., 2001). AOM can lead to the consumption and buffering of over 90% of methane, underscoring its crucial role in mitigating methane release into the water column and atmosphere (Reeburgh, 2007). Due to its importance, numerous studies have concentrated on unraveling the mechanisms of AOM at cold seeps. In the Gulf of Cadiz, extensive methane venting known to have occurred in the past, as evidenced by the widespread distribution of MDACs (Diaz-del-Rio et al., 2003), contrasts with present-day methane emissions, where

complete methane consumption in the seafloor is measured for MVs across the region, showing lower seepage rates than other submarine MVs (Niemann et al. 2006a, 2006b; Hensen et al. 2007).

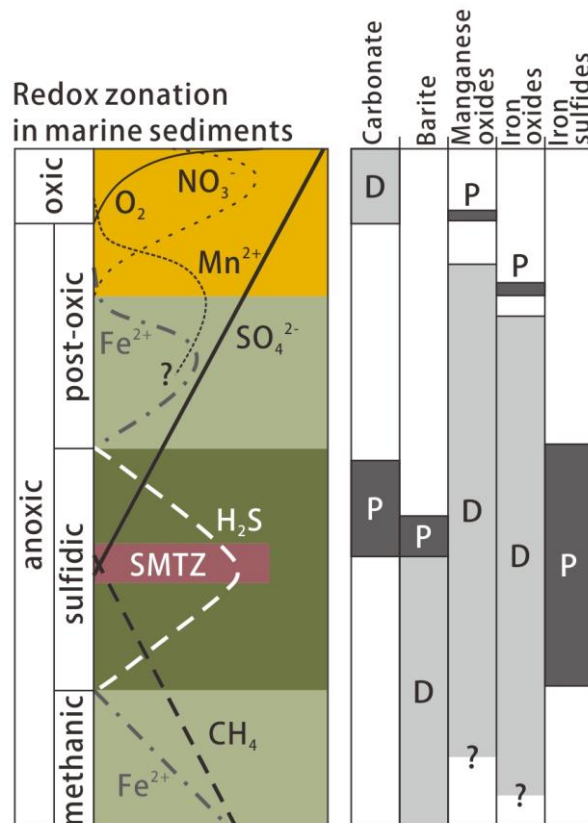


**Figure 1-7.** Schematic graph showing early diagenetic geochemical zonation of marine sediments (modified from Kasten et al., 2003, Henkel, 2011). The classification of redox zones is presented on the left side (Froelich et al., 1979; Berner, 1981). The zones of dissolution and authigenic formation of selected minerals are shown on the right side. *SMTZ* Sulfate-methane transition zone; *D* dissolution; *P* precipitation/formation.

Gas hydrate formation and dissociation is another important diagenetic reaction that is closely associated with cold seeps and occurs within the uppermost kilometer of marine sub-seafloor sediments (Kastner et al., 1991). The prevalence of gas hydrates in cold seep settings arises from a combination of factors ensuring their stability. The necessary conditions are facilitated by: i) relatively low seafloor temperatures; ii) deep-water depths where the pressure is sufficient for gas hydrate stability; and iii) the involvement of migrating methane from deep subsurface reservoirs. Thus, cold seeps, like MVs, serve as an important indicator of potential gas hydrate presence (Mazurenko and Soloviev, 2003). Reported findings from cold seep development areas include the Gulf of Mexico (Boswell et al., 2012), the Black Sea (Minshull et al., 2020), the Nankai Trough (Colwell et al., 2004), etc. In the Mediterranean Sea, the eastern region, including the Olimpi Field, the Nile Fan, and the Anaximander Seamount, is expected to host a significant amount of gas hydrates (Meroy and Longinos, 2018; Minshull et al., 2020), and in the Gulf of Cadiz gas hydrates have been inferred and retrieved from several

MVs (Gardner, 2001; Depreiter et al., 2005). The occurrence of gas hydrates modifies the chemistry and isotopic compositions of pore fluids, exhibiting anomalies in Cl concentrations and O and H isotopes. This is attributed to gas hydrates excluding Cl from their lattice structure and favoring the incorporation of heavier isotopes of O and H in their cage water (Hesse and Harrison, 1981; Ussler and Paull, 1995). Dissociation of gas hydrates, therefore, results in an increase in  $\delta^{18}\text{O}$  and  $\delta\text{D}$  of the diluted pore water (low Cl concentrations).

Clay mineral dehydration, specifically the transformation from smectite to illite, represents another important reaction responsible for the evolution of low Cl fluids observed in many cold seeps (e.g., Saffer and Bekins, 1998; Hüpers and Kopf, 2012). The decrease of Cl in pore waters can be attributed to the released water during this transformation process, consequently leading to the dilution of ambient pore water. In general, this process may be expressed as a reaction of smectite and K to illite, Mg, Na, minor elements such as Sr and Li, and  $\text{H}_2\text{O}$  (Scholz, 2010). The optimal temperature range for smectite-illite transformation is between 60 and 150 °C (Freed and Peacor, 1989; Srodon, 1999), which allows the reaction to occur over a considerable depth interval of several kilometers depending on the regional geothermal gradient. Its occurrence can be identified through water isotopic studies, as the interlayer water released from the expandable smectite structure is characterized by positive  $\delta^{18}\text{O}$  and negative  $\delta\text{D}$  values (Sheppard and Gilg, 1996). This distinct geochemical signature enables the distinction between different causes of pore fluid freshening, whether it's due to gas hydrate dissociation or clay mineral dehydration. Pore water freshening has been noted in many MVs, including the examples studied in this thesis: the Milano MV in the Mediterranean Sea and the Ginsburg and Yuma MVs in the Gulf of Cadiz. While the initial interpretation of this phenomenon in both regions was linked to gas hydrate decomposition (e.g., De Lange and Brumsack, 1998; Mazurenko et al., 2003), it has since been widely acknowledged as being caused by clay mineral dehydration (e.g., Dählmann and De Lange, 2003; Hensen et al., 2007).

In the case of deep burial or hydrothermal activity, the fluid–sediment alteration is characterized by high temperature and pressure, and the reactions with the oceanic or continental basement rocks can occur. But the basement fluids enter the sediment column is generally limited to the place where sediments are thin or in the proximity of faults (Spinelli et al., 2004; Fisher, 2005). Fluid circulation in the crust plays a central role in marine systems, primarily by facilitating the transport of heat and dissolved constituents (Suess, 2014). Generally, basement fluids tend to undergo greater geochemical evolution as basement temperatures rise. These temperatures are often dictated by the thickness of the overlying sediments. However, once the basement is fully sedimented, or if active tectonic processes cease to maintain permeability, it's unlikely for basement fluids to establish a hydrological connection with the ocean (Manning and Ingebritsen, 1999). In the cold seep environment, there have been reported findings of deep-sourced fluids, some of which may originate from the basement. An exceptional case can be observed in the Mariana Trench, where serpentinite MVs are found. The serpentinite materials forming these MVs result from the interaction of fluids originating from the subducting plate (Pacific Plate) with ultramafic rocks rich in olivine,

specifically harzburgite, within the overlying plate (Philippine Plate), thereby reflecting the impact of basement fluids on the sediment column (Fryer et al., 2020; Wheat et al., 2020). More direct support can be found at the South Chamorro Seamount located west of the Mariana Trench, where pristine deep-sourced fluids, enriched in sulfate and methane, originating from the subduction channel can reach the seafloor unchanged within the central conduit (Wheat et al., 2020). In the Mediterranean Ridge and the Gulf of Cadiz, seep fluids at MVs exhibit characteristics of the high-temperature regime (Hensen et al., 2007; Scholz et al., 2010a), with those for the later even displaying evidence of fluid-sediment interaction within hydrothermal regimes (>200 °C; Scholz et al. 2009).

## **1.4 Motivation**

As previously introduced, numerous previous studies have significantly advanced our comprehension of cold seeps, particularly those related to MV systems, encompassing geologic characteristics, geochemical processes, and biodiversity and ecology. However, there are still many research questions to be learned and improved. This thesis applies a range of methodologies, primarily focusing on pore water geochemical analysis, to a set of cores collected from the MVs in the Gulf of Cadiz. The aim is to address the following topics:

### **(1) What is the role of MVs in deep-seated fluid and solid migration through the Gulf of Cadiz accretionary prisms?**

The Gulf of Cadiz, situated offshore SW Iberia and NW Morocco, is an area of geological complexity that is grabbing increasing attention in the fields of mud volcanism and various phenomena associated with fluid seepage. While the occurrence of deep water MVs is closely tied to a set of strike-slip faults mediating fluid flow, the research on the correlation between MVs and faults, particularly in the context of the transform plate boundary traversing the accretionary wedge, remains relatively scarce. Based on the investigation of six MVs in locations adjacent to major strike slip faults, this study seeks to define fluid and solid mobilization depth and to identify the processes occurred during their ascent through the accretionary prism. Thus, the study focuses on understanding the role of MVs in relation to the faults and their variations between different parts of the accretionary prism.

### **(2) How do mud volcano geomorphological features affect the MVs' fluid circulation system?**

The evolving surface characteristics of MVs, including their morphology (mud flows, caldera collapsing, moat development), eruptive behavior (violent eruption, quiescent seepage), and product composition (fluidized sediments, gas and pore water), serve as indicators of the dynamic subsurface conditions, including variations in the source, alterations in reservoir pressure, and the influence of mud volcano conduits on fluid flow (whether enhancing or inhibiting). A deeper understanding of the evolution of these factors and the complex relationships among them require further investigation. During the M149 cruise, distinct salinity patterns (freshening at the summit vs. salinization at the moat) were detected at the

Yuma and Ginsburg MVs in the Gulf of Cadiz, and Dählmann and de Lange (2003) previously reported similar spatial distributions of Cl concentrations at the Milano MV in the Mediterranean Ridge. This spatial variation in chemical and fluid fluxes provides excellent data to further illuminate the structural implications behind its surface performance.

### **(3) To what extent do transform faults play a role in deep hydrologic cycle?**

In the study of fluid seepage, faults are among the most crucial elements, as they not only act as triggers for the formation of various cold seeps such as mud volcanoes and pockmarks but also function as integral components of the cold seep system by providing fluid pathways. While numerous venting and seepage activities are characterized by tectonic control and have been extensively studied along convergent plate boundaries, reported findings of fluid activity from transform faults are relatively limited. Across the Gulf of Cadiz, a set of WNW-ESE trending strike-slip faults forms the easternmost segment of the prominent transform system known as the Azores-Gibraltar fracture zone (AGFZ), making it a suitable area to study fluid flow along transform faults and allowing for comparisons with the fluids from nearby cold seep sites (MVs and pockmarks). Hence, this study primarily focuses on the chemical analysis of fluid composition, aiming to elucidate the impact of transform faults in concentrating crustal signals from the depths.

## **1.5 Outline of this cumulative dissertation**

The research presented in this doctoral dissertation was carried out at the MARUM – Center for Marine Environmental Sciences, University of Bremen, under the guidance of Prof. Dr. A. Kopf and Dr. W. Menapace. The specimens utilized in this doctoral dissertation were collected during the R/V Meteor research cruises M149 and M167 and the INSIGHT Leg 1 and 2 cruises (2018 and 2019). This dissertation is structured into five distinct chapters and encompasses three first-authored manuscripts. The primary content of each chapter is outlined below.

**Chapter 1:** This chapter serves as an introduction to this Ph.D. dissertation. It introduces the state-of-the-art knowledge in the field of seabed fluid flow, mud volcanoes and pore water geochemistry, outlines the motivations driving this Ph.D. study, details how this Ph.D. research is carried out, provides an overview of the main content covered in each chapter, and describes my individual contributions to each manuscript.

### **Chapter 2 (Manuscript I): Mud volcanoes in the Gulf of Cadiz as a manifestation of tectonic processes and deep-seated fluid mobilization**

This chapter focuses on the topic (1). Six MVs adjacent to major strike-slip faults in the Gulf of Cadiz, with three of them newly discovered during the R/V Meteor cruise M149, have undergone investigation utilizing a combination of morphology, sedimentology, physical properties, mineralogy, and geochemistry. The selected MVs are located along different strike-slip fault segments and are supposed to be hydraulically connected to deeper sedimentary layers, either through adjacent fault zones or deep-seated feeder channels. Based on marked variations

of morphologies and geochemical signals, their role in deep-seated fluid and solid migration through different parts of the Gulf of Cadiz accretionary prism has been defined. This work has been published on *Marine and Petroleum Geology*.

### **Chapter 3 (Manuscript II): The rise and fall of mud volcanoes: geophysical insights and geochemically enigmatic fluid signatures**

This chapter focuses on the topic (2) to further investigate the relationship between the evolving surface characteristics and the dynamic subsurface conditions within a MV. Five MVs situated in the Gulf of Cadiz and the Mediterranean Ridge have been studied. Among these MVs, three display variations in fluid compositions between their summits and moats/rim areas, while the other two exhibit different fluid seepage activities, representing different stages of evolution. By employing fluid geochemistry, pore water modeling, and high-resolution seismic data, fluid pathways associated with the MV rims have been identified, distinct from the central conduits within these MV structures. When related to the MVs evolution in the depletion and quiescence periods, the changing fluid composition as well as the fluid flux reflect the involvement of additional (shallow) fluid sources and the influence of mud volcano conduits on fluid flow (enhancing or inhibiting).

### **Chapter 4 (Manuscript III): Ascent of fluids through km-thick sedimentary cover links to active tectonics in the Gulf of Cadiz**

This chapter addresses the topic (3), and shifts the focus from MVs to transform faults in order to get a broader understanding of fluid seepage. This chapter examines the origin and distribution of fluid circulation along the South West Iberian Margin (SWIM) fault zones which form a transform-type plate boundary between Africa and Eurasia. Chemical and isotopic analysis have been conducted on the fault fluids, and in-situ heat-flow data has been collected across the fault. In comparison with the fluids from the nearby cold seep sites (MV's and pockmarks), geochemistry data reveal that fault fluids interact intensely with Triassic evaporites at depth and support the contribution of continental crustal fluids.

**Chapter 5:** This chapter provides a summary of the key findings from this Ph.D. dissertation and offers prospects for future research on seabed fluid flow.

## **1.6 Contribution to the manuscripts**

### **Manuscript I: Mud volcanoes in the Gulf of Cadiz as a manifestation of tectonic processes and deep-seated fluid mobilization**

S. Xu processed the multibeam data, conducted the Multi-Sensor Core Logger (MSCL) experiments, prepared the samples for X-ray diffraction (XRD), Inductively Coupled Plasma Optical Emission Spectrometer (ICP-OES) and Ion Chromatograph (IC) tests, analyzed and interpreted all the data presented in this study, prepared all the figures, wrote and revised the manuscript.

W. Menapace and A. Hüpers recovered all the sample used in this study during the R/V Meteor M149, interpreted the data, and revised the manuscript. A. Kopf contributed to the discussions and revised the manuscript.

**Manuscript II: The rise and fall of mud volcanoes: geophysical insights and geochemically enigmatic fluid signatures**

S. Xu processed the multibeam data, prepared the samples for Inductively Coupled Plasma Optical Emission Spectrometer (ICP-OES), Ion Chromatograph (IC) and H, O, Sr isotope measurements, wrote the MATLAB code for the advection-diffusion model, analyzed and interpreted all the data presented in this study, performed all the calculations, prepared all the figures, wrote and revised the manuscript.

W. Menapace recovered all the samples used in this study during the R/V Meteor M149 and M167, advised on the research idea, interpreted the data, and revised the manuscript. R. Urgeles, J. Ford, A. Calahorrano and R. Bartolomé collected the high-resolution seismic data during the INSIGHT Leg 1 and 2 cruises (2018 and 2019), processed the seismic data, contributed to interpretations and revised the manuscript. A. Kopf contributed to the discussions and revised the manuscript.

**Manuscript III: Ascent of fluids through km-thick sedimentary cover links to active tectonics in the Gulf of Cadiz**

S. Xu processed the multibeam data, prepared the samples for Inductively Coupled Plasma Optical Emission Spectrometer (ICP-OES), Ion Chromatograph (IC) and H, O, Sr isotope measurements, established and wrote the MATLAB code for the three-endmember mixing model, analyzed all the data presented in this study, performed all the calculations, prepared all the figures, wrote and revised the manuscript.

W. Menapace and A. Hüpers recovered all the samples and heat flow data used in this study during the R/V Meteor M149 and M167. W. Menapace advised on the research idea, interpreted the data, and revised the manuscript. A. Hüpers interpreted the data and revised the manuscript. A. Kopf contributed to the discussions and revised the manuscript.

## Chapter 2

# Mud volcanoes in the Gulf of Cadiz as a manifestation of tectonic processes and deep-seated fluid mobilization

Shuhui Xu, Walter Menapace, Andre Hüpers, Achim Kopf

MARUM – Center for Marine Environmental Sciences, University of Bremen, Leobener Strasse 8, D-28359 Bremen, Germany

Corresponding author: Shuhui Xu ([sxu@marum.de](mailto:sxu@marum.de))

Published in *Marine and Petroleum Geology* 132 (2021): 105188

### Abstract

Numerous mud volcanoes (MVs) are scattered through the Gulf of Cadiz (GoC), most of which are situated close to the WNW-ESE trending fault system in this region. In this study we have investigated six MVs in locations adjacent to major tectonic lineaments with the purpose of defining fluid and solid mobilization depth and ascent through the accretionary prism. Three of them, R2, D2 and Funky Monkey MVs, were discovered during R/V Meteor cruise M149 in 2018. Their morphologies were characterized by multibeam bathymetry and vary from flat-topped to cone-shaped, reflecting different nature of the emitted products and variable degrees of activity. Mud breccias and pore fluids were sampled at the summits of all MVs to determine their physical properties and composition of the solid and liquid fractions. The physical properties and lithological changes demonstrate recent activity of Yuma, Ginsburg, Meknes and Funky Monkey MVs. At these sites, we traced back the origin of venting fluids to clay mineral dehydration through major and minor elements geochemistry, high content of illite in the mud breccia matrix and calculated reaction temperatures of 60-100 °C using the Mg-Li geothermometer. Differences in fluid composition imply a dominant clay dehydration signal in the shallow MVs and a stronger crustal input in the deeper MV (Funky Monkey). In contrast, R2 and D2 MVs are textbook inactive mud domes, showing no venting and a chemical composition/reaction temperature similar to seawater. If crustal input in MVs fluids will be confirmed by subsequent studies (e.g., through Sr isotopes), this could lead to a rethinking of fluid migration in the GoC, where transform faults (and MVs located close to them) focus the crustal signal from depth. Based on the MVs active state and the geochemistry of the fluids, we can distinguish which structure would be more suitable for further analyses (boron isotopes, illite crystallinity) in order to identify possible sources of hydrocarbon-rich fluids channeled through MVs.

## 2.1 Introduction

Mud volcanoes (MVs) are well-known geological phenomena formed onshore and offshore by the rapid eruption of ascending sediments and fluids from deep sedimentary layers (Milkov, 2000; Kopf, 2002; Menapace et al., 2017a). The morpho-structure of MVs generally consists of a conical edifice varying in size and shape, formed by a feeder channel(s) rooted in the source layer(s), which records the history of fluids and sediments extrusion (Planke et al., 2003; Stewart and Davies, 2006). The main emission products of MVs – a mixture of gases (mainly methane), overpressured pore water, and sediments (fine mud containing clasts) generally known as mud breccia – offer a window into deep underlying sediments and their formation processes at depth. Examples of such processes are: i) diagenetic clay mineral transformation (e.g., Kastner et al., 1991; Dählmann and De Lange, 2003), ii) authigenic minerals precipitation or dissolution (e.g., Luff and Wallmann, 2003; Gieskes et al., 2005), iii) high-temperature interactions of sediments and crust (e.g., You et al., 1995; Chan and Kastner, 2000), and iv) microbial or thermogenic degradation of organic matter (e.g., Martin et al., 1993). Since MVs are related to enhanced geological, geochemical and biological activities and contribute to the global fluid and element budgets (Judd and Hovland, 2007), they have been extensively investigated and described worldwide since the early 1900s (Mazzini and Etiope, 2017).

To date, the majority of MVs are distributed in compressional settings, providing escape pathways for overpressured fluids and sediments originating from greater depth (e.g., Kopf, 2002). The enhanced pore fluid pressure, which is the main driving force to initiate mud volcanism, can be generated from recent tectonic activity, rapid sedimentation, disequilibrium compaction, dehydration reactions, gas hydrate decomposition and hydrocarbon generation (Dimitrov, 2002). As typical MVs emission products, hydrocarbon gases (predominantly methane), which are generated from the burial maturation of organic-rich sediments, are thought to sustain the buoyant ascension of fluidized sediments and trigger mud extrusion (e.g., Hedberg, 1974). MVs act as the surface expression of hydrocarbon seepage and migration, providing sign of hydrocarbon potential in the deep-sited sediments and indicating the redistribution of light hydrocarbon gases and petroleum in the region (e.g., Van Rensbergen et al., 2005; Mazzini and Etiope, 2017). With the evolution of MVs, its activity can be divided into four stages (Menapace et al., 2017a): i) eruption, active extrusion of mud breccia and formation of the MV edifice; ii) depletion, fluid seepage through cracks, gryphons and adjacent high permeable surroundings; iii) quiescence and build-up, subsidence of the edifice and accumulation of pore pressure; iv) reactivation, new episode of active mud flow extrusion. The various degrees of MVs activity, particularly i) and ii), are oftentimes linked to vigorous hydrocarbon seepage. Therefore, identifying MVs structures which are currently in one of these two stages is a key step in order to estimate the most suitable targets for further hydrocarbon exploration.

Over the last two decades, the Gulf of Cadiz (GoC) has become a target area for the study of mud volcanism (e.g., Diaz-del-Rio et al., 2003; Somoza et al., 2003; León et al., 2006).

Numerous submarine MVs have been identified along both the Iberian and African margins (Medialdea et al., 2009). According to several authors (e.g., Medialdea et al., 2009; Hensen et al., 2015), the MVs in the GoC present a close relationship with the tectonic structures of the region. In order to better investigate this connection, the M149 cruise was conducted in 2018 with R/V Meteor, focusing on both the GoC and the adjacent Alboran Sea. The expedition aimed to collect records of past and current tectonic and fluid flow activity, targeting strike-slip faults and adjacent MVs (Hüpers et al., 2020). During the M149 cruise various seafloor features have been investigated, whereas this article is specifically focusing on six MVs of the GoC including the newly discovered R2, D2 and Funky Monkey, the known Yuma and Ginsburg, and the isolated Meknes. The selected MVs are located along different strike-slip fault segments and supposed to be hydraulically connected to deeper sedimentary levels either through adjacent fault zones or deep-seated feeder channels (e.g., Scholz et al., 2009; Toyos et al., 2016). Since active MVs generally represent high flux seepage and play a significant role in the global budget of hydrocarbons and deep fluid circulation, identifying these structures will elucidate the aforementioned relationships and provide information on tectonic activity of the faults. Therefore, this work characterizes the MVs' morphology by multibeam bathymetry, and determines the properties and compositions of extruded sediments and fluids through sedimentology, physical properties, mineralogy and geochemistry. In agreement with other studies, which identified the major strike-slip fault systems in the region as fluid pathways connected to nearby MVs (e.g., Hensen et al., 2015; Schmidt et al., 2018), this article further reveals the various geochemical signals and sheds new light on their role in deep-seated fluid and solid migration through the GoC accretionary prism.

## 2.2 Study area

The GoC is located west of the Strait of Gibraltar, offshore Southwestern Iberia and Northwestern Morocco (Figure 2-1a). The tectonic evolution of the area is intimately linked to the convergence of the Iberian and the African plates, which collided in a N-S direction from Mid-Oligocene to Late Miocene and subsequently turned to a NW-SE direction from Late Miocene to present (Dewey et al., 1989; Rosenbaum et al., 2002). Between the converging Iberian and African plates, the Alboran Domain moved westward accompanied by folding and thrusting of the frontal sedimentary layers during the Early-Middle Miocene, which contributed to the development of the Betic-Rif Arc and the formation of an accretionary wedge (Gutscher et al., 2002). The accretionary wedge has a roughly arcuate boundary on its lower part and is divided in a northern and a southern lobe on its mid- to upper-part, occupying a central location in the GoC (Figure 2-1a). During the Late Tortonian, a large wedge-shaped allochthonous mass (the Allochthonous Unit of the Gulf of Cadiz, AUGC) constituted by a complex of imbricated thrusts was then emplaced in the region from the Iberian and Morocco coasts to the Horseshoe and Seine Abyssal Plains (Torelli et al., 1997; Maldonado et al., 1999; Medialdea et al., 2004). The AUGC consists of a mixture of Triassic to Neogene sedimentary units (Maldonado et al., 1999) and represents the thickest unit of the accretionary wedge's sedimentary cover (Figure 2-2). It is heavily dotted by MVs and salt diapirs, which mobilize undercompacted Miocene

marls and shales, and Triassic salt, respectively (Maestro et al., 2003). Across the accretionary wedge, a set of WNW-ESE trending lineaments, which are right-lateral strike-slip faults (the SWIM faults), form an active deformation band marking a modern transform plate boundary through the GoC (Zitellini et al., 2009). The SWIM 2 and SWIM 3 intercept the northern and southern segment of the accretionary wedge front and are referred to as the Lineament North and the Lineament South in this study, respectively. The SWIM 1, in the middle, is the longest lineament consisting of several segments, two of which are located within the southern lobe of the accretionary wedge (e.g., Crutchley et al., 2011) and will be hereafter referred to as the Lineament Center North and the Lineament Center South (Figure 2-1b).

Since the first MVs (Yuma and Ginsburg) were discovered in 1999 during the TTR-9 cruise (Ivanov et al., 2000; Gardner, 2001), numerous seagoing expeditions have been conducted in the GoC and over 90 MVs have been confirmed from cone-like morphologies, seismic profiles, coring of mud breccias and fluids geochemical analyses. These MVs are generally parallel to major strike-slip faults or situated at fault intersections, suggesting that their formation and fluid migration are closely tied to the activity of the adjacent fault system (Medialdea et al., 2009). While few MVs are located in the Deep Portuguese field along the lower slope, most of the MVs have been identified on the upper part of the accretionary wedge, in the Moroccan field (offshore the Moroccan margin), and in the Tasyo and Guadalquivir Diapiric Ridge fields (offshore the Spanish-Portuguese margin) (Figure 2-1a; Medialdea et al., 2009). These MVs' edifices display variable morphologies from small and smooth to large and complex, with symmetrical flanks in most sites and asymmetrical flanks mainly observed in the western Moroccan field (León et al., 2012). Their mud/fluid source layers are generally suggested to be the AUGC and/or deeper stratigraphic units of Mesozoic age, supported by tectonic, micropaleontological, and geochemical evidences (e.g., Pinheiro et al., 2003; Hensen et al., 2007; Toyos et al., 2016). The seismic images from the GoC generally indicate the AUGC as the potential sedimentary sources, while a deeper source below the AUGC is also proposed at least for the deep water MVs (Medialdea et al., 2009). Micropaleontological investigations of matrixes and clasts suggest predominant Eocene to Miocene ages with the oldest estimations dating back to Upper Cretaceous ages (Ovsiyannikov et al., 2003; Pinheiro et al., 2003). The fluids emanating from the active MVs are considered to be mainly formed by clay mineral dehydration occurring at up to 5 km depth below seafloor (Hensen et al., 2007). Crustal components are also reported in the fluids of Captain Arutyunov, Bonjardim and Porto MVs (Hensen et al., 2007; Scholz et al., 2009), where the crustally derived fluids in the latter structure are considered to be mediated by deep-reaching strike-slip faults (Hensen et al., 2015; Schmidt et al., 2018). The hydrocarbon gases (mainly methane) and varying proportions of petroleum in the mud breccia have predominantly a deep thermal origin, which was revealed by molecular and isotopic analyses (e.g., Stadnitskaia et al., 2006; Nuzzo et al., 2009). Jurassic and Cretaceous formations overlying the basement are considered as the main hydrocarbon source rocks (Van Rensbergen et al., 2005; Nuzzo et al., 2019). Hydrocarbon exploration in the GoC is mainly constrained to the Spanish shelf due to the intense tectonic deformation and nappes emplacement. Nonetheless, Van Rensbergen et al. (2005) suggested that the fault-

controlled MVs distribution could be consistent with seeping of hydrocarbon fluids through the allochthonous complex and indicates the migration pathways as well as the potential hydrocarbon accumulations in the region, especially in the eastern Moroccan field.

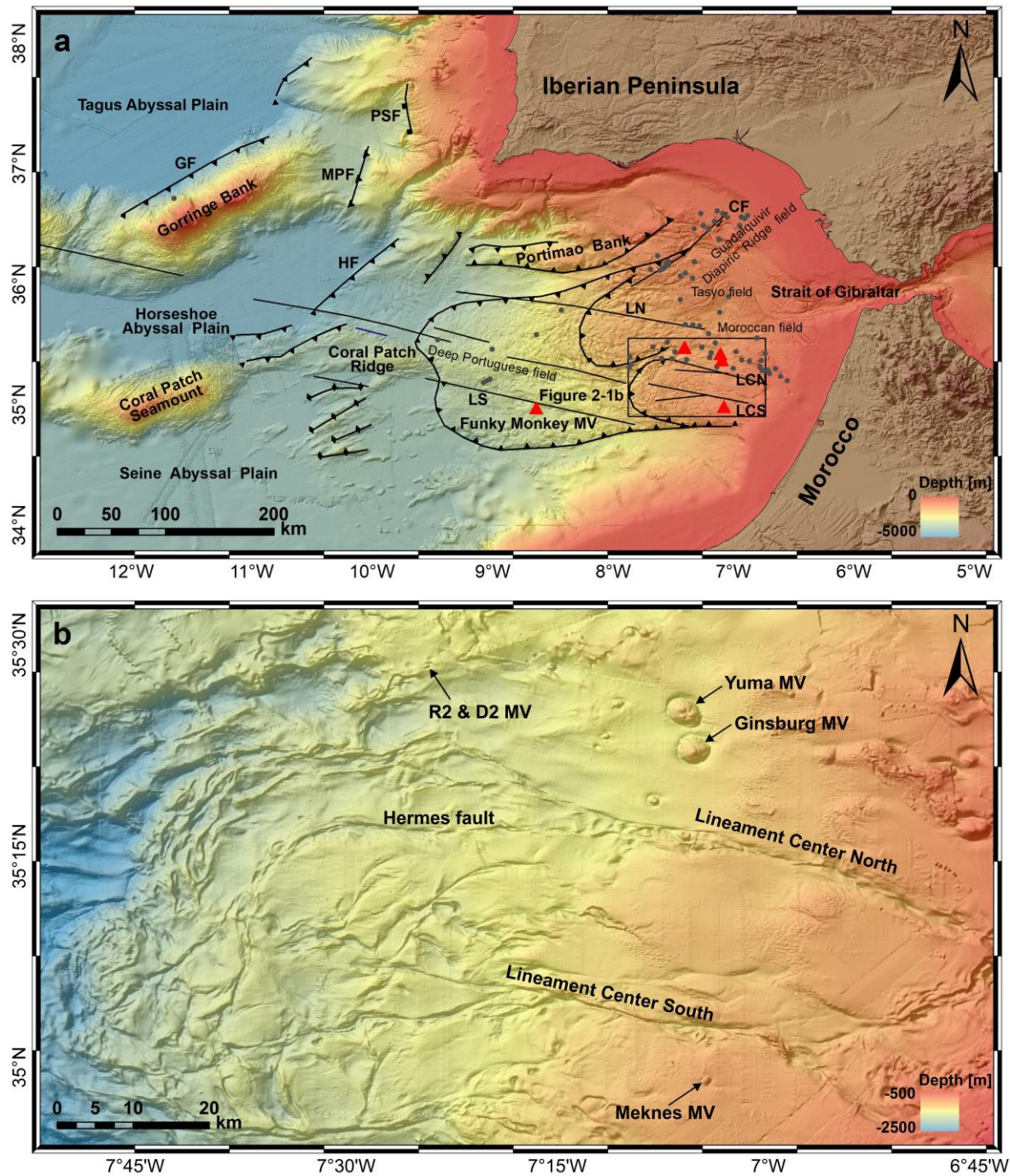


**Figure 2-1.** a) Bathymetry map of the GoC with main tectonic and morphological features depicted [modified from Cunha et al. (2012); bathymetry from the SWIM compilation of Zitellini et al. (2009)]. The locations of the six MVs investigated in this study (red triangles, Table 2-1), other MVs known to date (dark gray dots), as well as MV fields and major fault zones are shown. *CF* Cadiz Fault, *GF* Goringe Fault, *HF* Horseshoe Fault, *LN* Lineament North, *LCN* Lineament Center North, *LCS* Lineament Center South, *LS* Lineament South, *MPF*

Marques de Pombal Fault, *PSF* Pereira de Sousa Fault. b) Multibeam bathymetry map of the main study area produced during the M149 cruise.

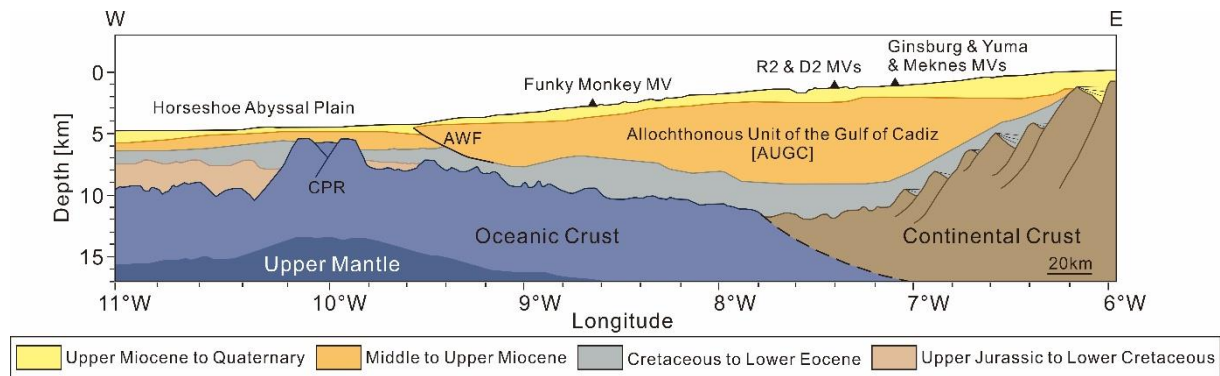


**Figure 2-2.** Schematic W-E cross section of the GoC region (roughly following the Lineament Center South) showing the main representative tectonic units [modified from Hensen et al. (2015)]. *AWF* Accretionary Wedge Front, *CPR* Coral Patch Ridge. Vertical exaggeration: ~5x.

**Table 2-1.** Locations, morphological characteristics and gravity cores for the MVs presented in this study.

Mud Volcano	Gravity Core	Latitude [°N]	Longitude [°W]	Water depth [m]	Height [m]	Diameter [m]
R2	GeoB23053-1	35°28.49'	7°24.25'	1163	75	900
D2	GeoB23054-1	35°28.82'	7°24.09'	1194	40	700
Yuma	GeoB23028-1	35°25.46'	7°06.07'	959	218	4400
Ginsburg	GeoB23024-3	35°22.36'	7°05.32'	908	280	3860
Meknes	GeoB23043-2	34°59.07'	7°04.43'	694	80	1400
Funky Monkey	GeoB23081-1	34°58.44'	8°37.95'	3143	42	1200

## 2.3 Methods

In this study, we employed multiple approaches to characterize six MVs. In order to determine the activity state of the MVs, their morphologies were examined by multibeam bathymetry, and gravity cores were recovered from each MV for lithology determination and physical property analysis. In addition, the mineral composition of the solids and the ion compositions of the pore water were analyzed to unravel diagenetic processes and to trace mud/fluid sources.

### 2.3.1 Hydroacoustics

During cruise M149, bathymetric data were acquired using a hull-mounted multibeam system, the Kongsberg Simrad EM122. A frequency of 12 kHz and 432 beams per ping were employed during operation and the maximum opening angle was up to 65° (130° in total), which was reduced to 60° in waters deeper than 2000 m. The dimension of a single beam footprint is 1° by 2° and the width of the swath can be up to six times the water depth on a flat bottom (Hüpers et al., 2020). An equidistant beam spacing was used to ensure a high beam density at the swath edge, and the acoustic velocity profiles were updated at least weekly or when the physical

properties of the water body changed. We processed the multibeam data with the program MB-System and visualized them by ArcGIS software. The pixel resolution of the bathymetric maps is 50×50 m for the main study area and 20×20 m for the individual MVs.

### **2.3.2 Sampling**

In order to sample the sub-seafloor sediments, a gravity corer consisting of a 1.5-ton-weight head and a 6 m-long steel barrel equipped with a plastic liner was employed. Upon recovery, the sediment-filled liners were segmented into sections of 1 m length and labelled according to the GeoB scheme (MARUM-own system of cataloguing sediment cores). Firstly, pore water specimens were collected from the cores for geochemical analyses. In contrast to sediment sampling, pore water samples were taken from whole-round sections as soon as possible once the cores were on deck, due to their time-sensitive nature. In a 4 °C laboratory, Rhizon samplers attached to syringes were used to extract pore water from gravity cores by creating a vacuum (Dickens et al., 2007). Three samples were taken per 100 cm, with a volume of up to 10 ml, and stored in 20 ml air tight PTFE vials at 4 °C for subsequent analyses. Secondly, the cores were cut lengthwise into a working half and an archive half. The working halves provided sediment samples for X-ray diffraction (XRD) analyses, while the archive halves were mainly used for core description, core imaging, and Multi-Sensor Core Logger (MSCL) measurements. All core sections were imaged immediately after being split by using the SmartCIS 1600LS line scanning system of the MARUM GeoB Core Repository. It was useful to freshly scrape the cores immediately prior to imaging in order to capture the ephemeral nature of some sedimentary features and colors. All images were acquired at a 500 dpi resolution.

### **2.3.3 Physical properties**

The physical properties of the sediments are indicators of sediment composition and environmental conditions, thus providing important constraints for the characterization of the sediments (Strasser et al., 2014). In this study, magnetic susceptibility and wet-bulk density were acquired using MSCL scans, to distinguish layers with different mineral content and compaction states (e.g., Feseker et al., 2010). MSCL measurements were carried out on the archive half of gravity cores at the MARUM-IODP Laboratory. Before the measurement, the archive halves were taken out of the core repository and held at room temperature for several hours to equilibrate with ambient temperature and the sediment surface was covered with foil to prevent loss of pore water. Then, high-resolution magnetic susceptibility (dimensionless) and wet-bulk density ( $\text{g}/\text{cm}^3$ ) records were obtained non-destructively with a sampling interval of 2 cm.

### **2.3.4 Mineralogy**

The mineralogical composition of matrix and clast from the mud breccia was analyzed by XRD in the Crystallography Laboratory at the University of Bremen. For the mud breccia matrix, specimens of 2-3  $\text{cm}^3$  were sampled from working halves, whereas clast samples with size of 1-3 cm were picked and carefully washed to remove contamination on their surface. All the

samples were dried in a convection oven for 24 h at 105 °C and then grinded into fine powder in an agate mortar.

In this study, 11 matrix and 8 clast samples were analyzed by a Philips X'Pert Pro© multipurpose diffractometer. Mineral identification and quantitative analyses were carried out using the QUAX© software package following Vogt et al. (2002). The standard deviation of the quantification is ±1% for carbonates, ±2% for quartz, and ±5-10% for feldspars and clay minerals.

### 2.3.5 Geochemistry

To determine the ion compositions in pore waters, 188 pore water samples from the six MVs were analyzed in the Sediment Geochemistry Group at the University of Bremen. To determine the concentrations of dissolved cations (i.e. Na, K, Ca, Mg, B, Li and Sr), we firstly used concentrated HNO<sub>3</sub> to dissolve any precipitates formed after sampling and then diluted the samples 10-/20-fold with 1% diluted HNO<sub>3</sub> to acquire the desired concentrations for measurements. After that, the diluted samples were introduced into an Inductively Coupled Plasma Optical Emission Spectrometer (ICP-OES). For the concentrations of anions (i.e. Cl<sup>-</sup>, Br<sup>-</sup> and SO<sub>4</sub><sup>2-</sup>), we firstly centrifuged the samples to remove any precipitates. Similar with samples for ICP-OES measurements, the pore water samples were diluted 50-/100-fold with Milli-Q water. Finally, 2 ml of the diluted samples was filled into a glass vial and measured through an Ion Chromatograph (IC).

In addition, based on the Mg and Li concentrations determined with the above methodology, the Mg-Li geothermometer was selected and applied to our geochemical data, in order to calculate the source temperatures of the fluids. The equation for the Mg-Li geothermometer is given by Kharaka and Mariner (1989):

$$t = \frac{2200}{\log\left(\frac{\sqrt{Mg}}{Li}\right) + 5.47} - 273 \quad e. q. (2.1)$$

where  $t$  (°C) is temperature and  $Mg$  and  $Li$  concentrations are in mg/l.

## 2.4 Results

### 2.4.1 Morphology

North of the Lineament Center North, the newly discovered R2 and D2 MVs are in close vicinity to each other, situated at a water depth of 1163 m and 1194 m respectively. The R2 MV in the southwest is a single cone elongated in the NE-SW direction, about 75 m high and 900 m wide, while the E-W elongated D2 MV in the northeast is composed of two partially merged cones, about 40 m high and 700 m in maximum diameter (Figure 2-3). The flanks of two MVs are generally homogeneous and continuous (Figure 2-3h, 2-3i), with slopes of 5-15° on the east and west sides and steeper slopes of 10-25° on the north and south sides. A moat of

about 10-25 m deep can be recognized on the north and south sides and its deepest point is located between R2 and D2 MVs (Figure 2-3i).

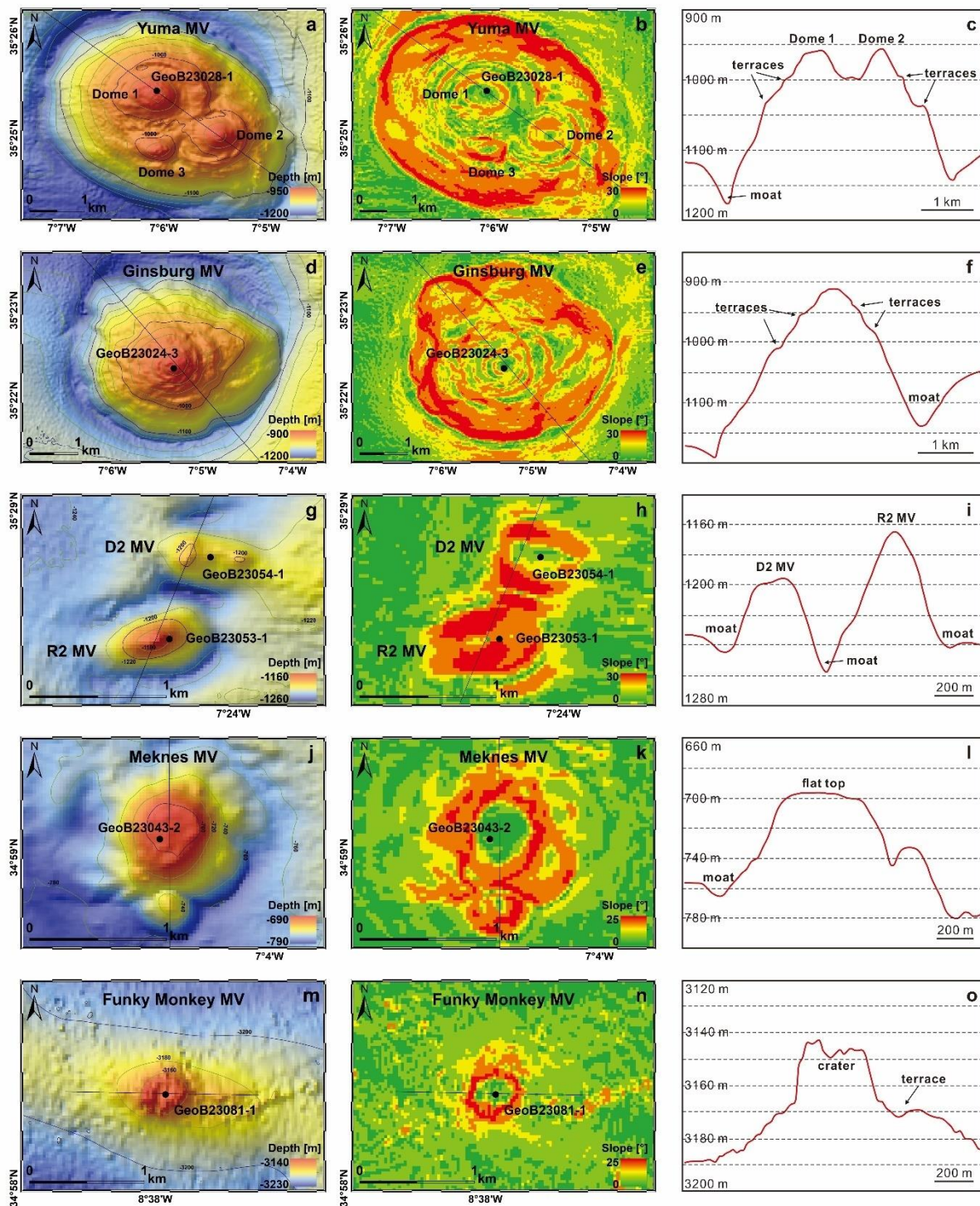


**Figure 2-3.** Bathymetry (a, d, g, j, m) and slope gradient maps (b, e, h, k, n), as well as cross sections (c, f, i, l, o) of the MVs analyzed in this study. a-c Yuma MV, d-f Ginsburg MV, g-i R2 and D2 MVs, j-l Meknes MV, m-o Funky Monkey MV. In the maps, locations of analyzed gravity cores are also noted.

About 30 km east of the R2-D2 group, the NW-SE aligned Yuma and Ginsburg MVs are two of the largest MVs in the area located at 959 m and 908 m water depth. While the Yuma MV, 218 m high and 4400 m in diameter, has three subcircular domes on top of the main edifice, the Ginsburg MV, 280 m high and 3860 m wide, has a single dome on its summit covered by scattered coral patches and rubble (Wienberg et al., 2009) (Figure 2-3). The flanks of two MVs show a predominantly terraced morphology with variably steep slopes, where two terraced sectors can be distinguished along the west and east flanks of the Yuma MV (Figure 2-3b, 2-3c) and the terraced flanks are pronounced in the northwest and northeast sides of the Ginsburg MV (Figure 2-3e, 2-3f). The slopes of two MVs mainly vary in the range of 8-15° and reach maximum values of 17-25° at the base. A ring-shaped irregular moat can be recognized in both MVs, with a maximum depth of 60 m on the northwest side of the Yuma MV (Figure 2-3b, 2-3c) and 80 m on the southeast side of the Ginsburg MV (Figure 2-3e, 2-3f).

In close proximity to the Lineament Center South, the Meknes MV is an isolated MV in the southernmost end of the Moroccan field, surrounded by small coral mounds (Akhmetzhanov et al., 2007). It has a N-S elongated, sub-elliptical morphology, approximately 1400 m in maximum diameter and 80 m in height, which contains a main cone with a flat top at 694 m water depth and a smaller dome on the southern side (Figure 2-3). The flanks of the MV are continuous with an average slope of 13°, which becomes gentler (2-8°) on the basal part (Figure 2-3k, 2-3l). A minor moat was observed surrounding the cone (Figure 2-3l).

Away from the predominant MV distribution, the Funky Monkey MV is located in the SW edge of the accretionary prism with a water depth of 3143 m, on the Lineament South. It is elongated in E-W direction with a maximum diameter of 1200 m and a height of 42 m, and has a flat top which contains a slight, central depression (Figure 2-3). The slopes vary from 10-20° for the upper part to 2-8° for the basal part (Figure 2-3n), and the MV shows a terraced morphology on its east side (Figure 2-3o), which is possibly related to different outflow episodes. As the slope inclinations at the base gently decrease before reaching the seafloor, no obvious moat is recognized around the cone.

#### **2.4.2 Sediment characteristics**

From the summits of R2 and D2 MVs, a 200 cm-long gravity core (GeoB23053-1) and a 35 cm-long gravity core (GeoB23054-1) were recovered at a water depth of 1163 m and 1194 m respectively, presenting similarities in lithology and physical properties (Figure 2-4c, 2-4d). The upper 27 cm and 20 cm of the core sections from R2 and D2 MVs present an oxidized layer of foraminifera ooze, bioturbated, with coral/shell fragments, and the sediment color gradually changes from yellowish brown at the top to gray at its lower boundary. The gray foraminifera ooze at 27-143 cmbsf and 20-35 cmbsf of R2 and D2 MVs are bioturbated and anoxic, containing mud clasts and bioclasts. While the bulk density of the foraminifera ooze layer stays constant at 1.95 g/cm<sup>3</sup>, the magnetic susceptibility decreases generally with depth from about 15\*10<sup>-5</sup> SI to 5\*10<sup>-5</sup> SI corresponding to the condition changes from oxic to anoxic. Due to the limitation of the recovered core length of D2 MV, the sediments below the

foraminifera ooze layer can only be seen in R2 MV. At 143-160 cmbsf the core is composed by greenish gray nannofossil ooze with cm-sized shell fragments, showing physical properties similar to the overlying anoxic foraminifera ooze. The cored sediments at 160-200 cmbsf are greenish gray to very dark greenish gray, mud-matrix dominated mud breccia, containing semi consolidated mud clasts. Between 168-187 cmbsf numerous carbonate concretions are also present. Furthermore, a 2 cm-thick very dark greenish gray mud breccia, which has a high content of fine disseminated pyrite crystals and a strong H<sub>2</sub>S smell, was observed at 173-175 cmbsf with sharp and straight top and bottom contact. Within the carbonates-rich mud breccia layer at R2 MV, the bulk density and magnetic susceptibility reflect different signatures from the upper section, showing lower values of 1.65-1.90 g/cm<sup>3</sup> and 0-7\*10<sup>-5</sup> SI.

In contrast to the thick foraminifera/nannofossil ooze overlying the mud breccia facies at R2 and D2 MVs, the 289 cm-long gravity core (GeoB23028-1) recovered from Dome 1 of Yuma MV and the 255 cm-long gravity core (GeoB23024-3) recovered from the single dome of Ginsburg MV are mainly consisting of mud breccias, with only 5 cm and 3 cm-thick olive brown hemipelagic cover at the top respectively (Figure 2-4a, 2-4b). The anoxic, dark greenish gray mud breccia of both Yuma and Ginsburg MVs has strong H<sub>2</sub>S smell and shows mousse texture with degassing voids and open cracks. Correspondingly, the physical properties of cored sediments from Yuma and Ginsburg MVs are mainly reflect the characteristic of mud breccia and considerably influenced by degassing processes. The bulk density is generally constant at about 1.9 g/cm<sup>3</sup> on the upper part, while the sediment degassing scatters the values in the 1.0-2.0 g/cm<sup>3</sup> range on the lower part. The magnetic susceptibility shows values mainly ranging between 10 and 13\*10<sup>-5</sup> SI, which reflect a uniform composition of the mud breccia.

Along the Lineament Center South, the gravity core (GeoB23043-2) sampled from the summit of Meknes MV show similar sedimentary features and physical properties to that from Yuma and Ginsburg MVs (Figure 2-4e). At the Meknes MV, the 144 cm-long gravity core recovered at a water depth of 694 m is constituted of a dark greenish gray mud breccia with few oxic sediments sitting at the top. The mud breccia has a strong H<sub>2</sub>S smell throughout the core and shows mousse-like texture below 34 cmbsf. The degassing processes result in large cracks and voids, especially at 44-49 cmbsf, 70-83 cmbsf, 126-129 cmbsf, 134-136 cmbsf and at the bottom of the core. The bulk density shows little variation with an average value of 1.85 g/cm<sup>3</sup>, despite scattered values at the bottom resulting from large cracks and voids. Consistently with the uniform lithology of the mud breccia, the magnetic susceptibility is characterized by low values mainly lying in the range of 9-14\*10<sup>-5</sup> SI.

However, in the deepest part of the accretionary prism, the gravity core (GeoB23081-1) taken from the summit of Funky Monkey MV at 3143 m water depth presents distinct characteristics from other cored sediments which contain thick ooze layers or gassy mud breccias (Figure 2-4f). The 220 cm-long gravity core from the Funky Monkey MV can be divided into four intervals where the physical properties are well consistent with the lithological changes. At 0-15 cmbsf, the core comprises an oxidized layer of brown to grayish brown hemipelagic

sediments, with the bulk density of 1.7-1.8 g/cm<sup>3</sup> and the magnetic susceptibility around 20\*10<sup>-5</sup> SI. At 15-73 cmbsf, the core yielded dark greenish gray fine mud breccia which may reflect the reduced seepage activity and a diffuse fluid flow, presenting bulk density of 1.8 g/cm<sup>3</sup> and magnetic susceptibility of 11\*10<sup>-5</sup> SI. From 73 to 220 cmbsf, two layers of mud breccia flow deposits can be distinguished implying two extrusion episodes. The dark greenish gray mud breccia at 73-149 cmbsf has a strong smell of H<sub>2</sub>S, which presents slightly higher bulk density values around 1.9 g/cm<sup>3</sup> and lower magnetic susceptibility values of 3-12\*10<sup>-5</sup> SI. The black mud breccia from 149 cmbsf to bottom instead has a strong smell of oil and contains sulphur-rich minerals and mm-sized pyrite crystals, showing similar bulk density values to the overlying mud breccia layer and higher magnetic susceptibility values of 10-36\*10<sup>-5</sup> SI.

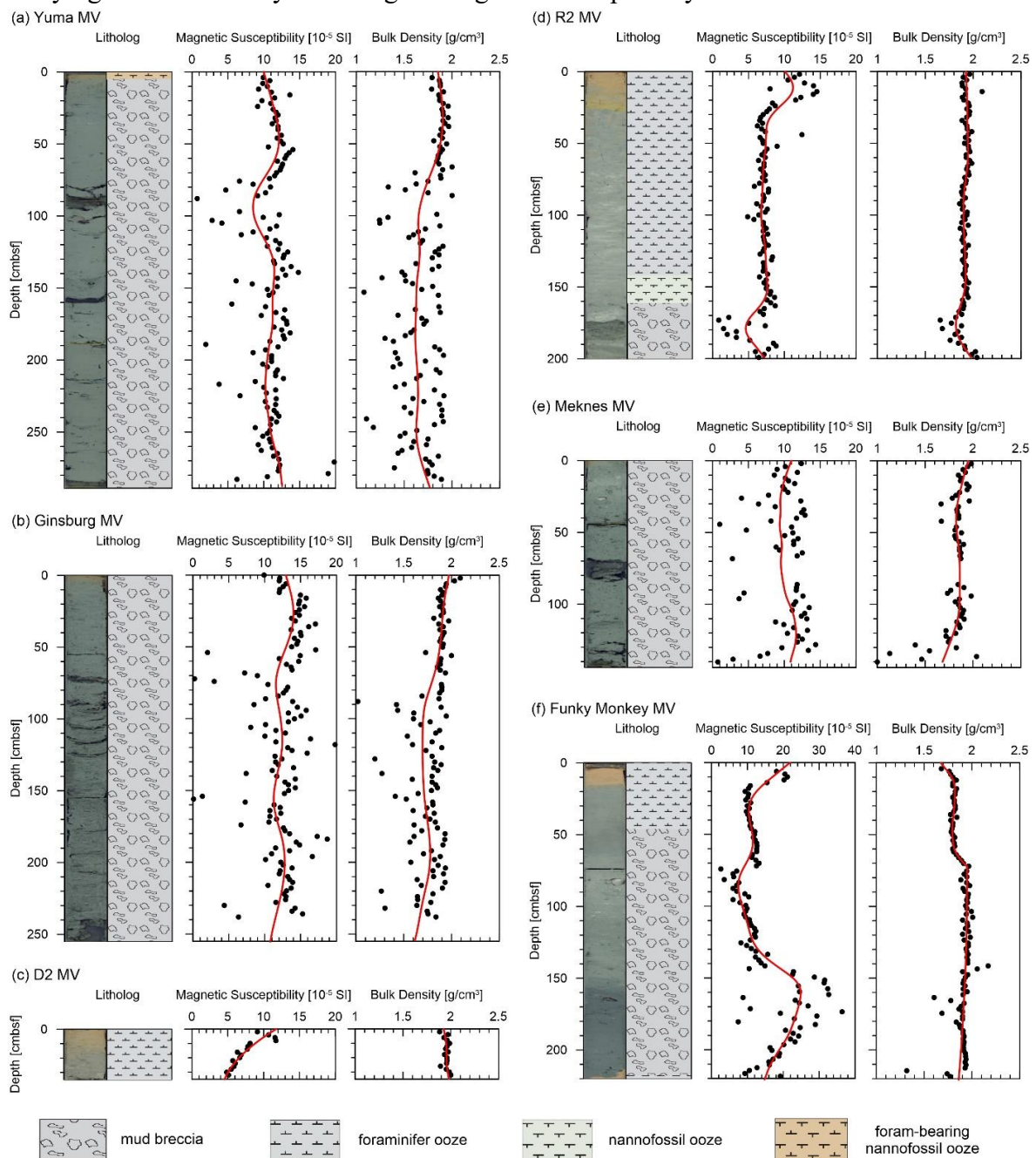


**Figure 2-4.** Core images and logs with vertical distribution of porosity, undrained shear strength, magnetic susceptibility, P-wave velocity and bulk density for the gravity cores

recovered on the MVs summits. **a** Yuma MV, **b** Ginsburg MV, **c** R2 MV, **d** D2 MV, **e** Meknes MV, **f** Funky Monkey MV.

### 2.4.3 Mineralogy

To define the origin of the solid emission components of the MVs, matrix and clast samples have been collected from each MVs for mineralogical analyses, with the exception of the D2 MV due to the limited core length.

Although the sampled MVs differ in sedimentary features and physical properties, the majority of matrix samples are quite similar in composition. Clay minerals, which are generally dominated by illite, are the major components (46-53 wt%) followed by quartz and feldspars (20-35 wt%) and carbonates (8-17 wt%) (*SI Appendix*, Table S2-1). Only three matrix samples demonstrate differences in composition, showing higher proportion of carbonates. Among them, one is from the shallow depth of the Ginsburg MV and the other two are from the R2 MV located where the carbonate concretions are abundant.

On the other hand, the clast samples, which usually originate from the same depth or a shallower one than the muddy matrix, show a wide variation in composition. In R2 MV, the clast sampled from the anoxic foraminifera ooze shows that carbonates represent the most dominant phases (93 wt%; *SI Appendix*, Table S2-1). In Yuma MV, different lithologies are observed in the clasts: clasts < 1 cm are commonly soft mudstones and marlstones while those > 1cm up to 4 cm are lithified siltstones and sandstones. Two mud breccia clasts sampled at 29-31 cmbsf and 150-152 cmbsf are lithified siltstone with carbonate cements and consolidated marlstone. In Ginsburg MV, the clasts are mainly composed of mudstone in mm-cm size. One lithified mudstone sampled at 197-199 cmbsf contains chlorite-rich clays and almost no carbonates (*SI Appendix*, Table S2-1). In Meknes MV, the clasts are mainly poorly consolidated to consolidated with a mean size less than 2 cm. Two of the sampled clasts are consolidated limestones with relatively abundant carbonate content from 52 wt% to 83 wt%. The dominant carbonate phases are represented by calcite at 27-29 cmbsf and ankerite at 64-66 cmbsf, respectively (*SI Appendix*, Table S2-1). In Funky Monkey MV, the two clasts sampled are lithified limestones which are mainly composed of carbonates (59-76 wt%) and relatively small amounts of clay minerals (8-21 wt%) and quartz (5-16 wt%) (*SI Appendix*, Table S2-1).

### 2.4.4 Geochemistry

To determine the source and migration of the fluids which liquefy clay-bearing strata to facilitate the extrusion process, pore fluids from the gravity cores have been analyzed for their chemical compositions.

The characteristics of pore water geochemistry in R2 and D2 MVs are distinct from that of other MVs, where all measured elements are constant and have similar values to that of seawater (Figure 2-5), mirroring bottom water chemical composition. At the other four sites,

however, the fluids show enrichment or depletion of element concentration to some degree, and the pore water data cluster into two groups. Along the Lineament Center North, the fluids from Yuma and Ginsburg MVs are depleted in  $\text{Br}^-$ , K, Ca and Mg and enriched in Li and B, and present little fluctuations in Sr with respect to seawater (Figure 2-5). The behavior of Na and  $\text{Cl}^-$  is not uniform whereas a slight enrichment of Na and depletion of  $\text{Cl}^-$  are observed. Pore water  $\text{SO}_4^{2-}$  at both sites is depleted within shallow depth and shows an enrichment in the lower part of the cores. Along the Lineament Center South and Lineament South, the fluids from Meknes and Funky Monkey MVs show seawater values at shallow depth and shifts to near-constant values in the lower core section, where the mixing effect of bottom water and ascending fluids is more prominent at the Funky Monkey MV. The concentrations of Na,  $\text{Cl}^-$ ,  $\text{Br}^-$ , K, Ca, Mg and  $\text{SO}_4^{2-}$  show a decreasing trend, among which the completely consumption of pore water  $\text{SO}_4^{2-}$  reached at 64 cmbsf at Meknes MV and almost reached at the deepest sample of Funky Monkey MV (Figure 2-5). In contrast, clear enrichments are observed in B, Li, and especially Sr which is as high as  $\sim 0.67$  mM in the Funky Monkey MV fluids.

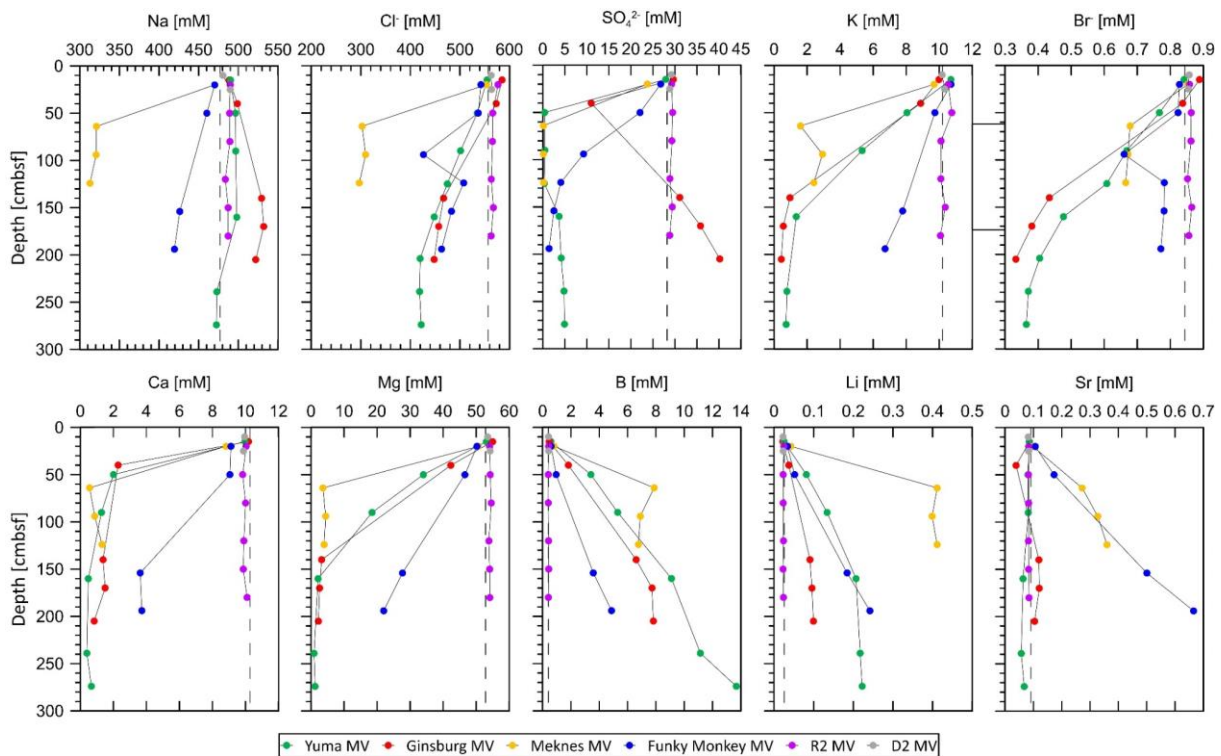


**Figure 2-5.** Pore water profiles of Na,  $\text{Cl}^-$ ,  $\text{SO}_4^{2-}$ , K,  $\text{Br}^-$ , Ca, Mg, B, Li and Sr in sediment cores from all study sites. Dashed lines indicate seawater values.

## 2.5 Discussion

### 2.5.1 Morphology related to mud extrusion and degree of activity

Our results show different morphological characteristics for the six MVs, which reflect the dynamics of mud extrusions and corresponding geological processes.

The shape of MVs is associated with various factors, and viscosity has been suggested as one of the key properties affecting eruptions. Low viscosities, which are typical of fluid-dominated MVs and generally lack of clasts, tend to produce flat edifices; whereas high viscosities, resulting from clast-rich, gas-poor mud ejections, contribute to vertical growth and result in classical conical shapes (Mazzini and Etiope, 2017). As a progressive decrease in sediment pore pressure during periods of tectonic reactivation, the mud flow generally evolved from less to more viscous with time. Near the Lineament Center North, the MVs Yuma, Ginsburg, R2 and D2 are characterized by a classical conical shape (Figure 2-3c, 2-3f, 2-3i), which seems to imply the extrusion of viscous mud breccia in the late stages of mud volcanism. Also, the three summit domes in Yuma MV and the two partially merged cones in D2 MV reflect multiple emission spots during the extrusive phase. On the other hand, the MVs along the Lineament Center South (Meknes) and the Lineament South (Funky Monkey) are flat-topped edifices (Figure 2-3l, 2-3o), which might be derived from vigorous, fluid-rich eruptions in the initial stages of mud volcanism (Ivanov et al., 1996; Lykousis et al., 2004). At Meknes MV, the blocky morphology corresponds to a distinct mousse-like texture of the mud breccia, index of gas-saturated sediments, and the small dome on its southernmost rim seems to be a separated emission site. Given the absence of a proper moat around the edifice, Funky Monkey MV is most likely a relatively young feature. Its flat morphology may be related to gas and water-dominated eruptions that normally lead to relatively poor vertical growth and lateral extension. In addition, the MV's terraced eastern flank implies multiple outflow episodes (Figure 2-3o), which might correspond to the different characteristics of the mud breccia layers, e.g., the hydrocarbon gas-saturated dark greenish gray mud breccia with lower magnetic susceptibility values and the petroleum-bearing black mud breccia with higher magnetic susceptibility values (Figure 2-4f).

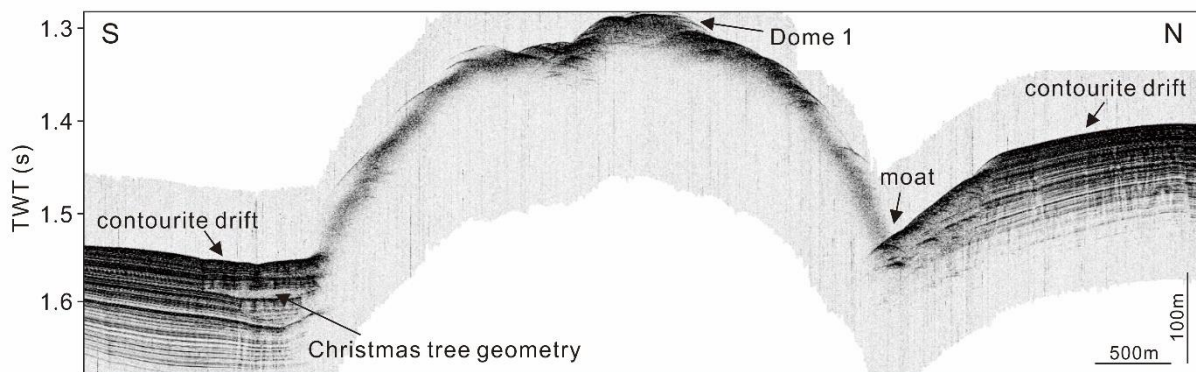


**Figure 2-6.** S-N trending parametric subbottom profile of the Yuma MV.

As a common feature present at the base of MVs in the GoC (e.g., Kenyon et al., 2000; Somoza et al., 2003; León et al., 2012), moats are related to a volume loss and/or relaxation of the compressional stress field as the consequence of the expulsion of sediments and fluids from the mud reservoir below the edifice (Camerlenghi et al., 1995; Van Rensbergen et al., 2005). While no/minor moat is observed in Funky Monkey and Meknes MVs, moats are pronounced in Yuma, Ginsburg, R2 and D2 MVs with semi-circular shapes, which is in consistent with the features being in an advanced stage of mud volcanism. Besides, the moats of the Yuma and

Ginsburg MVs seem to be reshaped by bottom currents (Figure 2-6), caused mainly by the Mediterranean Outflow Water, which is associated with contourite drift deposits and cold-water coral mounds surrounding the MVs (Foubert et al., 2008; Palomino et al., 2016; Vandorpe et al., 2016).

While MVs episodically experience violent eruptions of mud breccia and methane-dominated gas, quiescent periods are characterized by fluid seepage with variable intensity and account for a big part of MVs life cycles (over 97% as reported by Menapace et al. (2019)). Since the hemipelagic sedimentation is considered to be deposited during the quiescent phase of a MV evolution, its thickness provides information on MVs inactivity (Van Rensbergen et al., 2005) and can be defined by the physical properties of sediments which are uniformly consistent with lithological changes (Figure 2-4). At Yuma, Ginsburg and Meknes MVs, the presence of a 0-5 cm thick hemipelagic draping implies that they experience recent activity and currently lie in the phase with reduced sediment emission. At Funky Monkey MV, there are 15 cm of hemipelagic sediments overlying the mud breccia, which can also be clearly recognized through the distinct variations of physical properties. For example, the magnetic susceptibility is around  $20 \cdot 10^{-5}$  SI for the hemipelagic sediments, while three deeper intervals with different values each correspond to a diffuse fluid flow period and two extrusion episodes. Within the lowest mud breccia layer, a significant down-core decrease of magnetic susceptibility, accompanied by pyrite precipitation and sulfate depletion in pore water, record the activity of methane seepage and AOM (anaerobic oxidation of methane, further discussed in section 5.3). Moreover, at R2 MV, a decreasing trend in the magnetic susceptibility values from  $7-15 \cdot 10^{-5}$  SI to  $0-9 \cdot 10^{-5}$  SI corresponding to the lithological changes from foraminifera and nannofossil oozes to mud breccia is visible at 160 cmbsf, suggesting a longer period of inactivity.

Therefore, north of the Lineament Center North, the newly discovered R2 and D2 MVs have experienced a long period of inactivity since the last eruption, while the Yuma and Ginsburg MVs are long-lived features with activity for a long time all the way to present. Further south, the Meknes and Funky Monkey MVs are, relatively speaking, younger structures and provide evidence for recent activity.

### **2.5.2 Mud breccia composition**

According to the XRD results, the matrix of most mud breccia samples has little variation in mineralogy (Figure 2-7), suggesting consistent source materials. Potential sedimentary sources are generally considered to be the AUGC unit, mainly comprising Tertiary and Mesozoic shales and marls, and/or deeper units of Mesozoic age (e.g., Pinheiro et al., 2005; Medialdea et al., 2009). Moreover, the clay minerals in the matrix are dominated by illite (39 wt%-70 wt%), while the content of smectite is relatively low (10 wt%-37 wt%). This supports the hypothesis that clay mineral dehydration (most likely the conversion of smectite to illite) is the main fluid source and facilitates the formation of MVs in the GoC (e.g., Hensen et al., 2007). Furthermore, as the mousse textures with degassing voids and open cracks are extensive in the sediments from Yuma, Ginsburg, Meknes MVs and an oily smell is strong at the deeper Funky Monkey

MV, these active sites imply that the hydrocarbon fluids generated at depth participate in the MVs' extrusion. In previous literature work, Martos-Villa et al. (2020) showed that the 10B-rich illite at MVs in the GoC is related to the hydrocarbon fluids, since isotopically light B released from the kerogen is incorporated into the tetrahedral layer of diagenetic illite during the illitization process. We will explore the idea of further B isotope and illite crystallinity measurements on the illite-rich matrix samples in the future to evaluate the interactions of hydrocarbon fluids with clays and the organic matter maturation in the region.

On the other hand, three matrix samples, one from Ginsburg MV (GeoB23024-3; 40-42 cmbsf) and two from R2 MV (GeoB23053-1; 173-175 cmbsf, 181-183 cmbsf), are not following this trend and show an increasing carbonate content (Figure 2-7). This higher carbonate content seems to be related to the precipitation of authigenic carbonates, as a consequence of the high total alkalinity in correspondence to the AOM process or gas hydrate dissociation at these sites (e.g., Aloisi et al., 2000; Kenyon et al., 2000; Mazurenko et al., 2003).

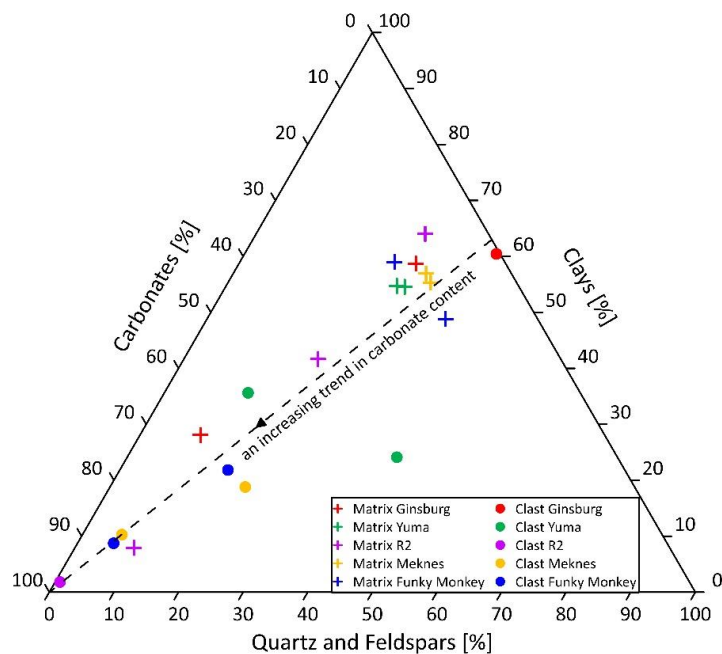


**Figure 2-7.** Normalized ternary plot of Quartz and Feldspars, Carbonates, and Clays for matrix (crosses) and clast (points) samples.

In addition, the clasts collected along the conduit by the ascending mud were also tested by XRD and can provide information on the composition and genesis of the deep-seated strata (Judd and Hovland, 2007). Contrarily to the matrix samples, the clasts from the mud breccia demonstrate distinct compositions and are representative of different lithologies, ranging from mudstones to limestones. Their mineralogical compositions are following an increasing trend in carbonate content and can be regarded as different mixtures of clay-rich grains and carbonates, where the clasts from Ginsburg and R2 MVs can roughly represent the clay-rich and carbonates endmembers, respectively (Figure 2-7). At Yuma and Ginsburg MVs, the clasts which are identified as mudstone, siltstone and marlstone are more clay-rich and contain a relatively high quantity of terrigenous minerals, likely formed by submarine gravity flows

(Ovsyannikov et al., 2003). In contrast, the clasts from Meknes, Funky Monkey and R2 MVs are mainly limestones which are probably derived from biogenic and/or hemipelagic sedimentation. Moreover, for R2 MV, carbonates are predominant in both matrix and clasts, and carbonate concretions are abundant throughout the core, which might also be explained by a shallow source in the accretionary wedge.

### 2.5.3 Diagenetic processes

For R2 and D2 MVs, the pore fluids are significantly affected by seawater showing constant chemical composition with depth, and diagenetic signals as well as evidences of mixing between ocean bottom water and deep fluids are not evident in the data (Figure 2-5). The absence of deep fluid signals indicates that R2 and D2 MVs are a classical example of inactive MVs, without recent upward fluid flow. Therefore, their geochemical profiles can be regarded as background values to compare with the ones derived from upward flow of deep fluids.

During the upward migration through overlying deposits, the pore fluids eventually mix with seawater and show geochemical signatures deviating from the original sources. One of the most important shallow subsurface processes is the AOM, where methane from deeper sources is oxidized by microorganisms using sulphate from seawater as the oxidant (Boetius et al., 2000). This process occurs extensively in the shallow subsurface of the GoC, especially at MVs (e.g., Niemann et al., 2006a). As a consequence of the sulphate - methane transition, pore water  $\text{SO}_4^{2-}$  is depleted within 50-200 cmbsf at most of our study sites (Figure 2-5). For example, the complete consumption of  $\text{SO}_4^{2-}$  occurs at 50 cmbsf in Yuma MV and 64 cmbsf in Meknes MV, and considerable depletion of  $\text{SO}_4^{2-}$  is also observed in Funky Monkey MV, although complete consumption is not fully reached through the extent of the cored sediments, probably due to a relatively low seepage rate. However, pore water  $\text{SO}_4^{2-}$  shows an enrichment at Yuma and Ginsburg MVs below the AOM zone (Figure 2-5), which may indicate a secondary deep source of  $\text{SO}_4^{2-}$  in both structures. According to Hensen et al. (2007) and Perez-Garcia et al. (2011), high  $\text{SO}_4^{2-}$  levels are caused by dissolution of anhydrite or gypsum at depth. Besides, during the AOM process,  $\text{HS}^-$  and  $\text{HCO}_3^-$  are produced and the latter leads to the increase in total alkalinity and the related carbonate precipitation. In the upper part of the Ca and Mg concentration depth profiles, the curvature observed indicates the co-precipitation of authigenic carbonates, due to Ca and Mg supply from seawater (Figure 2-5). By contrast, low concentrations of Ca and Mg are typical for the fluids below the AOM zone, which are mainly attributed to the high levels of alkalinity (Hensen et al., 2007) and the dolomitization of Cenozoic and Mesozoic carbonates at depth (Maldonado et al., 1999; Medialdea et al., 2004), respectively.

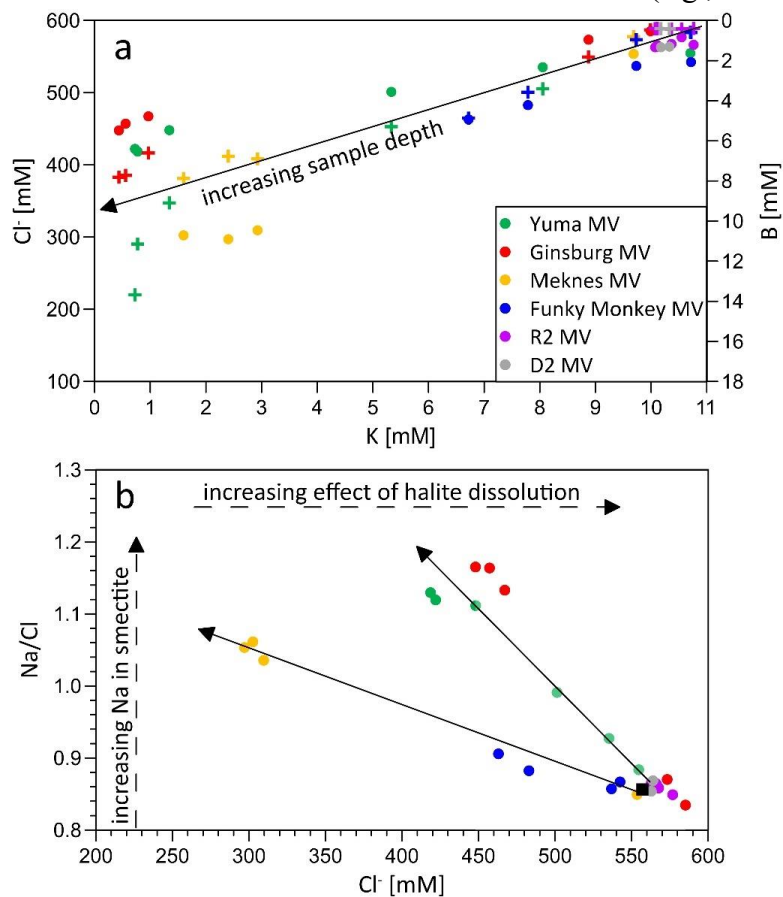
Below the AOM zone, the pore fluids presenting a negligible mixing effect with ocean bottom water are roughly referred to as deep fluids. Deep fluids generally present a distinct chemical composition inherited from various diagenetic processes at depth. Among those diagenetic signals, clay mineral dehydration (mainly the transformation of smectite to illite) has been identified as one of the most common mechanism of fluid formation driving MVs emissions

(e.g., Moore and Vrolijk, 1992; Brown et al., 2001; Dählmann and De Lange, 2003), and is the major fluid source in shallow MVs of the GoC (e.g., Hensen et al., 2007; Scholz et al., 2009). During the dehydration process, the release of mineral-bound water results in a general dilution trend of major solutes, and the effect is evident in conservative elements such as  $\text{Br}^-$  and  $\text{Cl}^-$  (Figure 2-5). Together with the freshening, the adsorption of K into illite controls the transformation kinetics and leads to K depletion in the fluids. The release of Na in the dehydration process further contributes to the relative Na enrichments over  $\text{Cl}^-$ . The fluid-mobile elements B and Li, which are suggested to be primarily released from clay minerals (Brumsack and Zuleger, 1992), also show enrichment during the process. As a consequence of clay dehydration, the fluid samples from the studied (active) MVs reveal a downcore trend of decreasing K and  $\text{Cl}^-$  together with increasing B (Figure 2-8a). In general, the samples from the MVs on the upper part of the accretionary wedge (Yuma, Ginsburg and Meknes) show the strongest signals, reflecting intense pore water freshening. A less intense effect is shown in the samples from Funky Monkey MV, possibly due to the westward thinning of the terrigenous sediments of the AUGC unit and the consequently reduced extent of clay mineral dehydration (Scholz et al., 2010b).

With the decrease of  $\text{Cl}^-$  concentrations, two different increasing trends of Na/Cl ratios were observed in the fluids (Figure 2-8b). Samples from Meknes and Funky Monkey MVs have similar increasing trends, although there is a certain difference between their absolute values. The relatively lower Na/Cl values at Funky Monkey MV can be explained by insufficient sampling depth where the stable region below the AOM zone was not reached, or by the thinner sedimentary cover at the site, close to the southwestern edge of the accretionary prism. By contrast, a relatively higher trend of Na/Cl has been detected in Yuma and Ginsburg MVs, which might reflect higher original Na content in the smectite (e.g., van de Kamp, 2008). However, the extent of freshening at the Yuma and Ginsburg sites is inconsistent with usual clay dehydration values and another possible mechanism, the leaching of halite, is likely to overprint the freshened fluids. As a consequence of the leaching of halite, the Na/Cl ratio would be shifted from 0.86 (seawater values) to close to 1.00 (e.g., Hensen et al., 2007). Our results with higher Na/Cl ratios of about 1.05 and 1.15 support both Na enrichment processes: Na released from clay mineral dehydration and simple addition of NaCl from halite dissolution. While the additional process of halite dissolution is relatively pronounced at Yuma and Ginsburg MVs, the Na release at Meknes and Funky Monkey MVs is mainly through smectite-illite transformation. Similar geochemical signals from evaporite dissolution were also observed at Hesperides MV, Captain Arutyunov MV and Mercator MV in the GoC (Hensen et al., 2007; Scholz et al., 2009; Haffert et al., 2013), and have been associated with widespread salt diapirs and their leaching effects (e.g., Perez-Garcia et al., 2011; Haffert et al., 2013).

Moreover, the behavior of Sr is not uniform at the studied (active) MVs. The fluids from Yuma and Ginsburg MVs show that Sr concentrations fluctuate within a narrow range and deviate from the mixing area characteristic of clay dehydration (Figures 2-5 and 2-8c). At Ginsburg MV, Sr is only slightly enriched and might originate from dissolution of evaporites, because

gypsum and anhydrite are Sr-enriched minerals (up to 5900 mg kg<sup>-1</sup> Sr; Usdowski, 1973) and elevated concentration of SO<sub>4</sub><sup>2-</sup> is observed at the site. At Yuma MV, no observable Sr enrichment suggests that the dissolution of sulfate minerals is negligible, which is consistent with only slightly enriched SO<sub>4</sub><sup>2-</sup> below the AOM zone. In contrast, Sr is enriched at the MVs near the Lineament Center South (Meknes) and the Lineament South (Funky Monkey) (Figure 2-5). The concentration of Sr at Meknes MV is up to 0.36 mM (Table 2-2), also parallel with B and Li enrichment (Figure 2-5) suggesting clay mineral dehydration. Consistently, the deepest data point plotted in Figure 2-8c lies in the range defined by mixing of Sr-enriched clay endmembers and seawater, which supports a clay dehydration origin of the Sr. At Funky Monkey MV, which is located at a water depth of 3172 m away from other study sites, the enrichment of Sr is more pronounced than B and Li enrichments (Figure 2-5). The fluids are offset from the mixing trend of clay water and seawater with high Sr concentrations (Figure 2-8c), which is similar to the ones of Abzu, Tiamat, and Michael Ivanov MVs (ATI MVs), suggesting a strong imprint of other Sr sources, i.e. recrystallisation of Mesozoic carbonates and/or leaching of oceanic crust (Hensen et al., 2015). Since Upper Jurassic carbonates are constrained in the westernmost part of the GoC near Coral Patch Ridge (Figure 2-1a) (Martinez-Loriente et al., 2013; Hensen et al., 2015), the Sr enrichment in the Funky Monkey MV where Jurassic strata is absent, is more likely related to the injection of crustal-derived fluids, possibly in connection to the Lineament South tectonic activity. The hypothesis also motivates future investigation on Sr isotope to determine the contribution of the oceanic crust underlying the Funky Monkey MV, where non-radiogenic Sr from fluid/basalt interactions can shift the pore water <sup>87</sup>Sr/<sup>86</sup>Sr ratios below that of modern seawater (e.g., Scholz et al., 2009).



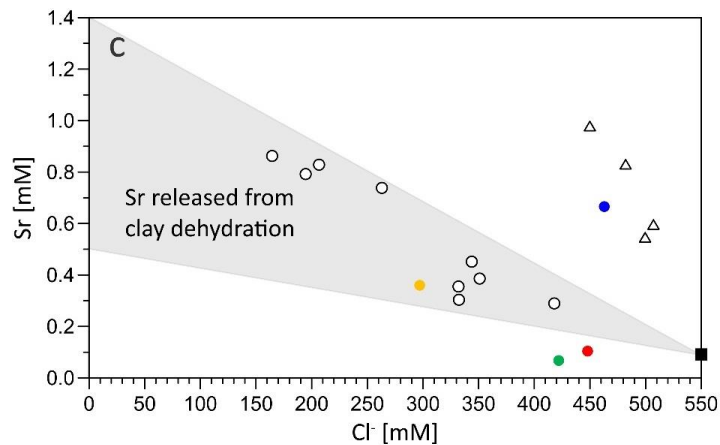


**Figure 2-8.** a) Plot of K vs.  $\text{Cl}^-$  (circles) and K vs. B (crosses) at all investigated sites. b) Plot of  $\text{Cl}^-$  vs.  $\text{Na}/\text{Cl}$  at all investigated sites [modified from Hensen et al. (2007)]. Two different trends are shown (solid lines with arrow), indicating variable degrees of potential processes, as well as the seawater value (black square). c) Plot of  $\text{Cl}^-$  vs. Sr for the deepest pore water samples of the studied (active) MVs [modified from Hensen et al. (2015)]. Gray field is defined by Hensen et al. (2015) using the published data (hollow circles) and marks the mixing area between minimum and maximum Sr endmembers at  $\text{Cl}^-=0$  and seawater. The seawater value (black square) and the data for the ATI MVs (hollow triangles) from Hensen et al. (2015) are shown for comparison.

#### 2.5.4 Fluid sources

As suggested by previous studies (Hensen et al., 2007), the MVs fluids in the GoC are mainly derived from clay mineral dehydration, which occurs at temperature between 60 and 150 °C (Freed and Peacor, 1989; Srodon, 1999). The Mg-Li geothermometer results for our studied (active) MVs are in the range of 60-100 °C (Table 2-2), supporting the idea that the released mineral-bound water is the major fluids source. While the calculated reaction temperatures at Yuma and Meknes MVs are about 93 °C, the one at Ginsburg MV is relatively lower (65 °C; Table 2-2), constraining the major source depth of the fluids at 2.4-3.1 km and 1.7-2.0 km below seafloor, respectively, by using the geothermal gradient of 30-38 °C/km (Grevemeyer et al., 2009). Besides, the presence of gas hydrates in the Ginsburg MV could also cause a difference in the fluids chemical composition, which results in the dilution of solutes concentrations and the underestimation of the reaction temperature. Since we did not sample pristine deep fluids from Funky Monkey MV, the temperatures calculated from our samples do not represent the maximum reaction temperature, but a close approximation. Nonetheless, the calculated temperature at Funky Monkey MV also reach the reaction range of clay mineral dehydration. In contrast, the calculated temperatures at R2 and D2 MVs are about 8-9 °C (Table 2-2), reflecting seawater temperature rather than the diagenetic reaction temperature from the deep fluids, which again supports inactive fluid seepage at these sites.

**Table 2-2.** Concentrations of B, Li and Sr, ratios of B/Li, and calculated reaction temperatures from Mg-Li geothermometer for the deepest samples of R2, D2, Yuma, Ginsburg, Meknes and Funky Monkey MVs.

Mud Volcano	Gravity Core	Depth [cmbsf]	B [mM]	Li [mM]	Sr [mM]	B/Li	Mg-Li geothermometer [°C]
R2	GeoB23053-1	180	0.41	0.02	0.08	17.2	9
D2	GeoB23054-1	25	0.42	0.02	0.08	18.3	8
Yuma	GeoB23028-1	274	13.68	0.22	0.07	61.5	93
Ginsburg	GeoB23024-3	205	7.82	0.10	0.10	78.8	65
Meknes	GeoB23043-2	124	6.77	0.41	0.36	16.4	93
Funky Monkey	GeoB23081-1	194	4.87	0.24	0.67	20.1	60

The enrichment of B and Li is commonly observed in venting fluids from accretionary prisms of subduction zones and their concentrations increase with increasing temperature (e.g., Chan et al., 1994; You et al., 1995). Before reaching 150 °C, sedimentary exchangeable B in clay minerals is released completely while Li does not vary, making B much more mobile than Li (You et al., 1995; You and Gieskes, 2001). In contrast, at moderate to high temperatures (150-350 °C), Li is enriched preferentially over B, but both of them are fluid mobile (Chan and Kastner, 2000; You and Gieskes, 2001). Hensen et al. (2007) compiled B and Li concentrations at various hydrothermal and cold vent sites suggesting that low B/Li ratios (<30) and high Li concentrations (>0.35 mM) are indicative for geochemical reactions occurring at temperatures above 150 °C. Taking the deepest data point from our core samples, several differences in relation to the MVs locations are also shown (Table 2-2, Figure 2-9). Yuma and Ginsburg MVs show high B/Li ratios of 61.5 and 78.7 respectively, but the concentrations of B and Li at Yuma MV are approximately twice those at Ginsburg MV (Table 2-2, Figure 2-9). This indicates that the pore fluids of Yuma MV may come from deeper sources, where more B and Li are generated by leaching from sediments at relatively higher temperatures, corresponding to the Mg-Li geothermometer results. By contrast, Meknes and Funky Monkey MVs have low B/Li values of 16.4 and 20.1 with enriched B and Li (Table 2-2, Figure 2-9), similar to the results of Captain Arutyunov MV and Bonjardim MV, which are considered to represent the cool end member of crustal derived fluids beneath the sedimentary cover (Figure 2-9; Hensen et al., 2007). The Li concentration is as high as 0.41 mM at Meknes MV, while Funky Monkey MV has a relatively lower Li concentration of 0.24 mM, which could be attributed to a lower seepage rate (thus more intense mixing with seawater). The low B/Li ratios and high Li concentrations indicate that crustal signals are preserved in Meknes and Funky Monkey MVs, in accordance with the Sr enrichment mechanism inferred for the latter. Previously, Nuzzo et al. (2019) suggested an open hydrocarbon system in the GoC through the He isotope analysis, as a result of the transpressive tectonic activity since the Late Miocene. The escaped petroleum accumulations participant in the illitization process and the diffused methane are transported and dissolved in the clay dehydration water. As Cretaceous formations are expected to be the source rock in the region, the higher concentrations of B and Li at Meknes MV compared to that at Funky Monkey MV may also reflect a higher maturation stage of the Cretaceous source

rock, which is assumed to reach post-maturation at near-shore sites and mid to late wet gas window maturities at the toe of the accretionary wedge. However, B and Li isotope fractionation analyses are needed to unambiguously evaluate the interactions of hydrocarbon-rich fluids with clays and trace the generation and migration of hydrocarbon related fluids.

As the active MVs investigated are part of a group of mud domes aligned parallel to the strike-slip fault system, the ascending fluids are expected to be channeled by their nearby deep-reaching, permeable strike-slip faults, which could provide a sufficient pressure gradient (Hensen et al., 2015, 2019; Schmidt et al., 2018). The Yuma and Ginsburg MVs are located along the Lineament Center North, which is mainly constrained within the southern lobe of the accretionary wedge, expelling mostly clay dehydration water without crustal signals. However, crustal signals carried from the ascending fluids are becoming focused along the Lineament Center South and the Lineament South, which are the major crustal-scale faults in the area. The admixing of crustal-derived fluid component is generally observed at distal MVs like Bonjardim, Porto and ATI MVs, consistently with our results of a pronounced crustal input at the Funky Monkey MV, at depths >3000 mbsl. However, in the upper part of the accretionary wedge, high temperature signals are also preserved in the Meknes MV indicating that the mediation of the Lineament Center South on crustal-derived fluids could be extended further shoreward. Therefore, the MVs effectively communicate with deep fluid systems in proximity of tectonic lineaments, and also advocate for an active role of the crustal-scale strike-slip faults in the GoC in mediating deep fluid seepage.

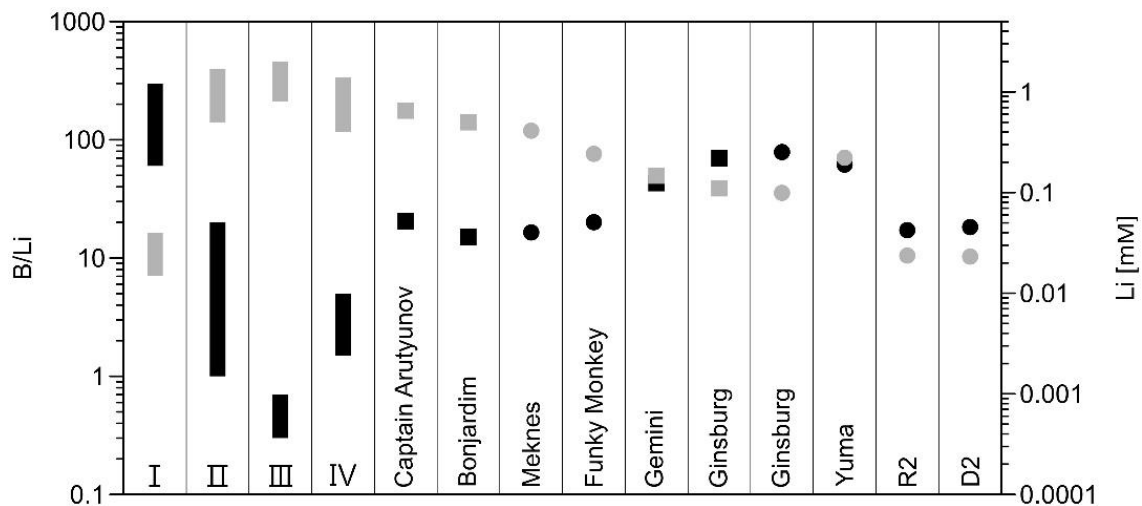


**Figure 2-9.** B/Li ratios (black) and Li concentrations (gray) from different vent environments [modified after Hensen et al. (2007), Haffert et al. (2013), and references therein]: (I) low-temperature cold vents, (II) high-temperature altered cold vents, (III) hydrothermal vents at ridge crests, and (IV) sediment-covered hydrothermal vents. The Data from Hensen et al. (2007) for Captain Arutyunov MV, Bonjardim MV, Gemini MV and Ginsburg MV are shown in squares for comparison. Values from the deepest samples of the six MVs in this study are given in circles.

## 2.6 Conclusions

Recently collected data from the M149 cruise, allowed us to characterize six MVs of the GoC according to their recent activity and mud/fluid sources, providing further insights into their relationship with the active tectonics of the region.

Close to the Lineament Center North, the newly discovered R2 and D2 MVs have classical conical shapes with pronounced moats, being in the late stages of mud volcanism. The thick nannofossil ooze retrieved on top of the mud breccia facies suggest an extended period of inactivity, and the pore fluids extracted from the sediments show similar chemical composition/reaction temperatures to seawater, indicating that no recent fluid seepage occurred. Due to the high carbonate contents in both matrix and clast samples, the two inactive MVs are expected to have a shallow source in the accretionary wedge.

In contrast, the other four MVs part of this study attest recent activity basing on the thin hemipelagic cover and the distinct pore water compositions. Yuma and Ginsburg MVs are long-lived features in an advanced stage of mud volcanism, characterized by a classical conical shape, multiple mud flow pulses and a pronounced moat. Meknes and Funky Monkey MVs are relatively younger structures in the initial stages of mud volcanism, showing a flat-topped summit with no/minor moat.

These active MVs have similar matrix compositions suggesting a consistent mud source in the AUGC unit and/or deeper units of Mesozoic age. Clay mineral dehydration is considered to be the major fluid source, which is also reflected in the high illite content of the matrix samples, in the pore water geochemistry and in the calculated reaction temperatures (from the Mg-Li geothermometer). The release of mineral-bound water during clay mineral dehydration results in the dilution of major solutes, with intense freshening at Yuma, Ginsburg and Meknes MVs and a less pronounced freshening at Funky Monkey MV.

Other diagenetic processes identified from deep fluid signals include AOM, carbonate precipitation and dolomitization, dissolution of halite and sulfate minerals, leaching of clay minerals and interactions with basement rocks. All these effects in the pore fluids show marked distinctions related to the MVs locations. Along the Lineament Center North, the process of halite and sulfate minerals dissolution has been found in the fluids of Yuma and Ginsburg MVs, and the Mg-Li geothermometer as well as the difference in B and Li concentrations indicate that the source depth of the pore fluids from Yuma MV is deeper than that of Ginsburg MV, at 2.4-3.1 km versus 1.7-2.0 km below seafloor. Along the Lineament Center South and the Lineament South, geochemical signals related to interactions with the underlying crust are present in Meknes MV and more pronounced in Funky Monkey MV, showing enrichment of Sr, Li and B with low B/Li ratios.

The strong crustal influence in the fluids of Funky Monkey MV is assumed to be influenced by the nearby deep-reaching strike-slip fault or a deep-seated feeder channel(s) which cut through the thinner sediment coverage of the upper plate, marking a notable difference from the shallow MVs, mostly showing clay dehydration signals. The crustal input therefore indicates the coupling of deep and shallow fluid systems through MVs and across the accretionary prism, further implying an active role of the crustal-scale strike-slip faults in channeling fluid seepage through the GoC accretionary prism.

## Supplementary material

**Table S2-1.** XRD results for matrix and clast samples from the recovered gravity cores.

Mud Volcano	Gravity Core	Depth [cmbfsf]	Analyzed part	Mineral Phase [wt%]								Relative Clay Abundance [wt%]			
				Qtz	Fds	Cal	Mg-Cal	Dol	Ank	Total Carbonates	Total Clays	Sm	Ill	K	Chl
R2	GeoB23053-1	50-52	Matrix	17	4	7	0	1	1	8	51	12	64	11	14
R2	GeoB23053-1	80-82	Clast	1	0	93	0	0	0	93	2	35	51	5	9
R2	GeoB23053-1	173-175	Matrix	8	0	57	14	1	4	75	7	17	75	1	7
R2	GeoB23053-1	181-183	Matrix	13	5	8	2	8	14	32	35	16	83	1	0
Yuma	GeoB23028-1	29-31	Clast	38	3	0	0	4	29	33	23	26	40	0	33
Yuma	GeoB23028-1	50-52	Matrix	16	7	9	0	2	6	17	48	30	55	8	8
Yuma	GeoB23028-1	150-152	Clast	9	3	48	0	1	1	50	34	27	64	6	3
Yuma	GeoB23028-1	239-241	Matrix	17	8	8	0	1	6	16	48	23	62	14	2
Ginsburg	GeoB23024-3	40-42	Matrix	7	1	53	0	0	1	54	24	16	73	8	4
Ginsburg	GeoB23024-3	140-142	Matrix	18	6	6	0	1	5	12	53	37	39	20	4
Ginsburg	GeoB23024-3	197-199	Clast	28	4	0	0	0	0	0	48	9	11	10	70
Meknes	GeoB23043-2	27-29	Clast	6	0	77	0	2	4	83	10	66	31	0	3
Meknes	GeoB23043-2	64-66	Clast	17	1	0	0	9	43	52	16	40	34	3	23
Meknes	GeoB23043-2	94-96	Matrix	17	9	5	0	1	5	12	50	28	50	21	1
Meknes	GeoB23043-2	102-104	Matrix	19	9	6	0	2	4	12	49	65	19	13	4
Funky Monkey	GeoB23081-1	50-52	Matrix	25	10	7	0	4	2	13	46	27	42	22	10
Funky Monkey	GeoB23081-1	84-86	Clast	5	0	73	2	0	1	76	8	0	64	26	10
Funky Monkey	GeoB23081-1	163-165	Clast	16	0	58	0	0	0	59	21	0	60	18	22
Funky Monkey	GeoB23081-1	195-196	Matrix	15	5	13	0	1	1	15	50	10	70	9	11

*Qtz* Quartz, *Fds* Feldspars, *Cal* Calcite, *Dol* Dolomite, *Ank* Ankerite, *Sm* Smectite, *Ill* Illite, *K* Kaolinite, *Chl* Chlorite

## Chapter 3

### The rise and fall of mud volcano systems: new insights on fluid circulation unravel their complex structural evolution

Shuhui Xu<sup>a,b</sup>, Walter Menapace<sup>a,c</sup>, Roger Urgeles<sup>c</sup>, Jonathan Ford<sup>d</sup>, Alcinoe Calahorrano<sup>c</sup>, Rafael Bartolomé<sup>c</sup>, and Achim Kopf<sup>a,b</sup>

<sup>a</sup> MARUM – Center for Marine Environmental Sciences, University of Bremen, 28359 Bremen, Germany

<sup>b</sup> Department of Geosciences, University of Bremen, 28359 Bremen, Germany

<sup>c</sup> now at ICM-CSIC, Institute of Marine Sciences, 08003 Barcelona, Spain

<sup>d</sup> National Institute of Oceanography and Applied Geophysics - OGS, Sgonico, Trieste, Italy

Corresponding author: Shuhui Xu ([sxu@marum.de](mailto:sxu@marum.de))

#### Abstract

Emission pathways in mud volcanoes (MVs) connect source layers with an extrusive edifice. While previous studies primarily focused on the central conduits we present evidence from MVs in the Gulf of Cadiz and the Mediterranean Ridge, suggesting the existence of rim-related fluid pathways that are actively expelling fluids. Among five examined MVs, three exhibit distinct fluid composition differences between summit (freshening) and moat/rim (salinization). At the Ginsburg MV, this rim-related fluid pathway is predominantly fueled by saline and Sr-rich fluid sources, resulting from evaporite dissolution and influenced by clay dehydration fluids. While freshened fluids are mostly channeled by central conduits, originating deep within (or below) the Allochthonous Unit of the Gulf of Cadiz (AUGC), seismic data suggest that saline fluids are likely related to nearby fluid accumulation at the AUGC's upper boundary. When considering the MVs' life-cycle, the younger Meknes MV exhibits freshening throughout its entire structure, whereas the inactive Rabat MV, at a later evolutionary stage, shows the disappearance of freshening at the summit but retains saline characteristics at the moat through diffusion. Thus, the evolution of MV systems governs the fluxes and composition of expelled fluids. In the case of Ginsburg MV, volumes of fluid emissions through the moat area are comparable to the summit area, highlighting the significant contribution of rim-related pathways to fluid circulation, especially during prolonged inactivity. Although this research is confined to two study areas, the identified salinity patterns and rim-related fluid pathways could represent a global phenomenon that merits further investigation.

### 3.1 Introduction

The marine environment hosts a variety of cold seep systems through which material can transfer from the geosphere to the biosphere and, eventually, to the atmosphere (Suess, 2014). With the release of gases through the ocean floor seep features such as mud volcanoes (MVs) and pockmarks are produced, altering the seabed morphology (Jones et al., 2010; Suess, 2014). The seafloor expression of these structures is controlled by several factors including flux rate and type of expelled material. Slow and vigorous fluid flux forms authigenic carbonates and pockmarks, respectively, whereas MVs result from much stronger eruptions with a high content of plastic sediments (Talukder, 2012). These active extrusions and subsequent mud flows contribute to the build-up of MV edifices, with low-viscosity and high-viscosity mud flows shaping the morphology into flat-topped or conical edifices, respectively (Kopf, 2002; Mazzini and Etiope, 2017). However, active mud eruptive phases are episodic, and most of the life span of a MV is characterized by intervals of depletion and quiescence, accompanied by continuous seepage of gas and volatiles (Kopf and Behrmann, 2000; Dimitrov, 2002; Menapace et al., 2019). Hovland (2002) and León et al. (2007) suggested an evolutionary path for MV edifices which, after the main eruption, continues with: i) slower fluid seepage, ii) edifice collapse forming the moat around the MVs (depletion), and iii) evolution to a hardground surface colonized by sessile organisms (quiescence). The varying intensity of fluid seepage during the evolution of a MV system is thought to be related to the clogging, changing, and reactivation of the conduit within the edifice.

The MV conduit, which promotes vertical migration of fluids from a source layer at depth to the extrusive seafloor edifice, is a crucial component in the MV system, affecting fluid circulation. As the conduits are highly transient in time and space, they are the least understood part of the MV system, contrary to their surface expression (Roberts and Carney, 1997; Hornbach et al., 2007). With recent advances in 3D seismic technology, vertical pipe-like structures (Davies and Stewart, 2005; Cartwright and Santamarina, 2015; Kirkham et al., 2018) have been increasingly recognized as MV conduits, in contrast to previous models that pointed to large diapirs (Brown, 1990) and to mud injections/diatremes (Pickering et al., 1988; Robertson and Kopf, 1998). The transmissivity of MV conduits affects the upward migration of fluids, which manifests as a change in fluid flux and fluid composition at the seafloor over time. During the R/V Meteor cruise M149 contrasting fluid signatures were detected at the summit (freshening) and moat (salinization) of the Ginsburg MV, in the Gulf of Cadiz. A similar spatial distribution of fluid composition has previously been reported at the Milano MV in the Mediterranean Sea (Dählmann and de Lange, 2003). In order to further illuminate the structural implications behind this spatial variation in chemical and fluid fluxes, we selected the Yuma, Ginsburg and Milano MVs (that have distinct fluid signatures), as well as the Meknes and Rabat MVs (that have much higher and lower activity levels, respectively). The aim of this study is to: i) identify fluid sources and diagenetic processes responsible for the variability in geochemical profiles from the summit to the rim of the MVs, ii) explain the complex fluid circulation below a MV edifice, related to the evolution of different

geomorphological units and iii) understand the contribution of fluid circulation to the emission rates during depletion and quiescence periods.

### **3.2 Geological setting**

The Gulf of Cadiz and the Mediterranean Sea, both situated in areas of convergence and tectonic compression between the Eurasian and African plates, host numerous fluid venting features, including MVs, that are related to their accretionary wedge (Figure 3-1). In the Gulf of Cadiz, most of the MVs are located on the upper part of the accretionary wedge and are distributed following NE-SW and NW-SE trends, due to the tectonic control exerted by thrust and strike-slip faults (Figure 3-1a; Medialdea et al., 2009). The sedimentary cover in the region consists of Triassic to Quaternary sediments, with variable thickness of 2-3.5 s two-way travel time (TWT) (Medialdea et al., 2004). It is worth noting that the Allochthonous Unit of the Gulf of Cadiz (AUGC), emplaced during the Late Tortonian, represents the thickest unit (up to 2.5 s TWT) and is characterized by chaotic facies in seismic reflection profiles (Maldonado et al., 1999; Medialdea et al., 2004). The Messinian to Quaternary successions overlying the AUGC contains three major discontinuities: i) the Top Miocene discontinuity (TM) at ca. 5.3 Ma; ii) the Base Quaternary Discontinuity (BQD) at ca. 2.6 Ma; and iii) the Mid-Pleistocene Discontinuity (MPD) at ca. 0.9 Ma (Toyos et al., 2016). The sediments underlying the AUGC are mainly upper Cretaceous to lower Eocene terrigenous sediments, with upper Jurassic carbonates present only near the Coral Patch Ridge and Triassic evaporites located at the base of the sedimentary cover. Previous studies of the MVs have shown that clay mineral dehydration occurring in the AUGC is the major fluid source, and that thermogenic gases originate in the deeper Jurassic/Cretaceous sediments where the formations have reached the oil to gas maturity window (Hensen et al., 2007; Nuzzo et al., 2019; Xu et al., 2021).

On the other hand, deformation along the Mediterranean Ridge accretionary complex occurs in response to collision and subduction of the African plate. The Mediterranean Ridge is composed of an outer and an inner domain, wrapped between the Cretan continental backstop and the Libyan passive continental margin (Figure 3-1c; Truffert et al., 1993; Chaumillon, 1995; Kopf et al., 2001). MVs are abundant in this region and the Olimpi MV field, located in the intensely deformed inner domain south of Crete, has the largest concentration, including several mud domes and complexes (Figure 3-1d; Camerlenghi et al., 1995; Cita et al., 1996). Messinian evaporites are ubiquitous and especially well imaged by seismic data across the outer domain (Chaumillon, 1995; Camerlenghi et al., 2023), forming a quasi-impermeable cap above the underlying Tertiary clastic sediments, but in the inner domain the salt sources are probably secondary brines or isolated evaporitic diapirs. Compared with the features in the Gulf of Cadiz, most MVs in the Mediterranean Ridge have a generally shallower depth of fluid origin (1-2 kmbsf, e.g., Deyhle et al., 2003; Panagiotopoulos, 2020), whereas some studies also suggest fluid and sediment mobilization depths of up to 3.5-6.8 kmbsf (Camerlenghi et al., 1995; Schulz et al., 1997).

In both regions salt tectonics has affected the mud volcanism, and in some MVs the corresponding geochemical effects are shown in the ascending pore water (e.g., Dählmann and de Lange, 2003; Haffert et al., 2013). In the Gulf of Cadiz, evaporitic deposits are of Triassic age and related to two different parent layers, the AUGC and the Triassic unit. While the AUGC containing such Triassic evaporites extends from the Iberian and Morocco coasts to the Horseshoe and Seine Abyssal Plains, the evaporitic Triassic unit covering the basement is mainly found in the northern sector and accumulated in half-grabens along the Morocco margin, forming a series of salt diapirs dotting the accretionary wedge (Maldonado et al., 1999; Tari et al., 2003). Their accumulation on top of the basement is related to the development of a rifted passive margin and to the opening of the Atlantic Ocean in Triassic-Jurassic times (Maestro et al., 2003; Tari et al., 2003). In the Mediterranean Ridge a shallower evaporitic sequence was formed in the Late Miocene (Messinian) on top of Paleogene to Tortonian sedimentary successions. While thick evaporite deposits generally trap deep fluids, the major MV fields are located at sites where Messinian evaporites are thin or absent (Masclé et al., 2014).

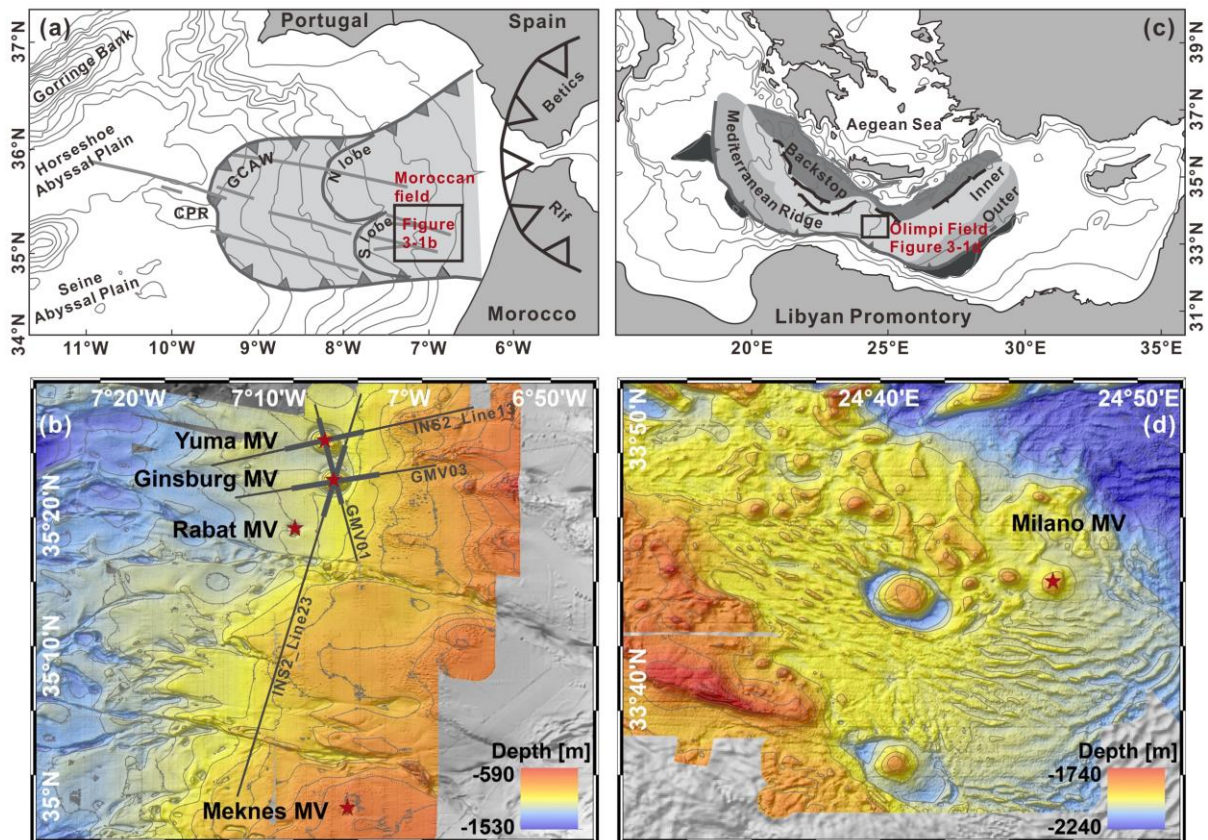


**Figure 3-1.** Study area and location of MVs in the Gulf of Cadiz and the Mediterranean Ridge. (a) General location map of the Gulf of Cadiz depicting the outline of the Gulf of Cadiz Accretionary Wedge (GCAW) including its shallower northern and southern lobes (modified from Gutscher et al., 2009). The long, grey lines show a set of WNW-ESE oriented strike-slip faults, the South West Iberian Margin (SWIM) fault zone (Zitellini et al., 2009). CPR Coral Patch Ridge. (b) Bathymetry map of the main study area in the Gulf of Cadiz, showing the location of the studied MVs (red stars) as well as the seismic profiles (dark grey lines). (c)

Geological setting of the Eastern Mediterranean with location of the Olimpi MV field (modified from Huguen et al. (2004), and references therein). (d) Bathymetry map of the Olimpi MV field, showing the location of the Milano MV (red star).

### **3.3 Materials and methods**

#### **3.3.1 Hydroacoustics**

We conducted seabed imaging surveys of the Gulf of Cadiz during R/V Meteor cruises M149 and M167, using the Kongsberg Simrad EM122 multibeam system that was operated with 432 beams per ping and at a frequency of 12 kHz. Hüpers et al. (2020) and Menapace et al. (2021) provide more details about the instrument's technical features and conditions of the survey. We employed the Kongsberg Seafloor Information System (SIS) software to monitor data quality in real time during the acquisition. We then processed the multibeam data with MB-System and Generic Mapping Tools (GMT) programs and displayed them with ArcGIS software. The main map of the Gulf of Cadiz and Olimpi MV field have a pixel resolution of 50×50 m and 30×30 m, respectively. The individual structures in the Gulf of Cadiz and Olimpi MV field have a pixel resolution of 20×20 m and 30×30 m, respectively.

#### **3.3.2 Seismic acquisition/processing**

To image the structure of Yuma and Ginsburg MVs, high-resolution multichannel seismic data was acquired in the Gulf of Cadiz during the INSIGHT Leg 1 and 2 cruises (2018 and 2019) (Gràcia et al., 2018; Urgeles et al., 2019). For the seismic survey, a source array comprising 10 G-GUN II air-guns (total volume 930 cu. in.) was utilized, with a shot interval of 12.5 m. Data acquisition was conducted using a GEOEEL Geometrics digital streamer with receiver spacing 6.25 m, with a total length of 443.75 m (72 active channels) for lines GMV01 and GMV03 and 343.75 m long (56 active channels) for lines INS2\_Line13 and INS2\_Line23. Real-time quality control was performed using shot gather and near-trace displays during the acquisition of the seismic lines. The seismic data was processed using RadExPro 2019.2 software with a CDP binning interval of 3.125 m (nominal fold of 18 and 14, respectively). A low-cut bandpass filter (2-4 Hz) was used to remove low-frequency swell noise, followed by time-frequency domain noise attenuation to reduce residual noise. Ghost arrivals, generated by the reflections at the ocean-air discontinuity, occurred due to the source and receivers being towed below the sea surface and have been removed using the “SharpSeis De-ghost” module in RadExPro 2019.2 software. The far-field source signature was estimated by flattening and stacking the waterbottom reflection in a near-offset gather, under the assumption that this approximates a zero-offset reflection from an isolated positive impedance contrast. The signature estimation used two iterations of flattening and rejection of traces with poor statistical correlation with the estimated signature (Blondel et al., 2023). Using this signature, deterministic de-bubble and zero-phasing operators were derived to remove the effect of the airgun source bubble pulse in the seismic data. The zero-phase correction adjusted the phase of the approximately minimum-phase airgun wavelet to zero-phase, improving the accuracy and resolution of the data.

The distance between the near- and far-offset channels (c. 400 m) in this experiment is relatively small relative to the water depth (>1 km), and the complex near-seafloor geology included many diffractions and out-of-plane reflections. Therefore, the semblance method was not suitable for the velocity analysis. Instead, we calculated a stacking velocity field assuming a constant water velocity of 1500 ms<sup>-1</sup> above the seafloor and an increasing velocity gradient of 500 ms<sup>-2</sup> below the seafloor. Considering that the stacking power is relatively insensitive to errors in the stacking velocity due to the low moveout of the reflections, the stacking velocity field was deemed appropriate. Data were normal moveout (NMO) corrected using the velocity field and stacked.

We similarly obtained a migration velocity field by assuming a uniform water velocity of 1500 ms<sup>-1</sup> above the seafloor and a velocity gradient of 125 ms<sup>-2</sup> below the seafloor. The velocity gradient was checked by conducting multiple migrations with different gradient values on two separate test lines. Finally, the stacked sections were migrated using a post-stack Kirchhoff time algorithm with the migration velocity field. Before migration a bottom mute was applied from the first waterbottom multiple to prevent multiple energy being migrated to the shallower part of the section as noise. After migration a Q-compensation filter (amplitude only), time-variant bandpass filter and top mute above the water bottom were applied to improve the image for interpretation.

### **3.3.3 Sediment and pore water sampling**

The pore water samples used in this study were acquired during cruises M149 and M167, where MeBo cores were recovered in the Ginsburg MV and gravity cores were collected in the Meknes, Yuma, Ginsburg and Rabat MVs (Hüpers et al., 2020; Menapace et al., 2021) (Table 3-1). The samples from the Milano MV are from the literature, and the methodology has been detailed in Emeis et al. (1996). The MeBo cores were drilled by a remotely operated seafloor drill-rig, the MARUM-MeBo70, whereas the gravity cores were recovered using conventional gravity coring with a 5.75 m-long corer. Both techniques employed a plastic liner to house the cores. To compare the characteristics of different geomorphological parts of a MV, core samples from the summit, flank and moat/rim areas were taken at each MV. Once the cores were on deck, they were cut into sections and sealed with plastic caps. Then, small holes were made in the plastic liner with an electric drill and pore water was extracted from the whole-cores using rhizons on syringes, as described by Dickens et al. (2007). Three pore water samples were taken every 120 cm for the MeBo cores and every 100 cm for the gravity cores. Before laboratory measurements, the pore water samples were stored in air-tight 20 ml PTFE vials in a refrigerated room at 4 °C.

### **3.3.4 Geochemical measurements**

After the cruise, geochemical measurements were conducted on the pore water samples extracted from the MeBo and gravity cores to determine their ion compositions and isotope ratios. We analyzed the soluble cation concentrations, including Na, K, Ca, Li, B, and Sr using an Inductively Coupled Plasma Optical Emission Spectrometer (ICP-OES). The anion

concentrations, such as Cl and SO<sub>4</sub><sup>2-</sup>, were examined using an Ion Chromatograph (IC). We measured Sr isotopes using a Thermal Ionization Mass Spectrometer and investigated water isotope ratios using a Cavity Ring-Down Spectrometer.

Prior to conducting the ICP-OES measurements, we acidified the collected pore water samples with concentrated HNO<sub>3</sub> to dissolve any solids that had precipitated during storage. We then diluted the samples with 1% HNO<sub>3</sub> and tested them with ICP-OES. The relative standard deviation based on duplicate measurements of IAPSO seawater standard was found to be <1% for Na, K, Ca and Sr, <3% for B, and about 10% for Li. Based on the resulting Sr concentrations, we separated ~1.5 µg Sr per sample using a SrSpec resin (Eichrom) via ion exchange chromatography and subsequently measured the Sr isotopes. We corrected the Sr isotope data for the decay of <sup>87</sup>Rb and normalized it to a value of 0.710248 for NIST SRM 987. The reproducibility of repeated tests on strontium carbonate isotopic standard (NIST SRM 987) yielded a value of 0.000004 (2SE, n=4). The measurement uncertainties were all below 0.000023 with a confidence level of 2 standard errors.

For water isotopes, we report the measured values relative to Vienna Standard Mean Ocean Water (V-SMOW) with a precision (2σ) of ±0.8‰ for δD and ±0.25‰ for δ<sup>18</sup>O. For IC measurements, we first centrifuged the pore water samples to remove precipitates and prevent the addition of anions to pore water. We then diluted the pore water samples with Milli-Q water and measured them with IC. The analytical precision for Cl and SO<sub>4</sub><sup>2-</sup> was about 1%.

### 3.3.5 Pore water modeling

To investigate the fluid flow in the selected MVs, an advection–diffusion model was used. The selected model describes the variation of interstitial solute concentration in a water-saturated one-dimensional sediment column and is expressed through the following differential equation (Boudreau, 1997):

$$\frac{\partial C}{\partial t} = D \cdot \frac{\partial^2 C}{\partial z^2} - v \cdot \frac{\partial C}{\partial z} \quad e. q. (3.1)$$

where  $C$  is interstitial solute concentration,  $t$  is time,  $D$  is the chemical diffusion coefficient in the sediment,  $z$  is depth, and  $v$  is fluid flow velocity. The selection of a one-dimensional model is justified by the significant vertical concentration gradient compared to the horizontal gradient prior to reaching concentration stability, indicating the dominance of vertical fluid flow. The differential equation was solved numerically with the finite difference method and the associated errors relative to the exact solution were negligible. The solution was obtained based on a depth–time grid. By employing the conservative element Cl, the program simulated the evolution of Cl concentration based on the advection and diffusion of solute and tested how long and at what fluid velocity the simulated solute concentration fits the measured geochemical profile. In our model,  $D$  was calculated from Boudreau (1996) as:

$$D = D_0 / (1 - \ln(\varphi^2)) \quad e. q. (3.2)$$

where  $D_0$  is the diffusion coefficient for chloride in free solutions at 5°C ( $D_0 = 1.12 \times 10^{-9} \text{ m}^2/\text{s}$ ; Boudreau, 1997) and  $\phi$  is the sediment porosity determined by averaging data obtained from moisture and density measurements (see metadata of Meteor cruises M149 and M167 published in [www.pangaea.de](http://www.pangaea.de)). The best-fit  $v$  and  $t$  will quantify the changing fluxes from the summit to the rim of the MVs and shed light on fluid circulation in different parts of the structure.

For the initial solute concentration, the seawater value was assigned from the top to a certain depth, below which a value similar to the maximum/minimum measured values at the bottom of the cores was specified, representing the solute concentration of pure fluids (another endmember). To simulate fluid advection, the fluid flow velocity was assigned a series of numerical values. For both the top and bottom boundaries, constant concentrations and fluid flow velocities were assigned during the model calculations, under the assumption that there is continuous fluid flow and that the concentration and velocity of pure fluids can be constrained with the model. However, the duration of fluid flow and the corresponding velocity were unknown, therefore a sensitivity analysis using a set of durations and velocities was conducted. The parameters that best predicted the measured data were determined by matching the model to the observed geochemical profiles.

### **3.4 Results**

#### **3.4.1 Morphology and sedimentology**

The morphology of the MVs, from summit to base, comprises: i) a crater, a flat top, or a central dome(s) on the summit; ii) homogeneous and smooth flanks, or terraced and lobe-shaped ones related to episodes of mud flows; iii) a moat at the base of the MV edifice or flanks merging with the seafloor adjacent to the rim area of the MV.

The Meknes MV (80 m high and 1400 m wide) and the Milano MV (122 m high and 3700 m wide) are cone-shaped edifices with a flat top (Figure 3-2). While the flanks of the Meknes MV are smooth and degrade to a gentle slope in the basal part, the Milano MV shows a terraced morphology with its outer edge delimited by a ring-shaped collapse-like structure. Around the two MVs, no significant moat is observed, but a moat-like structure buried beneath the lower flanks of the Milano MV corresponding to the outer ring faults is visible in seismic reflection profiles acquired prior to the ODP drilling (see Initial Reports of the Ocean Drilling Program Leg 160; Emeis et al., 1996). The cores recovered from the two MVs consist of mud breccia, with no or thin hemipelagic deposits at the top (Figure 3-2). The draping hemipelagic sediments are absent at the summits (GeoB23043-1, ODP 970D), and range in thickness from 0-3 cm at the flanks (GeoB23040-1, ODP 970C), to 5-60 cm at the rims (GeoB23039-1, ODP 970A). At the lower slope of the Milano MV, the rim area (ODP 970A) shows alternations of mud breccia and hemipelagic sediments, while the outer rim area (ODP 970B) is entirely hemipelagic sediments.

**Table 3-1.** Locations of sampled cores, for the MVs presented in this study, and parameters/results from the fluid flow modeling.

Sampling location	Core number	Core type <sup>a</sup>	Latitude	Longitude	Water depth (m)	Model column length (m)	Cl at surface (mM)	Cl at the model's bottom (mM)	Porosity	Upward fluid flow (cm/yr)
<i>Milano (Emeis et al., 1996)</i>										
Summit	ODP 970D	APC	33°44.04'N	24°46.61'E	1953	43	200	70	0.55	50.0
Flank	ODP 970C	APC	33°44.13'N	24°47.46'E	2037	10	509	350	0.50	11.6
Rim	ODP 970A	APC	33°44.19'N	24°48.12'E	2076	196	600	1715	0.50	0.0
Outer rim	ODP 970B	APC	33°44.21'N	24°48.69'E	2079	196	600	1715	0.60	1.5
<i>Meknes</i>										
Summit	GeoB23043-1	GC	34°59.07'N	7°04.44'W	687	1.5	590	298	0.61	129.2
Flank	GeoB23040-1	GC	34°59.10'N	7°04.20'W	735	1.8	590	480	0.53	21.9
Rim (no moat)	GeoB23039-1	GC	34°59.10'N	7°04.06'W	749	2.2	558.4	552	0.58	4.8
Background	GeoB23038-1	GC	34°59.12'N	7°02.04'W	744	3.7	560	560	0.59	0.0
<i>Yuma</i>										
Summit (dome1)	GeoB23028-1	GC	35°25.46'N	7°06.07'W	959	3	557	420	0.59	11.6
Summit (dome2)	GeoB24211-1	GC	35°25.06'N	7°05.45'W	950	2.5	595	465	0.61	15.0
Flank	GeoB23012-1	GC	35°24.73'N	7°05.66'W	996	4	595	580	0.57	0.0
Rim (mudflow)	GeoB23025-2	GC	35°24.31'N	7°05.52'W	1124	4.7	560	575	0.59	0.0
Depression (edge of mudflow)	GeoB23004-1	GC	35°23.92'N	7°05.74'W	1661	5	595	785	0.61	0.0
<i>Ginsburg</i>										
Summit	GeoB23024-3	GC	35°22.36'N	7°05.32'W	908	2.5	600	448	0.56	13.3
Summit	GeoB23024-4	MeBo	35°22.37'N	7°05.31'W	906	18	600	418	0.61	15.0
Summit	GeoB24222-1	GC	35°22.40'N	7°05.46'W	915	2.5	600	540	0.57	6.7
Summit	GeoB23005-1	GC	35°22.55'N	7°05.37'W	887	2	580	541.5	0.58	2.8
Flank	GeoB23010-1	GC	35°22.52'N	7°04.64'W	977	2.5	600	585	0.56	0.0
Rim (moat)	GeoB23007-1	GC	35°21.53'N	7°05.34'W	1121	45	590	2600	0.51	0.3 <sup>b</sup>
Rim (moat)	GeoB23009-1	GC	35°22.54'N	7°03.93'W	1072	45	590	2600	0.61	0.3 <sup>b</sup>
Rim (moat)	GeoB23047-3	MeBo	35°22.86'N	7°04.13'W	1126	45	590	2600	0.56	0.3 <sup>b</sup>
Background	GeoB23027-1	GC	35°22.38'N	7°01.16'W	962	4.4	583	605	0.61	0.0
<i>Rabat</i>										
Summit	GeoB23034-1	GC	35°18.90'N	7°08.04'W	1039	2.92	565	545	0.56	0.0
Rim (moat)	GeoB23052-1	GC	35°19.05'N	7°08.60'W	1186	4	570	735	0.60	0.0

<sup>a</sup>APC Advanced Piston Core, GC Gravity Core, MeBo Cores drilled by the seafloor drill-rig MARUM-MeBo70.

<sup>b</sup>The three cores from the moat of Ginsburg MV are combined into a single model, as their geochemical profiles show good agreement.

The Yuma and Ginsburg MVs, which have heights of 218 m and 280 m are two of the largest MVs in the Gulf of Cadiz. The MVs are shaped as elongated cones with central dome(s) at the summit and major axes of 4400 m and 3860 m, respectively, along the NW-SE direction (Figure 3-2). While the Ginsburg MV is topped by a single dome, there is a flat area consisting of two interconnected calderas on top of the Yuma MV with two central domes (Dome 1 and Dome 2) and one smaller dome (Dome 3) at the southern side. The flanks of both MVs show a predominantly terraced morphology with variable steepness. An annular, irregular moat is recognized in both MVs, being more pronounced at the northwest side of the Yuma MV (60 m) and the southeast side of the Ginsburg MV (80 m). The recovered cores (Figure 3-2) are composed of mud breccia overlaid by hemipelagic sediments that increase in thickness from the summits (0-5 cm-thick; GeoB23024-3/4, GeoB24222-1, GeoB23005-1, GeoB23028-1 and GeoB24211-1) to the flanks (94-134 cm-thick; GeoB23010-1 and GeoB23012-1), while the cores recovered at the rim of the MVs and the depression in between only contain hemipelagic sediments (GeoB23007-1, GeoB23009-1, GeoB23047-3, GeoB23025-2, and GeoB23004-1).

Southwest of the Yuma and Ginsburg MVs, the Rabat MV is a comparatively smaller feature with NW-SE elongation, 67 m high and major axis of 1577 m. It shows a central dome at the top, a terraced morphology on the NW flank, and an obvious moat of 10-30 m depth (Figure 3-2). The core recovered from the summit (GeoB23034-1) shows a thick layer of hemipelagic sediments (125 cm) followed by mud breccia, while the core recovered at the rim (GeoB23052-1) contains only hemipelagic sediments (Figure 3-2).

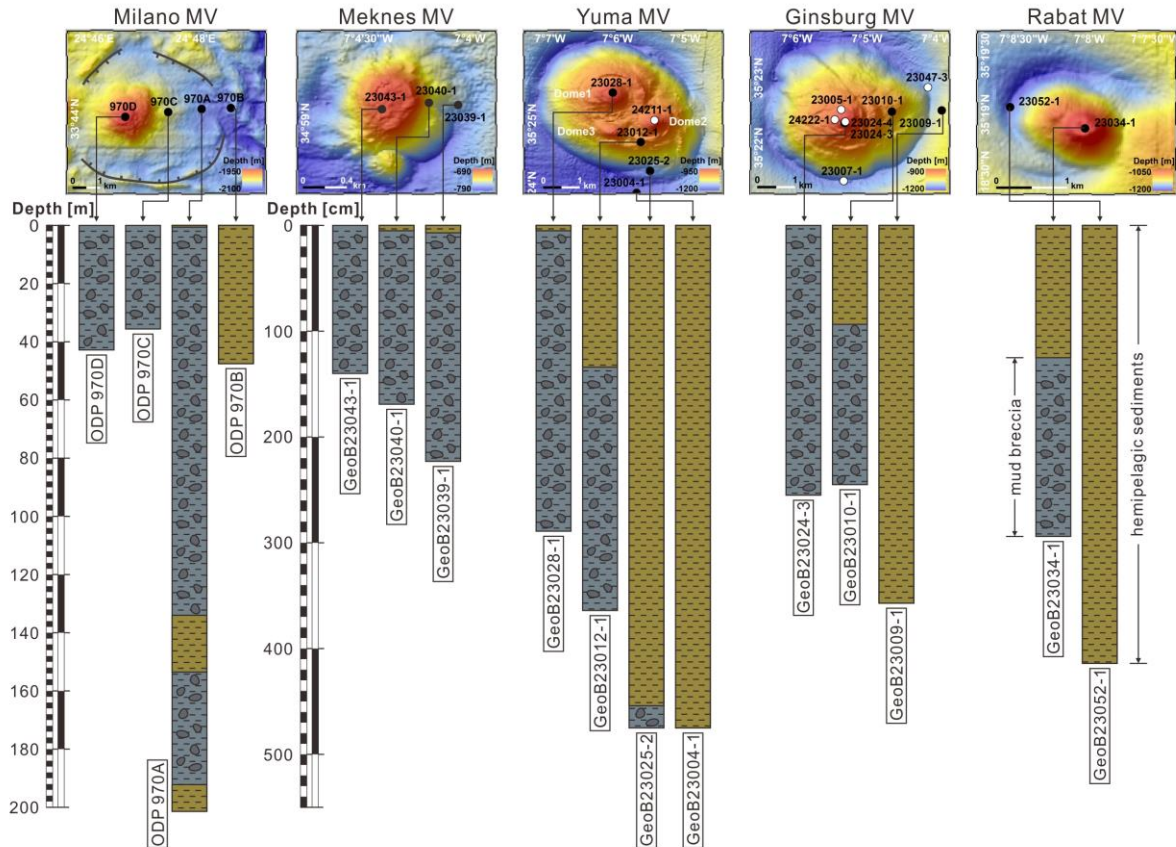


**Figure 3-2.** Lithostratigraphy of the sampled cores over the studied MVs. Data for the Milano

MV are taken from ODP drilling (Emeis et al., 1996) and core length is reported in meters, whereas for the other MVs core length is reported in centimeters below seafloor. In the maps, the core sites used in this study are noted as white and black dots. The black dots are the selected cores to show lithologies. Reference cores, GeoB23038-1 and GeoB23027-1, located to the east of the Meknes and Ginsburg MVs, are not included in the figure due to their positioning outside the figure's coverage area (see Table 3-1 for their latitude and longitude information).

### **3.4.2 Mud volcano internal structure**

High-resolution multichannel seismic profiles over the Ginsburg and Yuma MVs (Figure 3-1b) enable detailed characterization of their morphology and internal architecture. The Ginsburg and Yuma MV systems are composed of vertically stacked bicones and feeder complexes, with chaotic to transparent seismic facies disrupting the stratified seismic facies that characterize the surrounding sub-seafloor (Figure 3-3). Bicones, extrusive edifice morphologies characterizing MVs, are constituted of upward- and downward-pointing cones. There are two and four bicones stacked vertically under the Ginsburg and Yuma MVs, with their respective lowermost expressions overlying the Quaternary discontinuity and the upper boundary of the AUGC described by Duarte et al. (2022) and Toyos et al. (2016) (Figure 3-3c). The feeder complexes underlying the current extrusive MV edifices can be described as unstratified downward-tapering cones (Somoza et al., 2012) with chaotic to transparent reflection patterns (Figure 3-3). Beneath both the Ginsburg and Yuma MVs, the feeder complexes link the extrusive edifices to the AUGC.

The background sediments adjacent to the buried parts of the two edifices display chaotic, high-amplitude reflections in the AUGC unit, although high-amplitude stratified seismic facies are present locally (blue dashed boxes in Figure 3-3). The Upper Miocene to Quaternary sediments display parallel, continuous reflections with amplitude evolving from low to medium from bottom to top. The contact between the AUGC and the overlying units is characterized by a high-amplitude reverse polarity (i.e., downward decrease in impedance) reflector (Figure 3-3). On both sides of the buried edifices, reflections within the host sediments bend upwards against the edge of the feeder channel, especially between the Ginsburg and Yuma MVs (Figure 3-3b, 3-3c). Between the two MVs, in an area characterized by mounded seafloor (MF in Figure 3-3c), we highlight the presence of shallow subsurface lobes which have an internally chaotic seismic response.

The seismic line GMV03 across the Ginsburg MV (Figure 3-3a) shows the position of the MeBo core (GeoB23047-3), which was collected at the MV's eastern moat. Beneath the eastern moat, the boundary between the extrusive structure and the host sediments is characterized by a bright reflection zone (BR in Figure 3-3a). Similar bright reflection zones along the edge of the MV edifices are also observed in Figure 3-3b and 3-3d (marked with BR). As the central Dome 1 and Dome 2 of the Yuma MV are located in an interconnected caldera (Figure 3-2), the seismic line INS2\_Line13 across the central Dome 1 reveals the internal structure beneath the caldera area (Figure 3-3d). The upwards-bent, chaotic, enhanced reflections beneath the

moat-like depression at the top separate the Yuma extrusive edifice into two seismic facies: i) chaotic with high-amplitude reflections constrained to the caldera area (CF in Figure 3-3d); and ii) transparent along the slope area (TF in Figure 3-3d). A weak amplitude reflection of reversed polarity sometimes separates the two seismic facies (Figure 3-3c, 3-3d).

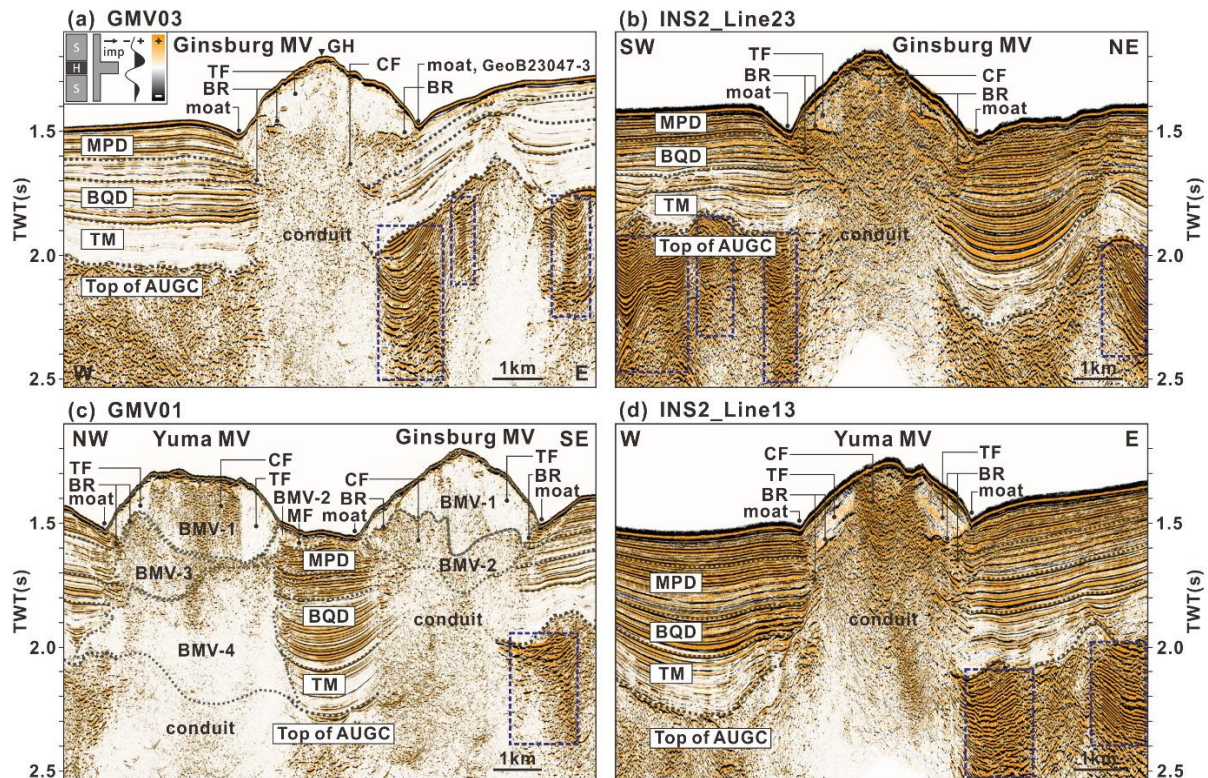


**Figure 3-3.** Seismic cross sections through the Yuma and Ginsburg MVs (see bold dark grey line in Figure 3-1b for location). Major discontinuities within Messinian-Quaternary sediments and *top of AUGC* (Allochthonous Unit of the Gulf of Cadiz) are shown: *MPD* mid-Pleistocene discontinuity, *BQD* base of Quaternary discontinuity, *TM* top of Miocene discontinuity. Two main seismic facies within the MV extrusive edifices have been defined: *TF* transparent facies and *CF* chaotic facies. The buried bicones of the Yuma and Ginsburg MVs are interpreted in Figure 3-3c, labeled as *BMV*, following Toyos et al. (2016). The location of gas hydrates recovered at the Ginsburg MV has been indicated as *GH* (Core AT206G/208G, Kenyon et al. 2000). The blue dashed boxes indicate the laterally-truncated bright reflectors at the top of the AUGC. Other abbreviations used in the figures are: *BR* bright reflector, *MF* mud flow, *TWT* two-way travel time.

### 3.4.3 Pore water geochemistry and modeling

For each MV, comprehensive sets of cores have been recovered from the summit to the rim, and pore fluids have been analyzed for their chemical and isotopic composition. The concentration-depth profiles for Na, Cl, K, Li, B and Sr for all study sites are shown in Figure 3-4.

While all measured elements do not vary with depth at the reference site of the Meknes MV

(away from the MV; GeoB23038-1), the fluids show depletion in Na, Cl and K and enrichment in B, Li and Sr, relative to seawater, at all of the Meknes MV sites (Figure 3-4b). The fluids from the summit show the strongest depletion or enrichment of element concentrations, while moving towards the rim site, the concentrations of Na, Cl, K, B, Li and Sr become closer to those at the reference site. East of the Yuma, Ginsburg and Rabat MVs, another reference site (GeoB23027-1; Table 3-1) shows pore fluids with a slight increase in salinity with depth. While the element concentrations from the summit of the Yuma and Ginsburg MVs follow the same trend as that in the Meknes MV, the pore water composition mirrors the bottom water chemical composition at the flank sites and shows marked differences at the rim sites (Figure 3-4c, 3-4d). Unlike the progressively changing fluid compositions across the Meknes MV, the Ginsburg MV fluids from the rim sites have diametrical changes compared to the summit ones, showing strong enrichment in Na, Cl and Sr, small enrichment in Li and depletion of B. A similar pattern is seen at the Milano MV in the Mediterranean Sea, showing Na and Cl depletion at the summit and an opposite trend at the rim, with the concentrations of K and Li at the rim exceeding those at the summit (Figure 3-4a). On the other hand, at the Rabat MV, apart from similar increasing Na and Cl trends at the rim, the element concentrations across the entire structure show minor fluctuations compared to seawater (Figure 3-4e).

Stable oxygen and hydrogen isotope analyses are summarized in Figure 3-5a and 3-5-b. At the MVs in both the Gulf of Cadiz and the Mediterranean Sea, there is a clear negative correlation between  $\delta^{18}\text{O}$  and  $\delta\text{D}$  (Figure 3-5a). While samples from the shallow subsurface have  $\delta^{18}\text{O}$  and  $\delta\text{D}$  values close to those of seawater, samples from greater depths tend to have more positive  $\delta^{18}\text{O}$  and negative  $\delta\text{D}$ . The strongest deviation from seawater composition occurs at the deepest summit samples. Pore water from the rim sites, however, follows the same trend but does not deviate strongly from seawater composition. One exception is core GeoB23047-3 at the rim of the Ginsburg MV, which shows a strong change to lighter  $\delta^{18}\text{O}$  and  $\delta\text{D}$  values from the surface to the base of the core. As the Yuma and Ginsburg MVs show considerable differences in Sr concentrations between their summit and rim sites (Figure 3-4c, 3-4d), we further analyzed their Sr isotopic ratios. The results are plotted in Figure 3-5c, illustrating similar  $^{87}\text{Sr}/^{86}\text{Sr}$  ratios in the range of 0.7085-0.7089.

In order to estimate the variation of advection velocity across the MV cores, an advection-diffusion model was used, with Cl as conservative parameter. The model-fitted curves, together with the measured data, are summarized in Figure 3-4 and the model parameters are given in Table 3-1. Apart from the Rabat MV, which has no fluid flow at both its summit and rim, the model results indicate high advection velocities of 129.2 cm/yr and 50.0 cm/yr at the summit sites of Meknes and Milano MVs respectively, and moderate values of 11.6-15.0 cm/yr and 2.8-15.0 cm/yr at the summit sites of Yuma and Ginsburg MVs, respectively. Overall, the advection velocities show a decreasing trend from the summit sites towards the rim sites. However, at the rim/moat of Milano and Ginsburg MVs, the fluids ascend at an estimated velocity of 1.5 cm/yr and 0.3 cm/yr, compared to absent flow at the flank of Ginsburg MV (GeoB23010-1) and Yuma MV (GeoB23012-1).

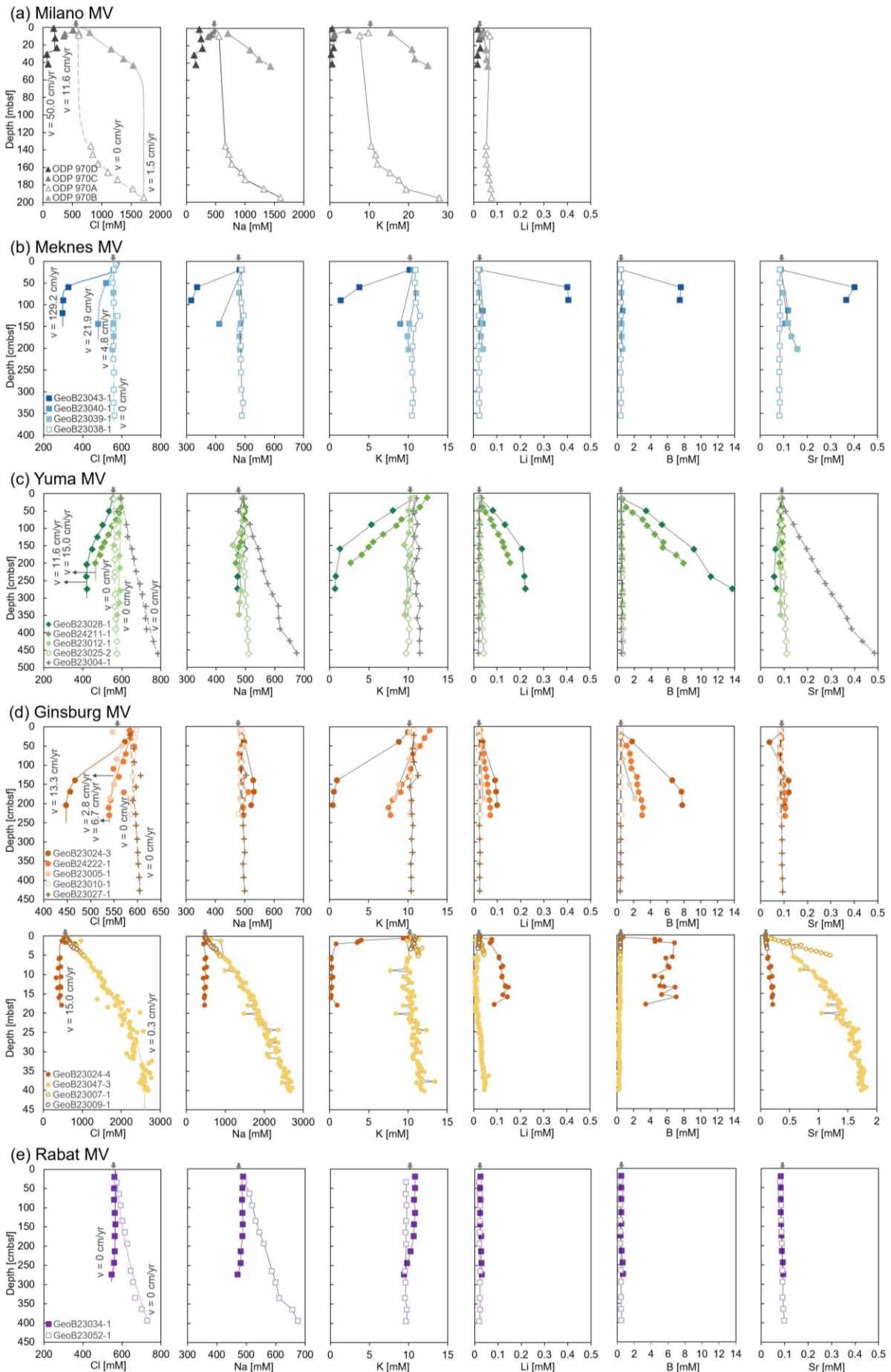


**Figure 3-4.** Pore water modeling results of Cl (shown in solid or dashed lines with fluid flow velocity values) and pore water depth profiles of Cl, Na, K, Li, B and Sr at the five MVs investigated in this study. Darker plot shades grading to lighter tone plots represent proximal (near central dome location) to distal (moat and off mud-volcano) sites. Vertical arrows (on x-axis) indicate seawater values.

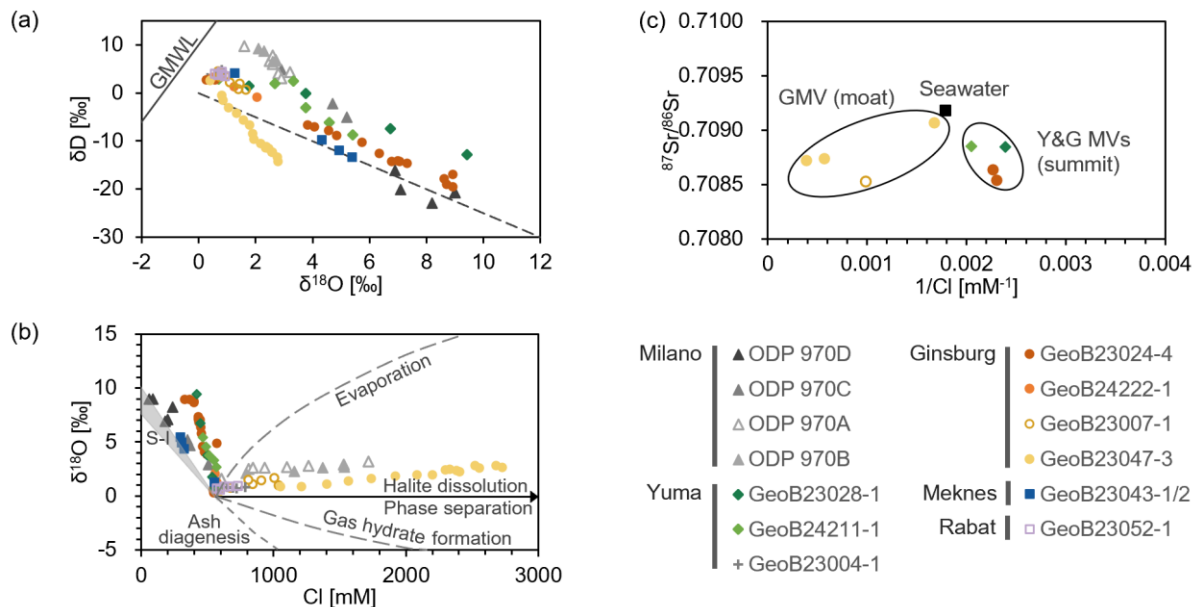


**Figure 3-5.** (a) Plot of  $\delta D$  vs.  $\delta^{18}O$  for MV fluids at study sites. The solid line represents the global meteoric water line (GMWL) (Craig, 1961). The dashed line represents the two-end member mixing between seawater ( $\delta D = 0$ ;  $\delta^{18}O = 0$ ) and clay-mineral-derived water ( $\delta D = -30$ ;  $\delta^{18}O = 12$ , Hensen et al., 2015). (b) Plot of  $\delta^{18}O$  vs. Cl concentration at study sites [modified after Haffert et al. (2013)]. The grey area for smectite-illite (*S-I*) transformation has lower and upper boundaries of  $\delta^{18}O = 7.5\text{‰}-10\text{‰}$ . (c) Plot of  $^{87}Sr/^{86}Sr$  vs.  $1/Cl$  for fluids at Yuma and Ginsburg MVs. The seawater value (black square) is shown for comparison. *GMV* Ginsburg MV, *YMV* Yuma MV.

## 3.5 Discussion

### 3.5.1 Fluid pathways: central conduit and rim system

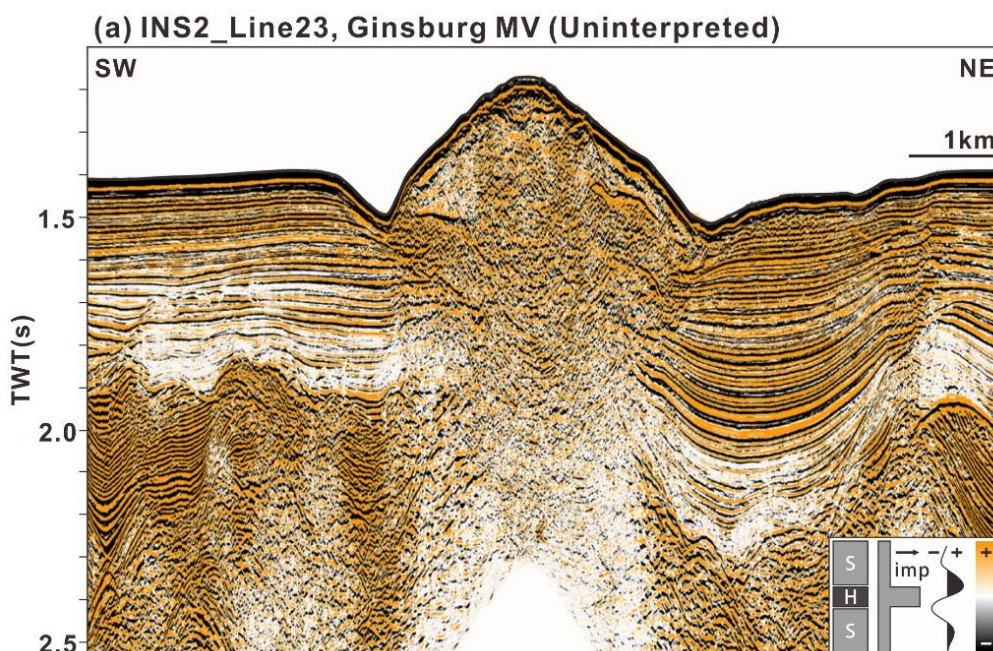
As demonstrated by the presented data, the Meknes, Ginsburg, Yuma MVs in the Gulf of Cadiz and the Milano MV on the Mediterranean Ridge show recent activity, with either a thin layer (< 3 cm) or absence of hemipelagic sediments on top of the mud breccia (Figure 3-2). Their chemical pore water compositions differ from seawater (Figure 3-4) and are hence to be attributed to seepage. On the other hand, Rabat MV is representative of a relatively long period of mud volcanic inactivity.

The seepage of deep fluids through MVs usually mix with bottom seawater close to the seafloor, thus being typically detectable in the upper section of a standard gravity core. This mixing process may cause different chemical gradients and pore water profiles in the sediments. Linear

pore water profiles attest that molecular diffusion is the dominant transport process in the sediments, usually occurring when seeping at MVs becomes inactive. In contrast, concave-down shaped profiles are related to a significant upward fluid advection, and concave-up profiles are commonly observed in e.g.  $\text{SO}_4^{2-}$  and  $\text{CH}_4$  due to their consumption by the anaerobic oxidation of methane (AOM). Concentration profiles of conservative elements (e.g. Na, Cl and B) for the recently active MVs have concave-down shapes (Figure 3-4), indicating the advective transport of deep fluids (Hensen et al., 2003). For each MV in our study, the most active sites of fluid advection are located at their summits, with upward fluid flow velocities varying over a wide range from 11.6 to 129.2 cm/yr. With increasing distance from the summit, the concentration gradient generally diminishes and the fluid flow velocities at the rim decrease to 0-4.8 cm/yr. This suggests that there is a central conduit through which the deep fluids are transported to the surface as confirmed by seismic data. While the Meknes MV shows a coherent geochemical change in elemental composition across the whole structure, similar to most previously reported cases (e.g., Vanneste et al., 2011; Haffert et al., 2013), the other three active MVs exhibit different characteristics. With respect to salinity, freshening at the summit (Cl depletion) vs. salinization at the rim/moat (Cl enrichment) is observed (Figure 3-4). For MVs in the Gulf of Cadiz and the Mediterranean Ridge, clay mineral dehydration has previously been identified as a major mechanism of fluid formation driving MVs emissions (Hensen et al., 2007; Xu et al., 2021), which causes a typical freshening signal. Nonetheless, the presence of brines/evaporites in both areas can significantly alter the diagenetic signal of the pore fluids, showing elevated salinities (Haffert et al., 2013). The high salinity observed at the rim/moat therefore indicates that the fluids experience different diagenetic processes or a different degree of mixing compared to those at the summit, suggesting the presence of an additional fluid pathway apart from the central conduit within these domes. This is further supported by the results from the modeled fluid flow velocities, as well as the distribution of enhanced reflections (bright spots) in the seismic data, characteristic of gas-bearing fluids. While the fluids from the central conduit do behave as reported in earlier studies on various MVs edifices (e.g., Vanneste et al., 2011), with fluid flow velocities rapidly decreasing from the highest value at the summit to 0 cm/yr at the flank, we recognize for the first time that advection also occurs at the rim/moat site in the Ginsburg and Milano MVs, reaching flow rates of 0.3 and 1.5 cm/yr respectively.

The high-resolution seismic profiles across Ginsburg and Yuma MVs clearly show both extrusive edifices and intrusive complexes, which clearly offer the geophysical support to explain the different geochemical patterns observed in the moat/rim area. Two distinct seismic facies are imaged in the extrusive MV edifices: a chaotic facies containing high-amplitude reflections, and a transparent facies which is seismically opaque. At both Ginsburg and Yuma MVs, chaotic acoustic facies occupy the majority of the extrusive edifice, especially in the central area, which is probably related to the fluid flow observed at the summit area (see also occurrence of gas hydrates on Ginsburg MV in Figure 3-3a). The transparent acoustic facies, however, is restricted to the flank areas overlying the chaotic acoustic facies, with bright negative polarity reflectors at their lower boundaries. Chaotic and transparent seismic facies

are expected in MV edifices given the significant presence of mud breccia (Figure 3-2) and mud mobilization structures. The presence of bright reflectors of negative polarity (i.e., downwards decrease in acoustic impedance) appears to indicate the significant presence of fluids, likely free gas, in areas characterized by chaotic facies within the MV body (particularly within the feeder system). Similar, yet more coherent, bright reflections have been imaged beneath the flanks of the Mercator MV in the Gulf of Cadiz, located to the east of the Ginsburg and Yuma MVs, and have been interpreted as bottom simulating reflectors (BSRs) by Depreiter et al. (2005). In our case, these bright negative polarity reflectors, which separate chaotic and transparent facies along the flank sites of the Ginsburg and Yuma MVs, may act as barriers to fluid flow, as attested by geochemical composition. Those sediments in the flank area (characterized by transparent acoustic facies) may represent paleo-mud flows that have already degassed and, together with the potential presence of gas hydrates as cementing material, can form a low-permeability barrier. In line with the geochemical observations of active fluid flow at the summit and absence of fluid flow along the flanks (Figure 3-4), these seismic signatures (Figure 3-3) further strengthen our interpretation. This highlights that already degassed “paleo-mud flows” may freely consolidate once the gas is released and develop lower porosities or, alternatively, that cooling of the interstitial fluids within the “paleo-mud flows”, allows the development of gas hydrates. Both situations result in the “paleo-mud flows” acting as flank seals, letting almost no fluids seep through. The hypothesized fluid circulation system at the moat area is represented in Figure 3-6. Consistent with the fluid flow detected at the moat sites, the background stratigraphy displays stacked enhanced reflectors beneath the moat, following the edge of the MV edifice (see BR in Figure 3-3 and orange area in Figure 3-6b). These stacked enhanced reflectors indicate upward fluid seepage of gas-enriched sediments, as detected in the pore water samples, and mark an additional fluid pathway within the edifice. Notice also that the shortest escape path (highest pressure gradient) for fluids within the main conduit is not through the main edifice, but at its rim, through the moat.



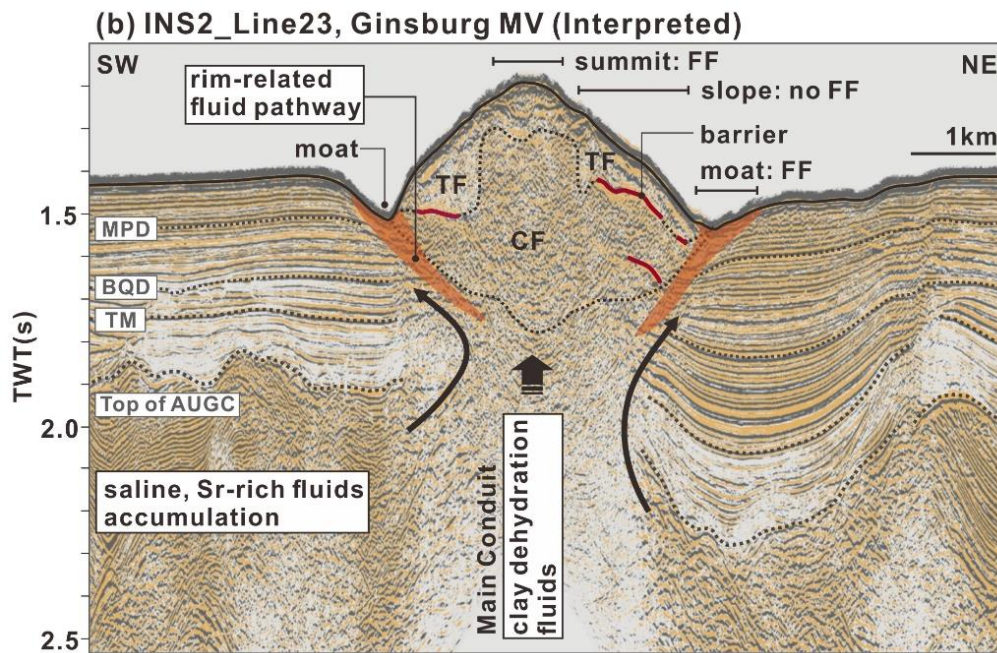


**Figure 3-6.** Uninterpreted (a) and interpreted (b) segment of seismic line INS2\_Line23 crossing the Ginsburg MV (see bold dark grey line in Figure 3-1b for location). Main conduit and rim-related fluid pathways along the edge of the extrusive edifice are indicated (orange areas). The curved black arrows show the rise of saline, Sr-rich fluids along the edge of the MV main conduit. *AUGC* Allochthonous Unit of the Gulf of Cadiz, *MPD* mid-Pleistocene discontinuity, *BQD* base of Quaternary discontinuity, *TM* top of Miocene discontinuity, *TF* transparent facies, *CF* chaotic facies, *FF* fluid flow, *TWT* two-way travel time.

### 3.5.2 Fluid sources

The fluids from the summit of the recently active MVs in both the Gulf of Cadiz and the Mediterranean Sea display typical geochemical characteristics of clay mineral dehydration, as evidenced by the freshening (Cl depletion) and distinct water isotope signatures (positive  $\delta^{18}\text{O}$  and negative  $\delta\text{D}$  values). Other geochemical signatures related to clay mineral dehydration, such as the uptake of K and the enrichment of fluid-mobile elements B and Li, can also be observed at the summit, while the increasing trend of Li concentrations at the Milano MV has been overprinted by the intense freshening. The smectite-to-illite transformation process has previously been identified as a major fresh water source in driving MV emissions in the region (Hensen et al., 2007), and occurred mainly in the terrigenous Upper Cretaceous-Miocene units. In the seismic data across Ginsburg and Yuma MVs, their central conduits are rooted within (or below) the AUGC (Figure 3-3), which we suggest serves as their root complex (although limited penetration does not allow to discard the possibility of a deeper source). Assuming a geothermal gradient of 30 °C/km for the upper accretionary prism of the Gulf of Cadiz (Grevemeyer et al., 2009) and 25 °C/km for the Olimpi MV field (Camerlenghi et al., 1995), clay mineral dehydration (60-150 °C) happens at depths of up to 5 and 6 km, respectively. The same depths coincide with the lower sedimentary units in the Gulf of Cadiz and the décollement in the Mediterranean Ridge (Deyhle and Kopf, 2001).

Since the moat fluids follow the same negative correlation of downcore  $\delta^{18}\text{O}$  increase and  $\delta\text{D}$  decrease, clay mineral dehydration clearly contributes to their pore water composition. Nonetheless, compared to the summit fluids, the moat/rim sites show less deviation from seawater composition, which could be related to a lower fluid ascend velocity. Chemically, in contrast to the freshening signature at the summit, the pore fluids from the moat/rim sites of Milano and Ginsburg MVs are highly saline. A significant contribution of residual brines can be ruled out as they normally cause an enrichment in both  $\delta^{18}\text{O}$  and  $\delta\text{D}$ , which is not observed here (Figure 3-5a, 3-5b). Halite dissolution is instead a possible source as it increases the Na/Cl ratio close to 1 and leaves the isotopic values unchanged, matching the observed characteristics. Additionally, the parallel enrichment of Sr with Cl for Ginsburg MV suggests a common fluid source for Sr and Cl, i.e. evaporite dissolution processes, at the moat sites. The fluids at Ginsburg MV contain less-radiogenic Sr that may be derived from dissolving gypsum and anhydrite minerals, as suggested by the high levels of both Ca and  $\text{SO}_4^{2-}$  at the sites (see *SI Appendix*, Figure S3-1). These calcium sulfate minerals are generally enriched in Sr due to the substitution of Sr by Ca and preserve the  $^{87}\text{Sr}/^{86}\text{Sr}$  record of contemporaneous seawater.

Due to a heterogeneous composition and internal deformation that form the accretionary wedge, the AUGC is seismically characterized by several seismic facies, and in most cases by chaotic reflectors (Medialdea et al., 2004). The seismic profiles across the Ginsburg MV show strong reflections within the host sediments of the AUGC, these laterally truncated bright reflectors at the top of the AUGC could possibly indicate gas-enriched fluid accumulations (see blue dashed boxes in Figure 3-3). The low amplitude Upper Miocene hemipelagic on top of the AUGC, likely fine-grained according to the seismic response, forms an unconformity trap for the gas-enriched fluids below. The AUGC, a mixture of Triassic to Neogene sedimentary units (Maldonado et al., 1999), contains Triassic evaporites which could fuel the saline, gas-(presumably methane; e.g., Nuzzo et al., 2019; Somoza et al., 2021b) and Sr-rich formation waters. Thus, the fluid accumulations in the AUGC may act as the source of saline fluids detected at the moat sites. In addition, the mobile element B is generally enriched in summit fluids due to desorption from clay minerals, consistent with intense fluid freshening, while B is scarce in the moat fluids. The low B concentration at the moat may also be explained by fluid formation under low temperature conditions. Alternatively, B depletion may be related to lower advective velocities, as B is strongly adsorbed to clays at low temperatures and most of the released B in the expulsion fluids can be re-absorbed or trapped by surrounding sediments during upward migration as the temperature decreases (You et al., 1995).

From the above reasoning, the moat fluids potentially consist of a mixture of three components: the predominantly saline, Sr-rich fluids, the clay dehydration fluids, and seawater. The saline, gas and Sr-rich fluids accumulated at the top of the AUGC are expected to migrate along the edge of the MV feeder conduit and extrusive edifices, taking advantage of this preferential pathway (Figure 3-6). During their ascent, the freshened fluids fueling the MVs are mixed with them at various degrees. In addition to the moat sites, the saline fluids have an influence on the summit sites; previous studies on the summit fluids at the Ginsburg MV show the presence of

halite leaching and gypsum/anhydrite overprinting the freshened fluids (Hensen et al., 2007; Xu et al., 2021), which is in agreement with a slight/no enrichment in less-radiogenic Sr.

In addition to the aqueous fluids, it is made evident in the seismic data that a significant component of the expelled interstitial fluids, both at the summit and moat, is gas (presumably methane). Similar to the aqueous fluid migration, this study suggests that the upper boundary of the AUGC is an intermediate trap and may fuel the gas migrating through the rim-related pathways toward the moat of the MVs. This is corroborated by the observation of biofilms in the MeBo core (GeoB23047-3) of the Ginsburg MV's eastern moat at a depth of 9.47-9.80 mbsf (see core description of GeoB23047-3 in et al., 2020). The depth at which the biofilm occurs generally corresponds to the sulfate-methane transition (SMT) depth, where the concentration of sulfate is depleted to near-zero (*SI Appendix*, Figure S3-1). Briggs et al. (2011) and et al. (2019) have reported such biofilms in fracture-dominated sediments with their vertical positioning close to the SMT depth, suggesting the production of the biofilm is closely associated with methane seeps. While thermogenic gases from dewatering sediments can be inferred, as evidenced by clay mineral dehydration contribution in moat fluids, whether there is coexisting microbial methane accompanying the shallower fluid accumulation deserves further investigation. In contrast, the origins of hydrocarbon gases feeding the summit have been extensively examined in many previous studies. Specifically in the Ginsburg MV's case, venting of thermogenic gases with different thermal maturities has been reported, which may be attributed to the presence of evaporitic deposits: i) clay mineral dehydration and thermogenic gas formation occur to a depth of approximately 4 km; and ii) further cracking of methane homologues (metagenesis) take place beneath salt deposits at greater depths (Nuzzo et al., 2009).

### **3.5.3 Role of rim-related fluid pathways during MV evolution**

In the evolutionary models of mud volcanoes (León et al., 2007, 2012; Menapace et al., 2017b), MVs episodically experience violent eruptions with edifice build-up, while interval phases of depletion and quiescence account for a large part of their life cycle (over 95-97%; Kopf and Behrmann, 2000; Menapace et al., 2019), characterized by reduced seepage activity and the development of moats.

The MVs investigated in this study are all in their depletion and quiescence phases, nonetheless, our results infer that they all have different “activity levels”. Among them, the Meknes MV is a relatively young structure in a depletion stage of mud volcanism, showing a flat summit with an absence of hemipelagic coverage and a minor or no moat at the base. The fluid seepage at the summit of the Meknes MV has a far higher flow velocity (129.2 cm/yr) than the other MVs reported here, which rapidly diminishes towards the periphery, indicating intense fluid emission fueled by the central conduit. In a more advanced stage of mud volcanism, the formation of moats at the base of the MV edifices is observed at the Milano, Yuma, and Ginsburg MVs, and is generally related to a depleted mud reservoir and a volume loss at depth in the phase of reduced seepage activity (Camerlenghi et al., 1995; Van Rensbergen et al., 2005;

Kirkham et al., 2018). Compared to the Meknes MV, the Milano, Yuma, and Ginsburg MVs have reduced fluid flow velocities at their summit sites and, more importantly, the development of moats provides an additional, shallower fluid circulation system within these features. Lastly, the Rabat MV, which has a thick layer of hemiplegic sediment in the summit core, has experienced a longer period of inactivity and is in a quiescent stage. While there is currently no evidence for upward advection on its summit, diffusion of saline fluids has been reported at its moat area.

Throughout the depletion and quiescence stages of MV evolution, the formation of a moat provides a conduit along the edge of the MV feeder channel and extrusive edifices where the pressure gradient is maximal and fluids preferentially ascend. Shallow fluid sources present around the MVs could significantly contribute to the MV fluid circulation system taking advantage of this additional pathway. Based on the modeled fluid velocities and bathymetry data, we calculated the flow rate in the moat area of the Ginsburg MV, in order to compare it to the summit area (central dome, Figure 3-7). The moat area extends from the MV base to the point with maximum curvature which separates it from the undeformed seafloor (Figure 3-7). The calculated flow rate in the moat area (estimated at  $1.5 \times 10^4 \text{ m}^3/\text{yr}$ ) demonstrates how significant it is compared to the flow rate calculated for the summit region, reaching an estimated at  $1.3 \times 10^4 \text{ m}^3/\text{yr}$ . These findings emphasize the crucial involvement of the moat area in the fluid circulation system of the MV, implying that the rim-related fluid pathway may contribute substantially to fluid emissions since depletion and quiescence periods prevail. While fluid seepage at both the summit and moat areas has much lower flux rates during periods of depletion and quiescence, the generally short-lived and intense nature of the eruptive phases results in these two phases making a comparable contribution to the global fluid and element budget.

Several previous studies estimate methane emission through MVs; among them Milkov et al. (2003) reported  $\sim 1.59 \times 10^{13} \text{ g/yr}$  during quiescent periods and  $\sim 1.71 \times 10^{13} \text{ g/yr}$  during eruptions. Moreover, field measurements of the methane flux on onshore MVs suggest that diffuse and invisible degassing surrounding the vents (mini- and micro-seepage, e.g., Etiope et al., 2002; Spulber et al., 2010) may result in higher gas emissions to the atmosphere compared to focused emissions in visible manifestations like craters (macro-seepage) (Etiope et al., 2007; Hong et al., 2013). According to Etiope et al. (2011), mini-seepage accounts for >75% of the total methane emissions for the Tokamachi MVs in Japan. Due to their widespread and extended presence throughout the structure, as well as their longer-lasting activity, mini- and micro-seepage can be more significant than macro-seepage, which is more commonly associated with eruptive events, a mere snapshot in the life span of MVs. However, previous estimates of methane flux from offshore MVs only considered macro-seepages, and mini-/micro-seepage of methane is expected to be insignificant due to oxidation and dissolution processes. Our findings in the moat area suggest that this sort of mini-/micro-seepage site in the MV structure must be re-evaluated as an important fluid emission feature which has the

potential, during non-active MV phases, for considerable fluid flux. Though methane flux is constrained by the AOM process, as confirmed by the occurrence of biofilm in our core, aqueous fluid flux plays a vital role in facilitating the transfer of elements from the lithosphere to the hydrosphere. Furthermore, for onshore MVs, this study can offer valuable insights into mini-/micro-seepage sites such as moat areas, and their evolution stages, particularly during depletion periods when the moat is forming. These aspects should be the primary focus of attention for further research.

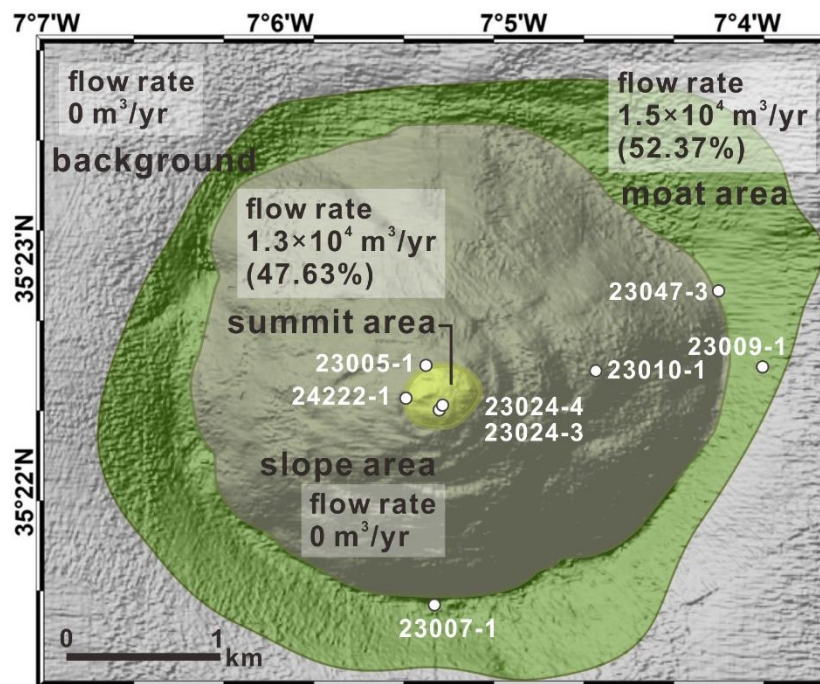


**Figure 3-7.** Geomorphological features used for flux estimation marked on the bathymetric map of Ginsburg MV. Locations of sampled sediment cores are indicated as white dots.

### 3.6 Conclusions

Anomalous salinity patterns (freshening at the summit vs. salinization at the moat) were detected at the Yuma, Ginsburg and Milano MVs, spanning from the Gulf of Cadiz into the eastern Mediterranean Sea and providing the initial scientific curiosity for this study. Fluid geochemistry, pore water modeling and high-resolution seismic data have been used to propose a model that explains the fluid circulation patterns behind these pore water signatures. The freshening signature at the summit of the MV structures is fueled by the clay dehydration process at depth up to 5-6 km, which moves along the central conduit and is generally constrained to these areas. The saline pore fluids at the moat/rim sites are instead related to shallower fluid accumulations, where the fluids' geochemistry is strongly affected by the widely distributed evaporites in both the Gulf of Cadiz and Mediterranean Ridge. Seismic data allows to infer that both fluid pathways channel a significant amount of methane. In particular, seismic imaging of the Ginsburg MV reveal that the additional fluid sources for the moat sites are probably trapped at the top of the AUGC by the overlying fine-grained Upper Miocene sediments, and migrate through the edge of the MV feeder conduit and the extrusive edifices.

While younger MVs demonstrate a strong influence of clay dehydration across the whole structure with a higher fluid velocity at the moat sites, the inactive MVs present different flow characteristics. This suggests that the rim-related fluid pathways are occupied by the freshening fluids during an early development stage of the MV structures, while further (shallow) fluid source(s) could contribute to the MV fluid circulation system and dominate the fluid composition through this additional pathway, especially during a later evolutionary stage when the moat is being developed. The calculated flow rates at the moat area, in the Ginsburg MV case study, indicate that the rim-related fluid pathways have an important significance in MV fluid circulation, showing a generally equivalent or even higher contribution to fluid emission compared to the summit area. Similar to terrestrial MVs areas away from summit sites, degassing through mini- and micro-seepage, this study on marine MVs further highlights that moat/rim areas, as mini-/micro-seepage sites, provide an important contribution to the global fluid budget, as well as to the global element budget. Given our overall findings, we advise to not only sample and study the summit areas of MVs, but also the peripheric systems of these complex, fascinating structures, in order to boost our understanding of cold seep systems and global geochemical balances.

### Supplementary material

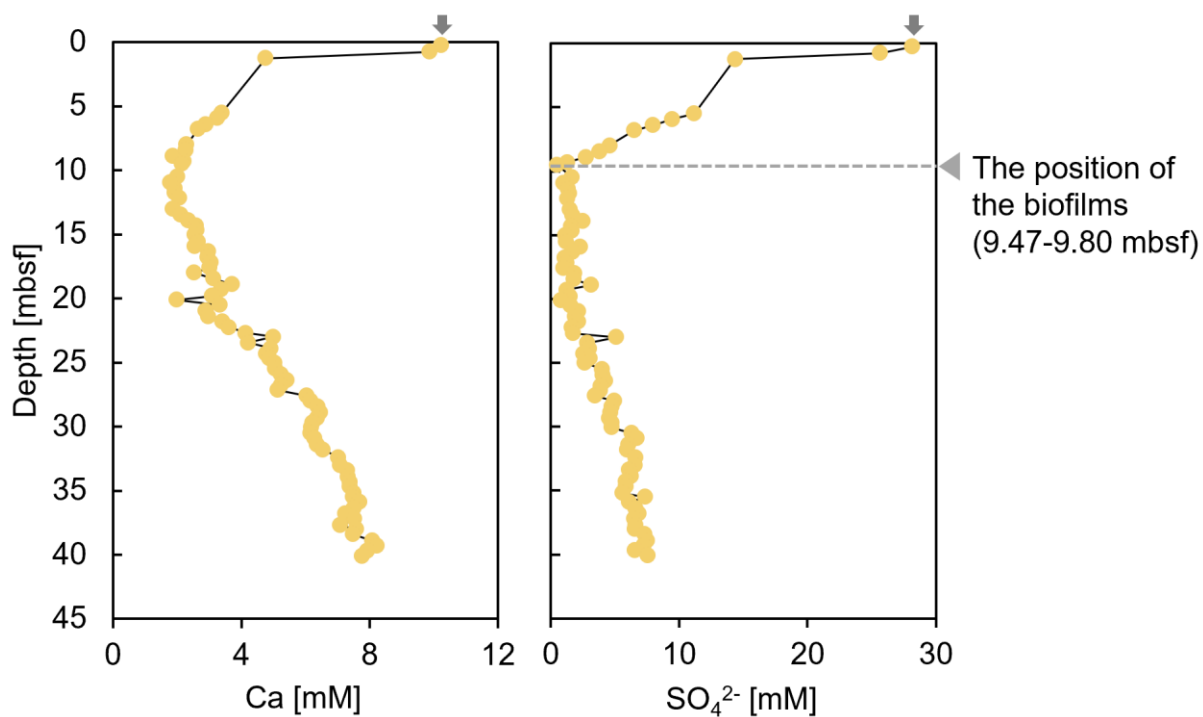


**Figure S3-1.** Pore water depth profiles of Ca and SO<sub>4</sub><sup>2-</sup> in the MeBo core (GeoB23047-3) of the Ginsburg MV's eastern moat. Vertical arrows (on x-axis) indicate seawater values. The dashed grey line in sulfate profile indicates the biofilm's location.

## Chapter 4

### Ascent of fluids through km-thick sedimentary cover links to active tectonics in the Gulf of Cadiz

Shuhui Xu<sup>a,b,1\*</sup>, Walter Menapace<sup>c,d,1</sup>, Andre Hüpers<sup>a</sup>, and Achim Kopf<sup>a,b</sup>

<sup>a</sup> MARUM – Center for Marine Environmental Sciences, University of Bremen, 28359 Bremen, Germany

<sup>b</sup> Department of Geosciences, University of Bremen, 28359 Bremen, Germany

<sup>c</sup> ICM-CSIC, Institute of Marine Sciences, 08003 Barcelona, Spain

<sup>d</sup> Institute of Geology, University of Innsbruck, 6020 Innsbruck, Austria

Corresponding author: Shuhui Xu ([sxu@marum.de](mailto:sxu@marum.de))

<sup>1</sup>S.X. and W.M. contributed equally to this work.

#### Abstract

Transform faults (TFs) represent important structures defining strike-slip boundaries between tectonic plates. The Gulf of Cadiz (GoC) hosts the easternmost part of a major North Atlantic TF system which defines the Africa-Eurasia plate boundary in the region, the South West Iberian Margin (SWIM) faults zones. Along this boundary are scattered abundant fluid seepage structures, most of which are associated to the faults' surficial expressions.

Here, we examine fluid geochemistry and in-situ heat-flow data to investigate the origin and distribution of fluid circulation in the GoC accretionary wedge. We show an intense interaction of the ascending fault fluids with Triassic evaporites at depth, as they present high Na, Cl, Ca, Br with decreasing Br/Cl and less radiogenic  $^{87}\text{Sr}/^{86}\text{Sr}$ , compared to present-day seawater values. When related to an evaporitic endmember from a nearby pockmark site, fault fluids exhibit more radiogenic  $^{87}\text{Sr}/^{86}\text{Sr}$  (0.7084-0.7087), suggesting amounts of continental crust fluids are admixed. Ternary mixing model indicates that up to 22% of the deep fluids expelled might be traced back to a crustal origin. Physically, deep fluid circulation is further supported by the anomalously high heat-flow values at the seafloor, when crossing the fault trace (73.3-121.9 mW/m<sup>2</sup>). We therefore present first evidence of active flow in the SWIM faults and crustal-scale fluid exchange spanning from the Horseshoe Abyssal Plain to the upper accretionary wedge. This study is advancing our understanding of the deep hydrologic cycle in transform-type plate boundaries, which is critical to define active tectonic patterns, fluid pathways and element exchange between geosphere and hydrosphere.

## Significance Statement

Since their discovery in the 1960s on the Atlantic seafloor, transform faults (TFs) have been identified all over the globe. These strike-slip fault zones accommodate the lateral movement of adjacent tectonic plates and can exist both in continental and oceanic lithosphere. While continental TFs are relatively well studied (i.e., San Andreas Fault), less is known about oceanic TFs due to limited accessibility. This work investigates the fluid-rock interaction in the easternmost Azores-Gibraltar Fracture Zone, providing evidence of fluid flow originating at several kilometers below the seafloor. The findings help characterize the Africa-Eurasia plate boundary in the region, further contributing to the thought of oceanic TFs as important settings for deep-sourced fluid flow circulation and their impact on global mass balances.

## 4.1 Introduction

Fluid discharge at the seafloor is a widespread natural process, which has a significant impact on the chemical and biological composition of the ocean, additionally influencing plate tectonics and slope stability (Judd and Hovland, 2007). In most cases, the emitted fluids have a distinct chemical composition resulting from various water-rock reactions at depth, which leads to element exchanges between the lithosphere and the ocean. While scientific research regarding fluid discharge has mostly been conducted on divergent and convergent plate boundaries, i.e., hydrothermal vents at mid-ocean ridges (Elderfield and Schultz, 1996) and cold seeps/mud volcanoes (MVs) in subduction zones (Mazzini and Etiope, 2017; Menapace et al., 2017b), the reported findings at transform plate boundaries are still limited (Hensen et al., 2019). Nonetheless, as strike-slip faults provide favourable conduits for vertical fluid flow due to their stress regime (Tobin et al., 1993), the transform-type plate boundaries, which consists largely of strike-slip faults, are expected to focus fluid discharge like the other types of plate boundaries. On the ocean floor, transform faults (TFs) are the loci of intense seismic activity and large earthquakes such as the 2012  $M_w$  8.6 Sumatra-Wharton Basin earthquake (Hill et al., 2015) and the 1941  $M_w$  8.4 Gloria Fault earthquake (Baptista et al., 2016). Fluid-related processes play an important role in the occurrence of seismicity (Hensen et al., 2019): fluid flow can affect the stress state thus determining the fault strength (Saffer and Tobin, 2011) and fluid-rock interactions can alter the composition of fault material, which is a key factor controlling the frictional properties of faults (e.g., Lauer et al., 2017). Therefore, fluid seepage in transform systems is closely related to tectonic activity and earthquakes.

The Atlantic segment of the Africa-Eurasia plate boundary named the Azores-Gibraltar fracture zone (AGFZ) is a prominent transform system (Figure 4-1). At the easternmost segment of the AGFZ, a set of WNW-ESE trending strike-slip faults, the South West Iberian Margin (SWIM) faults zone, cuts across the Gulf of Cadiz (GoC) and has been proposed as one of the candidate sources for the 1755 Great Lisbon earthquake (Zitellini et al., 2009). Along the SWIM faults, widespread fluid emissions features like MVs and pockmarks have been reported from the upper accretionary wedge to the Horseshoe Abyssal Plain (Baraza and Ercilla, 1996; Pinheiro et al., 2003; Xu et al., 2021), and the role of strike-slip faults to serve as pathway for the

ascending fluids has been established only for the deep-sea area, outside the GoC accretionary wedge (Hensen et al., 2021). While there the fluid circulation along the SWIM faults has been speculated to originate in oceanic crust older than 140 Ma (Scholz et al., 2009; Hensen et al., 2015, 2021; Schmidt et al., 2018), no crustal-sourced fluid flow has been reported in the upper accretionary wedge, where the ocean-continent transition crust is concealed beneath up to 13 km thick sediments (Thiebot and Gutscher, 2006). Furthermore, the role of the strike-slip faults in the upper accretionary wedge (Figure 4-1) is still debated, since active tectonic (prolongation of the SWIM faults) or gravitative deformation (surficial structures unrelated to the SWIM faults) have been both identified as possible mechanisms (Zitellini et al., 2009; Crutchley et al., 2011; Somoza et al., 2021a). In this study, we present the first direct evidence of active fluid flow along the easternmost segments of the SWIM1 fault and investigate the origin and distribution of the fluid circulation in the tectonic structures of the upper accretionary wedge.

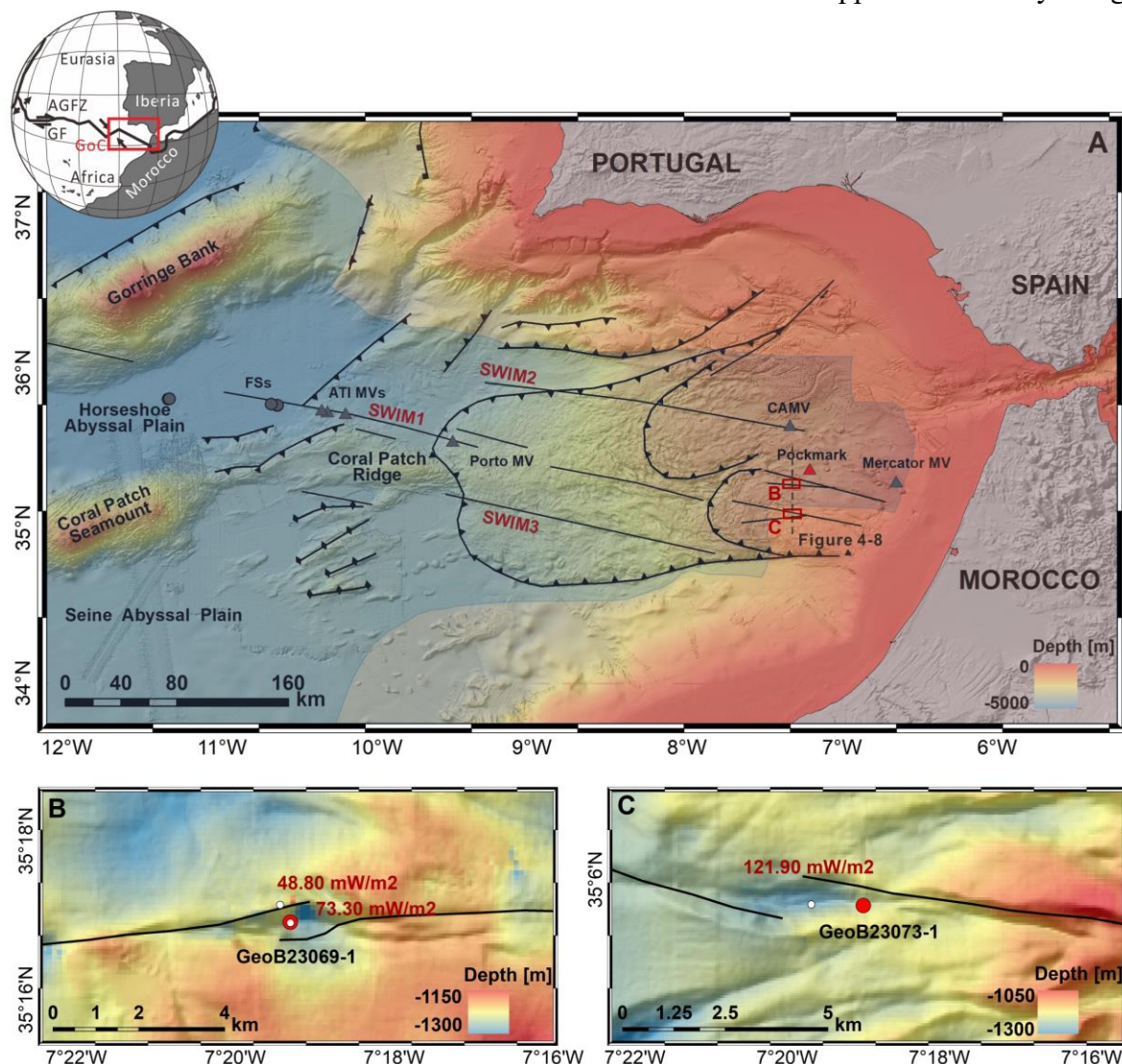


**Figure 4-1.** (A) Bathymetry map of the GoC with its main tectonic features. 50 m grid collected during the expeditions M149 and M167. The core sites used in this study (*SI Appendix*, Table S4-1) are shown as red triangles (gravity core) and red dots (MeBo cores in Figure 4-1B, 4-1C). Other MVs and flower structure sites are shown as grey triangles and grey dots, respectively. The dashed line shows the inset location of Figure 4-8. The main crustal domains

defined by Martinez-Loriente et al. (2014) are grouped into continental affinity and oceanic affinity and shown in faded colors of pink and blue respectively. Other abbreviations used in the figures are: *GF* Gloria Fault, *CAMV* Captain Arutyunov MV, *ATI MVs* Abzu-Tiamat-Michael Ivanov MVs, *FSs* flower structure sites. (B-C) Detail of the pull-apart basin formed along the SWIM fault zones with sites of MeBo cores (red dots) and heat-flow measurements (white dots).

## **4.2 Materials and methods**

### **4.2.1 Bathymetry**

The bathymetric data of the GoC were acquired during cruises M149 (in 2018) and M167 (in 2020) onboard R/V Meteor, using the Kongsberg Simrad EM122 multibeam system operated at a frequency of 12 kHz with 432 beams per ping. Further information about the technical specifications of the instrument is given in Hüpers et al. (2020) and Menapace et al. (2021). Monitoring and quality control of the data was conducted with the Kongsberg Seafloor Information System (SIS). The multibeam data were processed using the programs MB-System and Generic Mapping Tool (GMT) and visualized by ArcGIS software. The pixel resolution of the bathymetric maps is 50×50 m for both the main study area map and the insets with the individual structures.

### **4.2.2 Heat flow**

During the M149 cruise, heat flow measurements were conducted on the pull-apart basins along the SWIM1 faults by using the 6 m long heat flow probe of the University of Bremen. The heat probe is equipped with 21 thermistors over a 5.2 m long sensor tube and has a classical “violin bow” design (Hyndman et al., 1979). To measure the in situ thermal conductivity, a heater wire which can generate high energy heat pulses is installed on the heat probe. For each measurement, the heat probe firstly penetrates the seafloor and then stays in the sediments for 7-8 minutes to equilibrate to in situ temperatures. After equilibration, the heat probe takes 8 additional minutes to wait for the heat pulse decay. The temperature sensors have an accuracy of 1 mK. Detailed description of heat flow measurements can be found in Hüpers et al. (2020).

### **4.2.3 Sediment coring and pore water sampling**

During cruises M149 and M167, two MeBo cores (GeoB23069-1, GeoB23073-1) were taken along the path of the SWIM1 faults and one gravity core (GeoB24208-1) was recovered from a pockmark structure. Gravity cores were taken using a corer which utilizes a 5.75 m-long steel barrel with a plastic liner inside, while MeBo cores were sampled by a remotely operated seafloor drill-rig, the MARUM-MeBo70 (Hüpers et al., 2020; Menapace et al., 2021). The MeBo core barrel is only 2.5 m, but MeBo cores can be recovered using a wire locked to the inner core barrel with an overshot, process during which the outer drill string stays in the drilling hole (Freudenthal and Wefer, 2007). Therefore, long cores up to 70 m can be obtained by the MARUM-MeBo70 with the wire-line coring technique. After retrieval on deck, the plastic liner was removed from the core barrel, cut into 1.5 m (MeBo cores) or 1.0 m (gravity

cores) sections, sealed with plastic caps and labelled. Right after that, electric driller was used to make small holes on the plastic liner and the pore water was extracted from whole-rounds with Rhizon samplers attached to syringes following Dickens et al. (2007). For MeBo cores, three pore water samples were taken every 120 cm, whereas the sampling frequency for gravity cores is three samples per 100 cm. 20 ml air-tight PTFE vials were used to store the pore water specimens in a 4 °C cool room prior to laboratory measurements.

#### 4.2.4 Chemical analyses

The collected pore water samples were analyzed for their ion compositions in the shore-based laboratories at MARUM (GeoB23069-1, GeoB23073-1) and GEOMAR (GeoB24208-1), with an Inductively Coupled Plasma Optical Emission Spectrometer (ICP-OES) and an Ion Chromatograph (IC). The ICP-OES was used to determine the soluble cation concentrations (Na, K, Ca, Mg, B, Li and Sr). Before ICP-OES measurements, pore water samples were firstly acidified with concentrated HNO<sub>3</sub> to dissolve the solids precipitated during storage, and then diluted with 1% HNO<sub>3</sub> to suitable concentrations. Instead, the anion concentrations (Cl<sup>-</sup>, Br<sup>-</sup> and SO<sub>4</sub><sup>2-</sup>) were determined by IC. To avoid the addition of anions to pore water, the samples were firstly centrifuged, and the precipitates removed. Subsequently, the pore water samples were diluted with Milli-Q water and finally measured.

#### 4.2.5 Isotopic analyses

Water isotopes of fluids were analyzed in the MARUM Inorganic Geochemistry Lab at the University of Bremen, using a Cavity Ring-Down Spectrometer. The measured values are reported relative to Vienna Standard Mean Ocean Water (V-SMOW) with a precision (2σ) of ±0.8‰ for δD and ±0.25‰ for δ<sup>18</sup>O. Sr isotopes were measured in the Marine Isotope Geochemistry Lab at GEOMAR with a Thermal Ionization Mass Spectrometer. Based on Sr concentrations from ICP-OES measurements, ~1.5 μg Sr per sample was separated for samples through ion exchange chromatography using a SrSpec resin (Eichrom). Repeated tests on strontium carbonate isotopic standard NIST SRM 987 yield a reproducibility of 0.000004 (2SE, n=4). All the results were corrected for decay of <sup>87</sup>Rb and normalised to a value of 0.710248 for NIST SRM 987 (McArthur et al. 2004). The 2SE uncertainties for all the measurements are < 0.000023.

#### 4.2.6 Fluid mixing models

In this study, fluid mixing models based on Sr concentration and the <sup>87</sup>Sr/<sup>86</sup>Sr isotope ratio were used to evaluate different fluid sources. Both binary and ternary mixing models were considered. In the plot of <sup>87</sup>Sr/<sup>86</sup>Sr vs 1/Sr, fluids resulting from binary mixing fall along a line between the two endmembers (Wang et al., 2020), while those from ternary mixing lie in a triangle. The triangle is constructed by connecting the binary mixing lines of any two of the three endmembers. The contribution of each component can be quantified with ternary mixing simultaneous equations for the three endmembers:

$$X_A + X_B + X_C = 1 \quad e. q. (4.1)$$

$$C_{Mix} = C_A \cdot X_A + C_B \cdot X_B + C_C \cdot X_C \quad e. q. (4.2)$$

$$R_{Mix} = \frac{C_A \cdot X_A \cdot R_A \cdot (R_B + 1) \cdot (R_C + 1) + C_B \cdot X_B \cdot R_B \cdot (R_A + 1) \cdot (R_C + 1) + C_C \cdot X_C \cdot R_C \cdot (R_A + 1) \cdot (R_B + 1)}{C_A \cdot X_A \cdot (R_B + 1) \cdot (R_C + 1) + C_B \cdot X_B \cdot (R_A + 1) \cdot (R_C + 1) + C_C \cdot X_C \cdot (R_A + 1) \cdot (R_B + 1)} \quad e. q. (4.3)$$

where  $X$  is the proportion (i.e., contribution) of each endmember,  $C$  is the Sr concentration,  $R$  is the  $^{87}\text{Sr}/^{86}\text{Sr}$  isotopic ratio, and the subscript  $A$ ,  $B$ ,  $C$  and  $Mix$  denote the three endmembers and their mixed fluids with the predetermined proportion  $X$  for each component. For binary mixing, it suffices to assign a proportion  $X = 0$  to one of the endmembers.

### 4.3 Results

As pore fluid movement affect the thermal structure of the seafloor sediments, surface heat flow distribution is a sensitive tracer for fluid discharge at the seafloor. For example, heat flow anomalies caused by pore fluid movement have been reported in subduction zones, transform faults and active fluid venting structures (Lachenbruch et al., 1980; Yamano et al., 1992; Vogt et al., 1997). In order to find out if the easternmost segments of the SWIM1 fault is currently discharging fluids, heat flow measurements have been performed at two pull-apart basins on different fault segments (Figure 4-1). For further tracing and constraining fluid sources, the composition of pore waters sampled from sediment cores recovered during Meteor cruises M149 and M167 including measurements of H, O and Sr isotopes are used in this manuscript. Fault fluids are from 2 MeBo cores (GeoB23069-1, GeoB23073-1), which sampled two different pull-apart basins on the SWIM1 fault segments (Figures 4-2A and 4-3). MeBo is a seafloor drill rig remotely operated from a research vessel deployed during the M149 in addition to the gravity corer (see M149 Cruise Report, et al., 2020). The gravity core data shown in Figures 4-2B and 4-3 are from a nearby pockmark site (Figure 4-1; also see M167 Cruise Report, Menapace et al., 2021), where its chemical and isotopic composition is selected for comparison with the fault sites, and are correlated to previously published data from MVs distributed across the GoC (Hensen et al., 2007, 2015; Scholz et al., 2009; Haffert et al., 2013).

In the central area of the two pull-apart basins, high heat flow values of 73.30 mW/m<sup>2</sup> and 121.90 mW/m<sup>2</sup> were obtained near two sites selected for MeBo coring, GeoB23069-1 and GeoB23073-1 respectively (Figure 4-1B, 4-1C and *SI Appendix*, Table S4-1), while the northern margin of the northernmost basin showed a heat flow of 48.80 mW/m<sup>2</sup>, consistent with background values in the region. The background heat flow in the upper accretionary prism reported from the literature is 45 mW/m<sup>2</sup> (Grevemeyer et al., 2009).

Pore water profiles of major and minor ions present differences between the fault sites and other fluid emission structures (Figure 4-2). Similar to the trends on the MVs, the pockmark pore fluids show a general decrease in  $\text{SO}_4^{2-}$ , Ca, Mg, K and Br and an increase in B, Li, and Sr with depth. While most MVs show typical clay dehydration signals (Cl depletion), the pockmark site displays increasing Na and Cl concentrations with Na/Cl ratios close to one, similar to that observed at the Mercator MV (Haffert et al., 2013). In contrast, pore fluids from

the faults show major differences in chemical composition. Due to the greater drilling depth of MeBo (compared to conventional gravity coring), the fraction of deep fluid signals is greater thus offering a better understanding of the fluid-mixing processes. These fluids are considerably enriched in Na and Cl and have low Br/Cl ratios of  $0.79 \times 10^{-3}$  (GeoB23069-1) and  $0.52 \times 10^{-3}$  (GeoB23073-1) in the deepest samples (*SI Appendix*, Figure S4-1). While  $\text{SO}_4^{2-}$  depletion is also observed in fault fluids, the behaviour of Ca, Mg, K, Br and B is different from the trends observed in MV fluids. The fault fluids show no enrichment or even depletion of the fluid-mobile element B, and strong enrichment of Ca, Li and Sr.

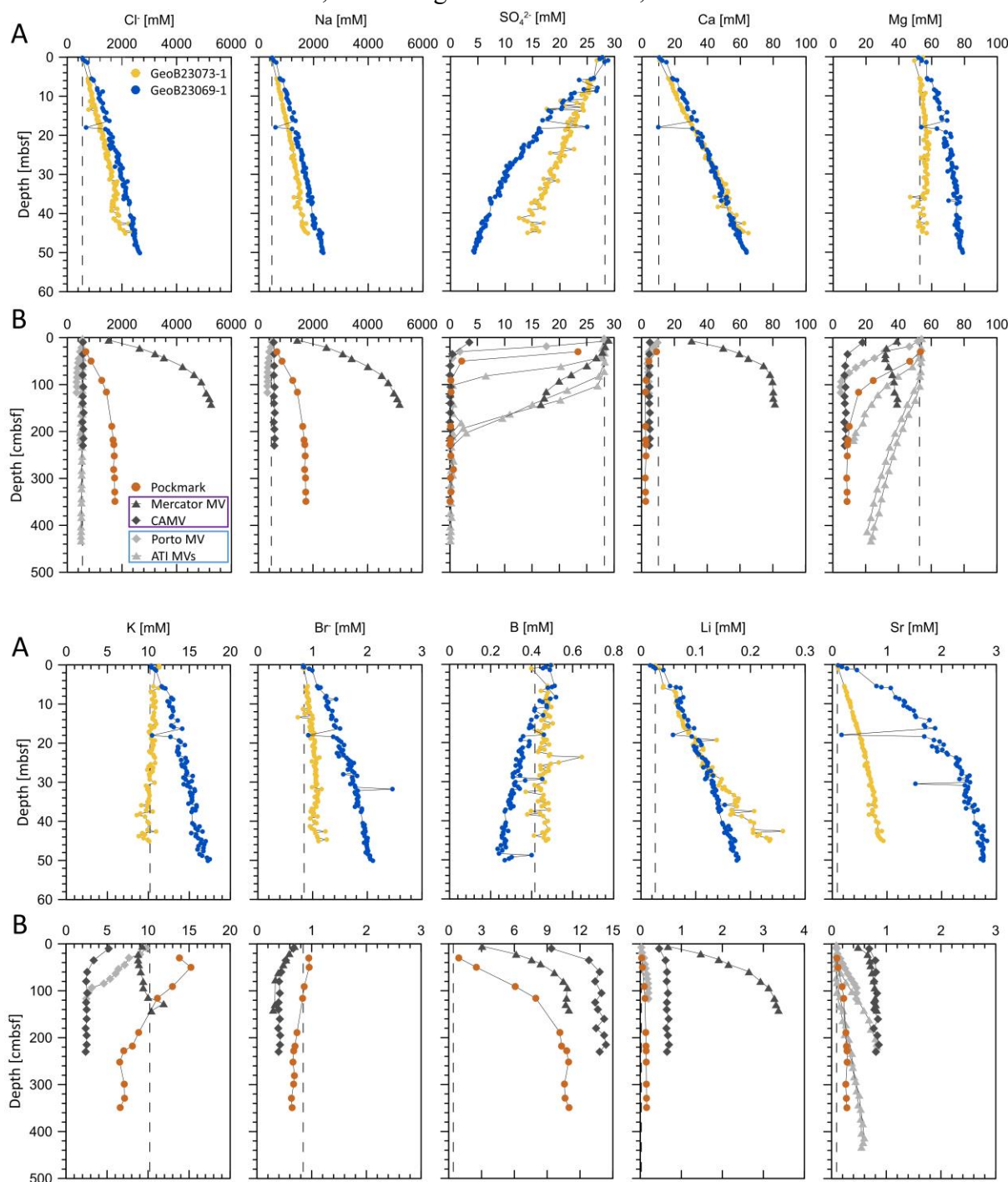


**Figure 4-2.** Pore water profiles of  $\text{Cl}^-$ , Na,  $\text{SO}_4^{2-}$ , Ca, Mg, K, Br, B, Li and Sr in sediment cores from fault sites (A) and pockmark site with literature data of other MVs (B). Dashed lines

indicate seawater values. Data for the Mercator MV, CAMV, Porto MV and ATI MVs are from Haffert et al. (2013), Hensen et al. (2007), Scholz et al. (2009) and Hensen et al. (2015). Violet square represents proximal MVs, while light blue one represents distal MVs.

Results of water isotope analyses are summarized in Figure 4-3A together with previously published data from proximal MVs (Mercator and CAMV, close to mainland Morocco) and distal MVs (Porto and ATI MVs, close to or on the abyssal plain) (Hensen et al., 2007, 2015; Haffert et al., 2013). The end member fluids from the pockmark show positive  $\delta^{18}\text{O}$  (5.13‰ to 6.25‰) and negative  $\delta\text{D}$  values (-13.33‰ to -16.01‰), consistent with the trend depicted from previous findings on MVs. However, pore waters from the fault sites do not deviate much from the seawater composition with  $\delta^{18}\text{O}$  and  $\delta\text{D}$  values between +0.06‰ to +0.57‰ and -7.98‰ to +3.10‰, respectively (Figure 4-3A). The Sr concentration and isotopic composition of pore fluids are plotted in Figure 4-3B. Previous studies reported high radiogenic Sr isotopic compositions for proximal MVs (Haffert et al., 2013) and low radiogenic Sr isotopic compositions for distal MVs (Hensen et al., 2015) compared to seawater values, whereas the pore fluids of pockmark and fault sites analyzed in this study display  $^{87}\text{Sr}/^{86}\text{Sr}$  ratios in the range of 0.7083-0.7089 below that of modern seawater.

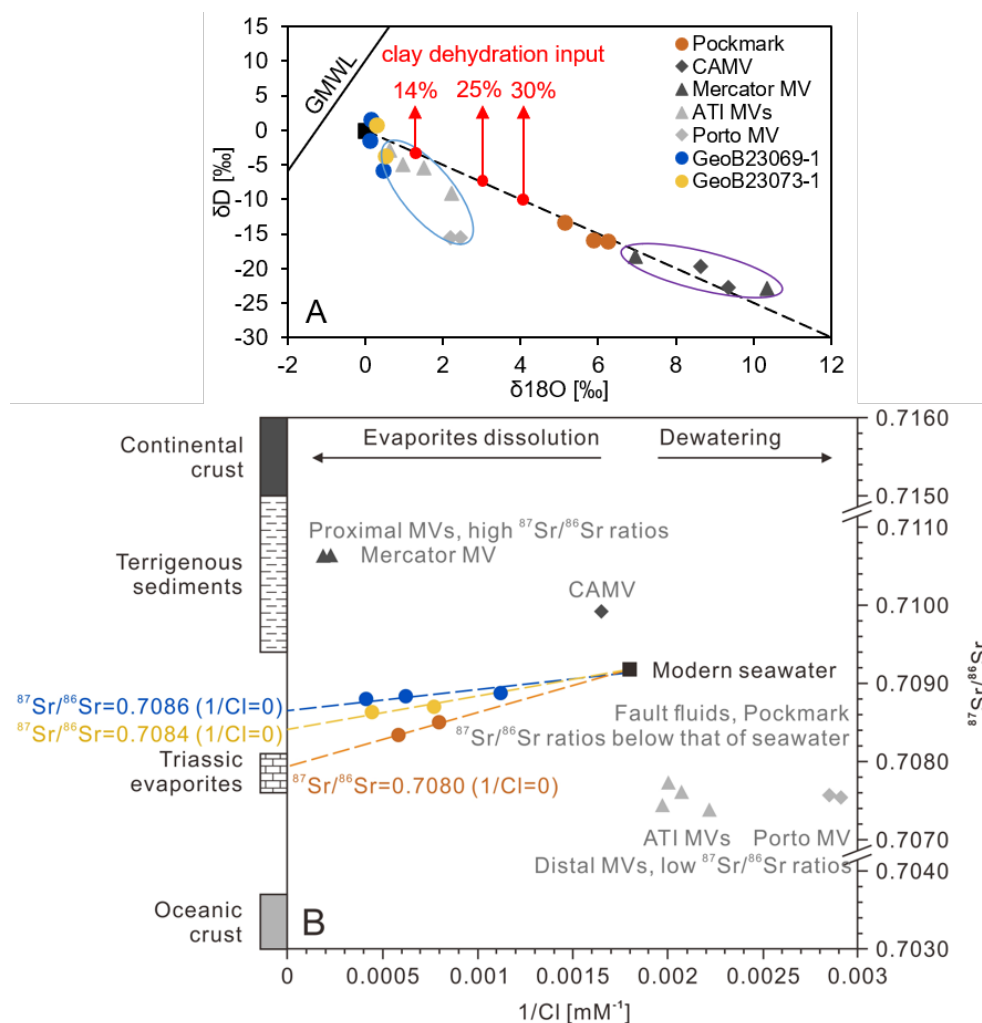


**Figure 4-3.** Plots of  $\delta\text{D}$  vs.  $\delta^{18}\text{O}$  (A) and  $^{87}\text{Sr}/^{86}\text{Sr}$  vs.  $1/\text{Cl}$  (B) for end member fluids at faults and pockmark sites. The seawater value (black square) and the data for Mercator MV, CAMV,

Porto MV and ATI MVs are shown for comparison. Violet oval encloses proximal MVs while light blue one encloses distal MVs. The solid line in A represents the global meteoric water line (GMWL) (Craig, 1961). The dashed line in A represents the two-end member mixing between seawater ( $\delta D = 0$ ;  $\delta^{18}O = 0$ ) and clay-mineral-derived water ( $\delta D = -30$ ;  $\delta^{18}O = 12$ , Hensen et al., 2015). Theoretical water isotope values for inputs of 14%, 25%, and 30% clay dehydration are represented by red points. The  $^{87}Sr/^{86}Sr$  values for terrigenous sediments, Triassic evaporites, continental and oceanic crust are indicated in B by the vertical bar on the left side (Banner, 2004; Scholz et al., 2009; Ortí et al., 2014).

## 4.4 Discussion

### 4.4.1 Elevated heat flow as an indicator for upward fluid flow

At the selected fault sites, elevated heat flow values are observed along the fault traces, suggesting upward fluid flow. While the measurements taken away from the faults show a mean of  $50.52 \text{ mW/m}^2$  (Figure 4-4 and *SI Appendix*, Table S4-1), in agreement with the background heat flow ( $45 \text{ mW/m}^2$ ; Grevenmeyer et al., 2009), the high heat flow values obtained at the fault sites indicate active fluid seepage, with all measurements on faults being up to 2 times higher than background values (Figure 4-4). Similarly, Hensen et al. (2021) present high heat flow of  $74.5 \text{ mW/m}^2$  (compared to background values of  $52\text{-}59 \text{ mW/m}^2$ ; Grevenmeyer et al., 2009) and element fluxes at the westernmost segment of the SWIM1 fault, in the Horseshoe Abyssal Plain (flower structure sites in Figure 4-1A). Further west, the Meteor cruise M162 also detected elevated heat flow values along the Gloria fault in early 2020 (Hensen et al., 2020), showing seamlessly uninterrupted fluid flow emissions all over the AGFZ. Interestingly, other transform faults such as the Vema TF, in the central Atlantic, show similar heat flow patterns (Khutorskoi and Polyak, 2017). In the active part of the Vema TF, high heat flow values of  $250\text{-}270 \text{ mW/m}^2$ , compared to a background of  $220 \text{ mW/m}^2$ , are caused by convective discharge of the oceanic crust (Khutorskoi and Polyak, 2017).

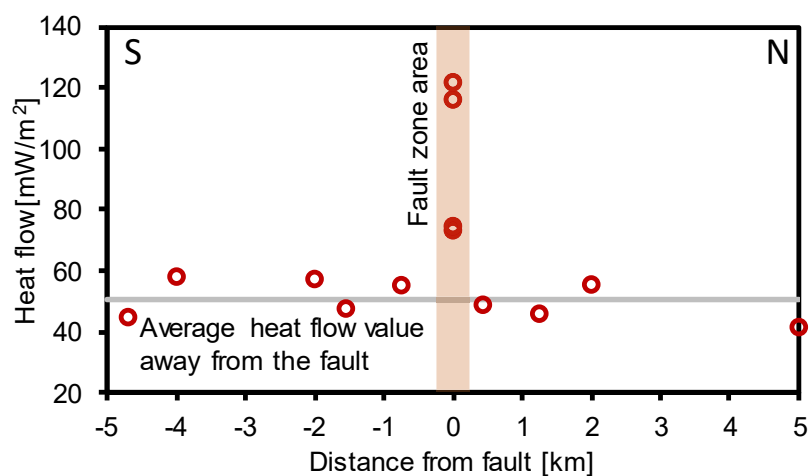


**Figure 4-4.** Heat flow data across the easternmost segments of the SWIM1 fault.

#### 4.4.2 Fluid origins: evaporites dissolution versus clay dehydration

In order to determine the fluid sources along the SWIM1 fault system, we summarized the stratigraphy, lithology, potential fluid sources and their geochemical characteristics of typical elements in the upper accretionary wedge of the Gulf of Cadiz (Table 4-1). The origin of the fluids can be deduced by analyzing the composition of fault fluids. In addition, a pockmark site (Figure 4-1) was selected for comparison. The key geochemical characteristics of pockmark fluids include: i) enrichment of Na and Cl in pockmark fluids, indicating significant evaporite influence on pore water geochemistry (Figure 4-2B; Menapace et al., 2021); ii) similar overall composition and variation trend of pockmark fluids compared to MVs fluids (Figures 4-2B and 4-3A); and iii) lower  $^{87}\text{Sr}/^{86}\text{Sr}$  ratios in the pockmark fluids compared to modern seawater, which are also a primary characteristic of the fault fluids reported here (Figure 4-3B).

At both fault and pockmark sites, a clear geochemical signature resulted from interaction with evaporites is evident in the ascending pore water (Figure 4-2), and thus a contribution from an evaporitic end member can be inferred for these samples. Basing on the behaviour of  $\delta^{18}\text{O}$  and Br/Cl with increasing salinity (Figure 4-5 and *SI Appendix*, Figure S4-1), the generation of evaporitic fluids is attributed to halite dissolution with little contribution from late stage evaporites or brines (Gieskes and Mahn, 2007). While the high Na and Cl concentrations in the pockmark and fault fluids show that halite is the main component of the dissolved salts, the contribution of other evaporite minerals like gypsum and late-stage potash minerals (sylvite and carnallite) is also observed in the fault samples. High Ca concentrations beyond gypsum equilibrium (Ca: ~40 mM; Fontes and Matray, 1993) and the parallel enrichment of K, Mg and especially Br (up to 2.10 mM in GeoB23069-1, Figure 4-2) support this hypothesis (McCaffrey et al., 1987; Gieskes and Mahn, 2007). While some solutes in the pockmark site are expected to be involved in diagenetic processes like shallow carbonate precipitation and clay mineral dehydration (see also discussion below), the pore water constituents in the fault samples, especially in GeoB23069-1, are consistent with the influence of dissolution of the Triassic evaporites in the GoC which contains halite, gypsum, shallow-water carbonates and minor amounts of carnallite and sylvite (Holser et al., 1983; Maldonado et al., 1999; Scholz et al., 2009).

Triassic evaporites cover extensive parts of the basement forming a series of salt diapirs dotting the accretionary wedge (Table 4-1; Maestro et al., 2003). Their accumulation on top of the basement is related to the development of a rifted passive margin and the opening of the Atlantic Ocean in Triassic-Jurassic times (Maestro et al., 2003; Tari et al., 2003). During the Late Tortonian, the Allochthonous Unit of the Gulf of Cadiz (AUGC) was emplaced in the region and represents the thickest unit of the sedimentary cover, which is a mixture of Triassic to Neogene sedimentary units containing such Triassic diapirs (Maldonado et al., 1999; Medialdea et al., 2004). With the seaward advance of the AUGC, the extension at the back of the AUGC favoured mud and salt diapirism of Miocene marls and Triassic evaporites, piercing the AUGC until and reaching, in some cases, the seafloor surface (Medialdea et al., 2004). Thus, the AUGC is hosting both Triassic salt (diapirs) and terrigenous sediments, showcasing

**Table 4-1.** The stratigraphy and lithology of the sedimentary cover at the upper accretionary wedge, along with the potential fluid sources, their  $^{87}\text{Sr}/^{86}\text{Sr}$  values, and their respective impacts on the concentration of typical elements in pore water.

		Stratigraphy <sup>a</sup>	Lithology <sup>a</sup>	Thickness <sup>d</sup>	Fluid sources	Na	Cl	$\delta^{18}\text{O}$	$\delta\text{D}$	Sr	$^{87}\text{Sr}/^{86}\text{Sr}$	
Salt diapir		U. Miocene to Quaternary	Miocene marly clays and sands, and Pliocene-Quaternary hemipelagic deposits, contourites and turbidite beds	~ 1.5 km	Evaporitic fluids (salt diapir dissolution)	(+) <sup>e</sup>	(+)	/	/	(+)	Contemporaneous seawater 0.7076-0.7081 (Orti et al., 2014)	
		Mid to U. Miocene (Inc. AUGC)	a mixture of Triassic salt units and under-compacted Miocene plastic marls and shales	2.7-5.5 km		Clay mineral dehydration (60-150 °C)	(-) <sup>e</sup>	(-)	Positive <sup>e</sup>	Negative <sup>e</sup>		(+) vary
		Cretaceous to L. Eocene	terrigenous sediments (shales with chert layers and limestones at the base)	1-1.5 km	Hydrocarbon generation (> 150 °C, wet gas to post-maturity stage)	/	/	/	/	/	/	
		U. Jurassic <sup>b</sup>	clayey limestones									
		Triassic	evaporites (halite, anhydrite, and minor amounts of potash minerals)		Evaporitic fluids (evaporites dissolution)	(+)	(+)	/	/	(+)	Contemporaneous seawater 0.7076-0.7081 (Orti et al., 2014)	
		Basement (OCT) <sup>c</sup>		Fluid injection from basement					(+)	Continental crust (radiogenic): >0.7150 (Banner, 2004) Oceanic crust (non-radiogenic): 0.7030-0.7037 (Banner, 2004)		

<sup>a</sup>Stratigraphy and lithology in the Gulf of Cadiz are defined by Maldonado et al. (1999), Medialdea et al. (2004).

<sup>b</sup>U. Jurassic unit is constrained to the westernmost part of the Gulf of Cadiz near Coral Patch Ridge and is absent on the accretionary wedge.

<sup>c</sup>The basement located in the study area consists of Ocean-Continent Transition (OCT) crystalline crust.

<sup>d</sup>U. Miocene to Quaternary unit: 1.5 s TWT (about 1.5 km assuming a velocity of 2.0 km/s, after Gonzalez-Fernandez et al., 2001);

Mid to U. Miocene unit: 2.5-5 s TWT (about 2.7-5.5 km assuming a velocity of 2.2 km/s, after Gonzalez-Fernandez et al., 2001);

Mesozoic to L. Eocene unit: 0.6-0.8 s TWT (about 1-1.5 km assuming a velocity of 3.7 km/s, after Medialdea et al., 2004, Gonzalez-Fernandez et al., 2001).

<sup>e</sup>The '+' (increase) and '-' (decrease) signs represent changes in element concentration caused by respective fluid sources. "Positive" and "Negative" represent the sign of  $\delta^{18}\text{O}$  and  $\delta\text{D}$  values of clay dehydration-derived water.

evaporite dissolution and clay mineral dehydration, where the latter is the major fluid source fuelling mud volcanism in the area (Haffert et al., 2013; Xu et al., 2021).

The pockmark pore waters show major and minor elements trends similar to the MVs (Figure 4-2B), suggesting they are rooted within the AUGC unit and their chemical composition is altered by the same diagenetic processes: anaerobic oxidation of methane (AOM), associated carbonate precipitation in the shallow subsurface, and clay mineral dehydration at depth (e.g., Hensen et al., 2007). For the fault fluids, the characteristic  $\delta^{18}\text{O}/\delta\text{D}$  signature of clay mineral dehydration is almost absent (Figure 4-3A). For comparison, the ATI MVs, located outside the accretionary wedge, show consistently higher signals of clay mineral dehydration (Figure 4-3A). Moreover, the absence of other associated geochemical clues such as the uptake of K or the enrichment of desorbed B (Figure 4-2A) is consistent with a missing signal from clay mineral dehydration. This suggests an almost absent connection with the terrigenous sediments, thus showing how the fault fluids are in fact “bypassing” the AUGC. The distinct chemical signatures carried by fluids at the fault sites consequently imply a different, likely deeper fluid source(s) below the AUGC.

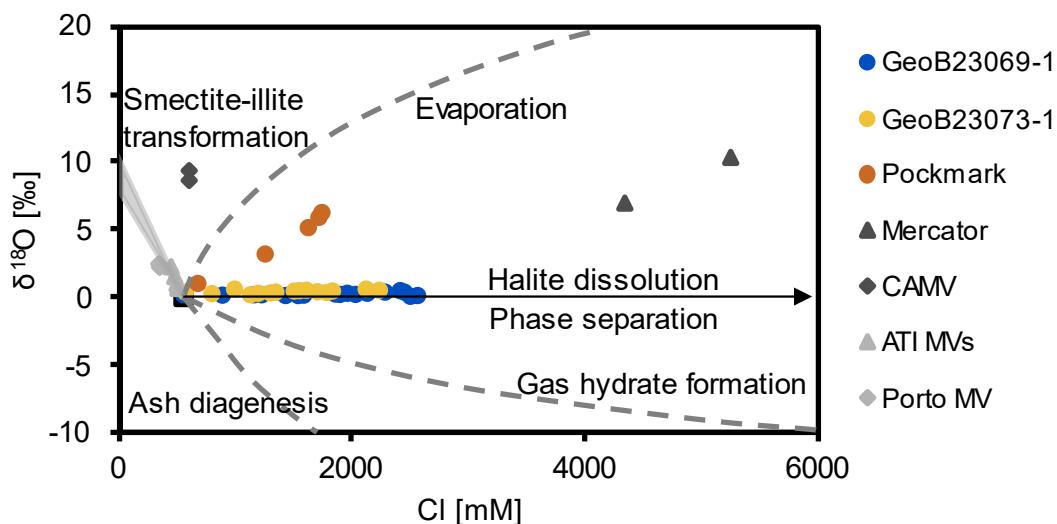


**Figure 4-5.** Plot of  $\delta^{18}\text{O}$  vs. Cl concentration at faults, pockmark and MVs sites [modified after Haffert et al. (2013)]. The grey area for smectite-illite transformation has lower and upper boundary of  $\delta^{18}\text{O} = 7.5\text{‰}-10\text{‰}$ . The seawater value (black square) and the data from Hensen et al., (2021) for Mercator MV, CAMV, Porto MV and ATI MVs are shown for comparison.

#### 4.4.3 Continental crust fluids as a potential fluid origin

The isotope geochemistry of Sr is a powerful proxy for deducing fluid origins (e.g., Dia et al., 1995; Chao et al., 2013, 2022). Here we utilized Sr data to: i) reinforce the confirmation of evaporite influence on both fault and pockmark fluids, and ii) infer the contribution from a third endmember to the fault fluids. The  $^{87}\text{Sr}/^{86}\text{Sr}$  data from different sites were plotted against  $1/\text{Cl}$  (Figure 4-3B). It is evident that data from the same site generally align along a continuum between an endmember and seawater (i.e., binary mixing), suggesting that samples from different depths represent mixtures with varying proportions of seawater. Extrapolating this

continuum line to the maximum dissolved Cl concentrations ( $1/Cl = 0$ ) yields an isotopic ratio reflecting the  $^{87}\text{Sr}/^{86}\text{Sr}$  value in evaporites. For the pockmark samples, the extrapolated  $^{87}\text{Sr}/^{86}\text{Sr}$  ratio is 0.7080, which falls within the range of 0.7076-0.7081, as reported for Triassic sulfates onshore in Spain (Ortí et al., 2014). This further supports the assertion that Triassic evaporitic fluids constitute a predominant source for these samples. It should be noted from the prominent negative correlation of  $\delta^{18}\text{O}$  and  $\delta\text{D}$  (Figure 4-3A) that intense clay mineral dehydration is happening at the pockmark (Sheppard and Gilg, 1996); however, the radiogenic Sr released during that process is negligible, which could be related to the hypersaline fluids composition (Rafferty et al., 1981). Therefore, Sr isotope ratios in the pockmark fluids indicate that interactions with Triassic evaporites is likely to represent the pure, non-radiogenic end member. This is clearly different from Mercator MV and CAMV, where highly radiogenic  $^{87}\text{Sr}/^{86}\text{Sr}$  ratios derived from interactions with terrigenous material and/or continental crust are reported (Scholz et al., 2009; Haffert et al., 2013). However, the fault fluids have a slightly higher radiogenic isotopic signature than the pockmark (Figure 4-3B;  $^{87}\text{Sr}/^{86}\text{Sr} = 0.7084\text{-}0.7086$  at  $1/Cl = 0$  for the fault samples), pointing towards a third fluid source that can shift the  $^{87}\text{Sr}/^{86}\text{Sr}$  ratio from the dominant evaporitic endmember values.

In the upper accretionary wedge, the upwelling fluids may interact with continental crust or terrigenous material and produce a highly radiogenic  $^{87}\text{Sr}/^{86}\text{Sr}$  signal (Elderfield and Gieskes, 1982). While leaching of terrigenous sediments cannot be observed from the geochemical data presented in this paper (see previous discussion), a deeper fluid source, the underlying continental crust, is then expected to alter the  $^{87}\text{Sr}/^{86}\text{Sr}$  values (Table 4-1). Due to the significantly high  $^{87}\text{Sr}/^{86}\text{Sr}$  values ( $>0.7150$ , Banner, 2004; Scholz et al., 2009) originating from the continental crust, admixing of minor amounts of crustal fluids can elevate the  $^{87}\text{Sr}/^{86}\text{Sr}$  values from the evaporitic endmember to the measured level in the fault fluids. Besides, the influence of Sr from the modern seawater contamination cannot be ignored in the fault fluids, as their geochemistry profile does not reach steady state at the lowermost samples (Figure 4-2A).

In order to test our hypothesis regarding the fluid origins in the fault system and better constrain the contribution of possible sources, we set up two scenarios with as many three-endmember mixing models (Figure 4-6). The first scenario tested whether the mixing of seawater, evaporitic fluids, and clay dehydration water can produce the observed  $^{87}\text{Sr}/^{86}\text{Sr}$  values, whereas the second scenario examined a mixing model involving seawater, evaporitic fluids, and continental crust fluids.

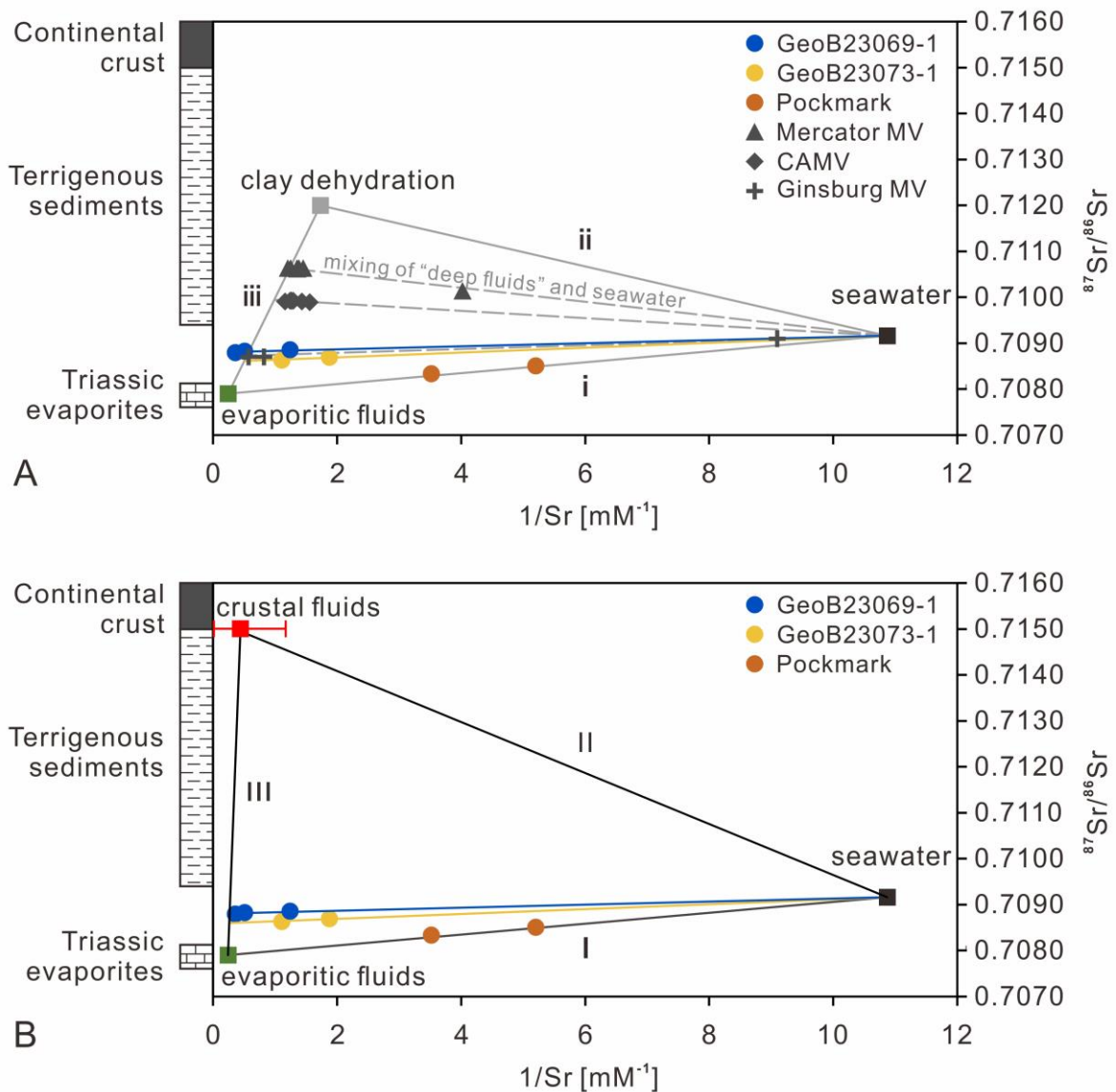


**Figure 4-6.** Relationship among  $^{87}Sr/^{86}Sr$  and  $1/Sr$  of possible sources for faults, pockmark and MVs fluids. (A) Scenario I, the three-endmember mixing between seawater, evaporitic and clay dehydration fluids (a triangle constituted by the grey solid binary mixing lines i, ii and iii). The grey dashed lines indicate the mixing of MV “deep fluids” and seawater. (B) Scenario II, the three-endmember mixing between seawater, evaporitic and continental crust fluids (a triangle constituted by the black solid binary mixing lines I, II and III). The red bar of the continental crust endmember indicates a Sr concentration varying from 0.85 to 68.5 mM (Yardley, 2013), and the red square represents a value of 2.2 mM taken from Benito et al. (1999) as a good approximation for the Gulf of Cadiz. The  $^{87}Sr/^{86}Sr$  values for continental crust, terrigenous sediments and Triassic evaporites are indicated by the vertical bar on the left side of the figure (Banner, 2004; Scholz et al., 2009; Ortí et al., 2014).

#### 4.4.3.1 Clay mineral dehydration cannot explain $^{87}Sr/^{86}Sr$ data

The first scenario assumes a mixing of seawater with the upwelling “deep fluids” which are composed of evaporitic fluids and clay dehydration-derived fluids. The parameters for each

endmember are as follows: i) seawater ( $Sr = 0.092$  mM, Anthoni, 2006;  $^{87}Sr/^{86}Sr = 0.7092$ , Banner, 2004), ii) evaporitic fluids ( $^{87}Sr/^{86}Sr = 0.7079$ , Ortí et al., 2014), and iii) clay dehydration-derived fluids ( $^{87}Sr/^{86}Sr = 0.7120$ , Scholz et al., 2009). Since there is no Sr concentration data reported in the literature for evaporitic fluids in the Gulf of Cadiz, we followed the procedure described by Benito et al. (1999) to estimate the Sr concentration for both evaporitic fluids and clay dehydration-derived fluids, using published data for MV fluids in the Gulf of Cadiz.

Previous studies have shown that the fluids of CAMV, Mercator and Ginsburg MVs in the Gulf of Cadiz are mainly derived from evaporite leaching and clay dehydration (Hensen et al., 2007; Haffert et al., 2013; Hüpers et al., 2020). Assuming a mixing with seawater, the recovered MV fluids represent a ternary mixing of seawater, evaporitic and clay dehydration-derived fluids. In turn, this ternary mixing can be regarded as a mixing of seawater and the upwelling MV fluids composed of evaporitic and clay dehydration-derived fluids. This is supported by the fact that the fluid samples from these three MVs and the endmember of seawater fall on linear lines in the plot of  $^{87}Sr/^{86}Sr$  vs  $1/Sr$  (grey dashed lines in Figure 4-6A). We also note that the MV fluid samples plot on different lines, indicating that distinct proportions of evaporitic and clay dehydration-derived fluids are mixed at different MVs. Purely “deep fluids” (i.e., without seawater) should fall on the binary mixing line of evaporitic and clay dehydration-derived fluids. Since seawater accounts for a minor percentage in the MV fluids with increasing sample depth, the deepest samples, which have the lowest seawater contents, can be used to estimate this mixing line. The samples from Mercator and Ginsburg MVs were finally employed because the line defined by them is farthest from the seawater endmember (grey solid line iii in Figure 4-6A). By intersecting a horizontal line with an average  $^{87}Sr/^{86}Sr$  value of evaporitic fluids and clay dehydration-derived fluids with the binary mixing line, the Sr concentration of evaporitic fluids (4.1 mM) and clay dehydration-derived fluids (0.58 mM) were obtained (green and grey squares in Figure 4-6A).

With the Sr concentration and  $^{87}Sr/^{86}Sr$  isotope ratio of each endmember determined, we used e.q. (4.1) to e.q. (4.3) to calculate the relative contributions of seawater, evaporitic fluids and clay mineral dehydration to our fault fluid samples (Table 4-2). This was undertaken to determine whether the Sr concentration and Sr isotope composition can be explained by Scenario I. The results yield a contribution of clay mineral dehydration up to 25% for the deepest sample at GeoB23073-1 and a contribution  $>100\%$  for the deepest sample at GeoB23069-1 (Table 4-2). The high percentage of clay dehydration input is not consistent with the water isotope data (Figure 4-3A). Moreover, negative values were yielded for seawater from GeoB23069-1, suggesting that no practical solution exists for the mixing of these three endmembers. This agrees with the observation that two samples fall out of the triangle composed by the three endmembers (Figure 4-6A). Therefore, the deviation of Sr isotope ratio from the evaporitic endmember values in the fault fluids cannot be explained by clay mineral dehydration.

**Table 4-2.** Results of three-endmember mixing models.

Core Number	depth [mbsf]	endmember contribution in total fluids [%]			endmember contribution in deep fluids [%]	
		seawater	evaporitic fluids	clay dehydration	evaporitic fluids	clay dehydration
Scenario I		seawater	evaporitic fluids	clay dehydration	evaporitic fluids	clay dehydration
GeoB23069-1	5.50	56.02	14.23	29.75	32.36	67.64
GeoB23069-1	19.70	-14.57	37.26	77.32	32.52	67.48
GeoB23069-1	42.60	-61.34	53.76	107.58	33.32	66.68
GeoB23073-1	19.70	76.60	9.31	14.09	39.79	60.21
GeoB23073-1	42.60	57.66	17.20	25.14	40.62	59.38
Scenario II		seawater	evaporitic fluids	crustal fluids	evaporitic fluids	crustal fluids
GeoB23069-1	5.50	80.08	15.56	4.36	78.12	21.88
GeoB23069-1	19.70	47.96	40.71	11.33	78.24	21.76
GeoB23069-1	42.60	25.68	58.56	15.76	78.80	21.20
GeoB23073-1	19.70	88.00	9.94	2.06	82.80	17.20
GeoB23073-1	42.60	78.00	18.32	3.68	83.26	16.74

#### 4.4.3.2 Continental crust fluids as a fluid origin and its quantification

The second scenario assumes a mixing of seawater, evaporitic and continental crust fluids, and is established by replacing the clay dehydration endmember in the first scenario with the continental crust fluids (Sr = 0.85-68.5 mM, Yardley, 2013;  $^{87}\text{Sr}/^{86}\text{Sr} = 0.7150$ , Banner, 2004; Scholz et al., 2009). The effects of changing crustal Sr concentrations on the calculated contribution of each endmember are shown in Figure 4-7. Taking a Sr concentration of 2.2 mM (red line in Figure 4-7) which is derived from the continental crust fluids in southeast Spain (Benito et al., 1999) and could be also representative for the GoC, the results show that at sites GeoB23069-1 and GeoB23073-1, seawater contributes to 26% and 78% for the deepest samples (crossed points at solid lines in Figure 4-7; Table 4-2), respectively, while in the pure “deep fluids”, continental crust fluids amount to 22% and 17% (evaporite contribution/continental crust contribution = 3.6 and 4.9; crossed points at dashed lines in Figure 4-7; Table 4-2) respectively. Thus, the Sr signature of the fault fluids can be explained by this three-endmember mixing model, and the underlying continental crust is a reasonable fluid source fuelling the “deep fluids” component at the fault sites. Although uncertainties exist due to the challenges of obtaining endmember samples, we have utilized the published data to constrain the endmembers, and established a framework for re-evaluating the results as more data becomes available. Due to the model's complexity, a four-endmember mixing model involving seawater, evaporitic, clay dehydration-derived, and continental crust fluids is not considered. However, considering that the first scenario cannot explain the  $^{87}\text{Sr}/^{86}\text{Sr}$  data, we suggest that the involvement of continental crust fluids is indispensable. Therefore, the continental crust signal inferred in this study is reliable.

In the second scenario presented in this work, crustal-derived fluids act as the fluid sources to initiate fluid flow and carry the evaporitic signals upward. The dominant process of evaporite dissolution do not release water, but instead alter diagenetic signals of ambient pore water. The SWIM faults here provide high permeability pathways for the upward advection of fluids through otherwise thick, impermeable sediment cover, allowing fluid and energy exchange between lithosphere and hydrosphere (Figure 4-8). This key finding is also supported by

prominent heat flow anomalies at the seafloor, in correspondence of the fault sites (Figure 4-4).

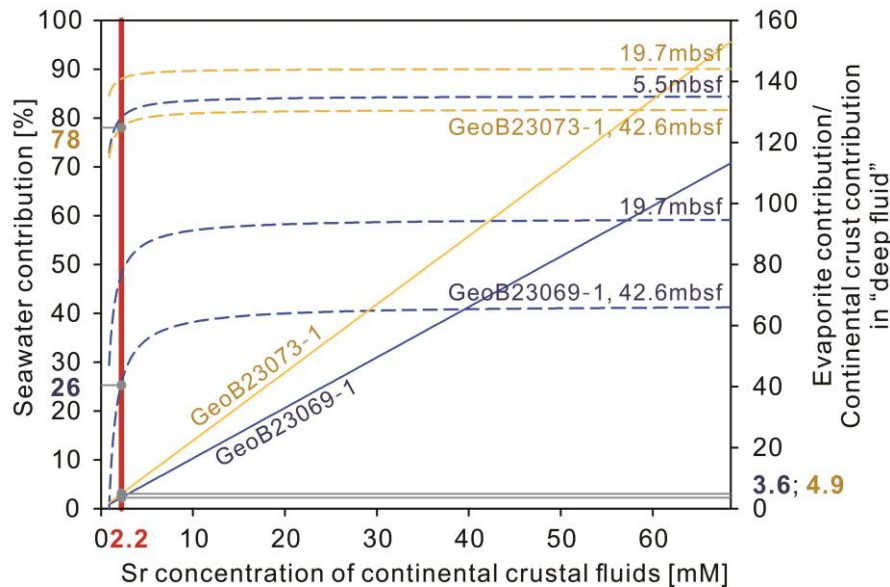


**Figure 4-7.** Diagram showing the effects of different Sr concentrations of continental crust fluids on the results of the three-endmember mixing model. The dashed lines represent the seawater contribution in the three-endmember mixing model. The solid lines represent the contribution of evaporitic fluids with respect to continental crust fluids in the pure “deep fluid”.

In the Horseshoe Abyssal Plain, similar mechanisms driving fluid flow through the SWIM faults have been previously reported on top of flower structures (Figure 4-1A), indicating a hydrological connection between the seafloor and the old (>140 Ma) oceanic crust (Hensen et al., 2015, 2021). Our work provides instead new evidence of fluid flow from the continental crust in the upper part of the accretionary wedge, where the SWIM faults offer important pathways for crustal fluids exchange through km-thick sediments (Figure 4-8). We therefore recognize through geochemical and geophysical evidence the continental-ocean boundary for the tectonic domains identified in the literature (Figure 4-1A; Martinez-Lorient et al., 2014; Silva et al., 2017), which then acknowledge the SWIM faults as the main tectonic features cross-cutting the upper accretionary prism. Confirming the presence of continental crust in the area, we further corroborate the idea that enhanced source rock maturation and hydrocarbon generation can be caused by higher radiogenic heat (i.e., from the continental crust) compared to the rest of the GoC, which is underlain by oceanic crust (Nuzzo et al., 2019). Moreover, we disprove that strike-slip faulting in the upper accretionary prism is happening due to pure deformation, in order to accommodate downslope compression and upslope extension (Crutchley et al., 2011), and unrelated to the dextral transform plate boundary system (SWIM). The deep geochemical signals at the sites analyzed in this paper highlight that modern faulting in the upper accretionary prism cut through km-thick sediment cover, reaching the continental crust.

While significant vent and seep activity is well known for convergent plate boundaries (Sahling

et al., 2008) and especially along the eastern Africa-Eurasia plate boundary (Deyhle and Kopf, 2001; Menapace et al., 2017c), reported fluid activity in TFs which have similar length as convergent boundaries (Bird, 2003) and cover vast areas of the seafloor is relatively limited. The SWIM fault zone described here offers a clear example of active fluid flow and heat exchange in a transform fault setting. Similar observations are reported for the Mendocino (Stakes et al., 2002) and Vema TFs (e.g., Devey et al., 2018; Prigent et al., 2020), where methane-rich cold seeps and hydrothermal circulation drive the deep fluids to the surface.

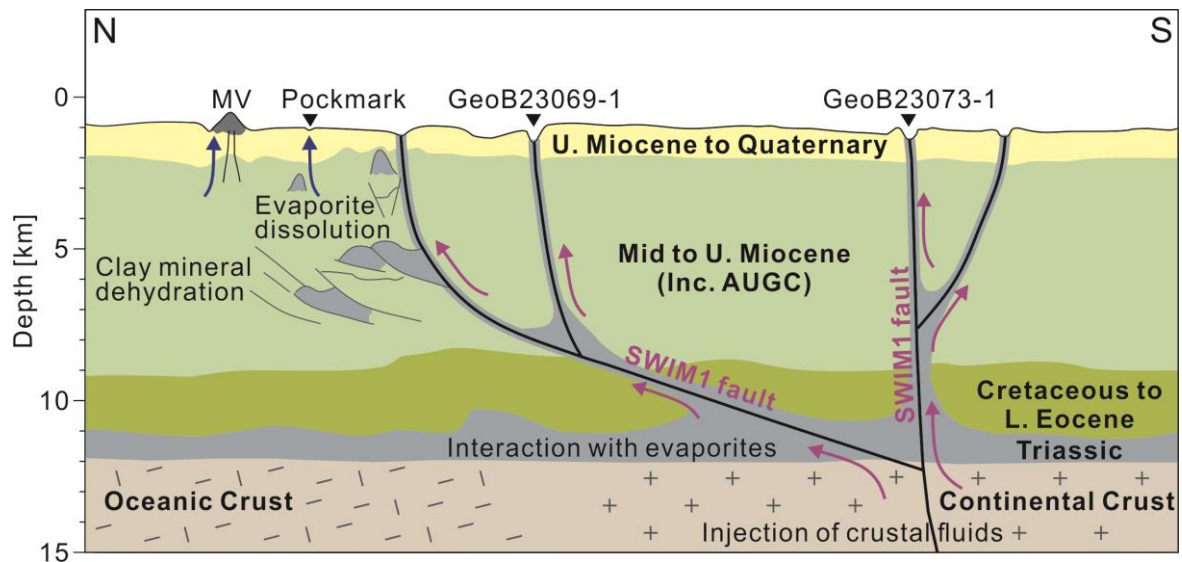


**Figure 4-8.** Schematic overview illustrating the fluid formation and flow processes in the GoC upper accretionary prism. The cores sites and seafloor features investigated in this study are projected along the profile. See Figure 4-1A for their exact location.

#### 4.5 Implications

The findings presented in this paper offer first evidence of crustal-scale fluid circulation on the easternmost part of the AGFZ. This suggests an active tectonic state of the SWIM faults along their whole surficial expression, in contrast to what previously speculated by Crutchley et al. (2011), which labelled them as surficial deformation structures in the upper accretionary prism. In light of this study the SWIM faults tsunamigenic potential should be reevaluated, as one of the possible sites expected to host high magnitude earthquakes in the GoC (Silva et al., 2017). Additionally, the absence of recent significant seismicity reported in the SWIM faults (Silva et al., 2017), can be now related to the rheological weakening and fault creep induced by the fluid circulation. Nevertheless, the transition from creep to stick-slip within the fault zones is a plausible rupture mechanism for large earthquake occurrence (Noda and Lapusta, 2013).

Given the large geographical extent of the AGFZ as a whole, further studies regarding the fluid circulation along its path will advance our understanding of elements exchange in the region with applications on a global scale, better defining the AGFZ's role in the Africa-Eurasia plate boundary. Transform-type plate boundaries could then bear a considerable potential for fluid exchange between ocean and lithosphere and are therefore ideal settings for future research.

## Supplementary material

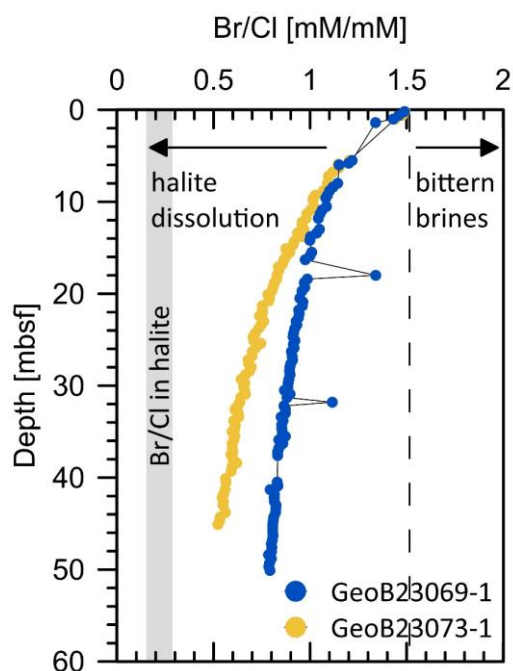


**Figure S4-1.** Br/Cl depth profile at fault sites. Dashed lines indicate seawater values. The grey area depicts Br/Cl ratio ranges in halite.

**Table S4-1.** Locations of sampled cores and heat flow measurements.

Location	Core Number	Gear	Latitude[°N]	Longitude[°W]	Water Depth [m]	Heat Flow [mW/m <sup>2</sup> ]
Pockmark	GeoB24208-1	GC	35°22.80'	7°12.23'	1190	
Pull-apart basin	GeoB23069-1	MeBo	35°16.98'	7°19.31'	1280	
Pull-apart basin	GeoB23073-1	MeBo	35°05.66'	7°19.00'	1281	
Pull-apart basin	GeoB23074-1	HF	35°05.68'	7°19.68'	1274	121.90
Pull-apart basin	GeoB23070-1	HF	35°16.97'	7°19.31'	1309	73.30
Pull-apart basin	GeoB23070-2	HF	35°17.20'	7°19.44'	1309	48.80
Heat flow transect	GeoB23016-1	HF	35°13.34'	7°05.33'	944	58.10
Heat flow transect	GeoB23017-1	HF	35°14.30'	7°05.33'	941	57.30
Heat flow transect	GeoB23018-1	HF	35°15.00'	7°05.32'	965	55.20
Heat flow transect	GeoB23019-1	HF	35°15.40'	7°05.31'	1021	116.30
Heat flow transect	GeoB23021-1	HF	35°16.50'	7°05.34'	1017	55.50
Heat flow transect	GeoB23050-1	HF	35°05.47'	7°04.19'	867	41.50
Heat flow transect	GeoB23050-2	HF	35°03.48'	7°04.26'	862	45.90
Heat flow transect	GeoB23050-3	HF	35°02.81'	7°04.28'	1016	74.70
Heat flow transect	GeoB23050-4	HF	35°01.98'	7°04.34'	883	47.60
Heat flow transect	GeoB23050-5	HF	35°00.26'	7°04.38'	759	44.80

## Chapter 5: Conclusions and outlook

### 5.1 Conclusions

In this Ph.D. study, cold seeps in the Gulf of Cadiz are investigated through a series of methodologies, having resulted in three manuscripts, each dedicated to a specific topic. Firstly, six mud volcanoes (MVs) in the Gulf of Cadiz have been reported and characterized using hydroacoustic methods, gravity coring, and extensive laboratory testing. This investigation has shed light on MV activity, diagenetic processes, and fluid sources. Subsequently, detailed analyses have been conducted on each individual MV, revealing distinct salinity patterns. To elucidate the origins of these patterns, comparisons have been drawn with the Milano MV in the Mediterranean Ridge. Links between MV evolution, fluid pathways, and salinity patterns have been established using geochemical analysis, high-resolution seismic data, and pore water modeling. Lastly, on a broader scale, a comparative analysis has been carried out regarding cold seeps occurring through MVs, pockmarks, and faults, and discussions have been engaged regarding the role of transform faults in the deep hydrologic cycle. The research presented in this Ph.D. dissertation offers crucial insights into fluid flow dynamics in the Gulf of Cadiz, holding significant implications for future studies. The primary conclusions are as follows:

1) Among the six MVs investigated, the two newly discovered R2 and D2 MVs are in the late stages of mud volcanism and have exhibited long periods of inactivity. In contrast, the other four MVs exhibit recent activity at different stages. The Yuma and Ginsburg MVs are long-lived features in an advanced stage of mud volcanism, while the Meknes and Funky Monkey MVs are relatively younger structures in the initial stages of mud volcanism. Clay mineral dehydration is considered to be the primary fluid source for the four active MVs. Several other diagenetic processes have also been identified, including AOM (anaerobic oxidation of methane), carbonate precipitation, dolomitization, dissolution of halite and sulfate minerals, leaching of clay minerals, and interactions with basement rocks. Yuma and Ginsburg MVs are primarily influenced by the dissolution of halite and sulfate minerals, while crustal contributions are inferred in the case of Meknes and Funky Monkey MVs.

2) Fluid geochemistry reveals distinct salinity patterns (freshening at the summit vs. salinization at the moat) in the MVs of the Gulf of Cadiz and the Mediterranean Ridge. The integration of fluid geochemistry, high-resolution seismic data, and pore water modeling in different MVs suggests that these salinity patterns appear to be controlled by the evolution of MVs and the fluid pathways along the edge of the MV feeder conduit and extrusive edifices. The freshening signatures at the summit are driven by the clay dehydration process in the deep central conduit, while the saline pore fluids at the moat/rim sites are significantly impacted by the shallower and widespread evaporites through the rim-related fluid pathways. However, for younger MVs, the entire structure is dominated by freshening since the rim-related fluid pathways are occupied by freshening fluids. Conversely, in older inactive MVs, the freshening at the summit disappears due to diffusion, coexisting with saline characteristics in the moats.

Quantitative calculations indicate that the rim-related fluid pathways play a substantial role in the MV fluid circulation. Although this research is confined to the Gulf of Cadiz and the Mediterranean Ridge, the discovered salinity patterns and rim-related fluid pathways could be a global phenomenon that has not been identified. This warrants further investigation in diverse regions.

3) Fluid samples extracted from the South West Iberian Margin (SWIM) faults zones in the Gulf of Cadiz show an intense interaction between the ascending fault fluids and Triassic evaporites at depth, as they present high Na, Cl, Ca, Br with decreasing Br/Cl and less radiogenic  $^{87}\text{Sr}/^{86}\text{Sr}$ , compared to present-day seawater values. Isotopic data reveal more radiogenic  $^{87}\text{Sr}/^{86}\text{Sr}$  ratios (0.7084-0.7087) in the fault fluids after subtracting the influence of Triassic evaporitic fluids, hinting a potential contribution from continental crust fluids. Three-endmember mixing model suggests that up to 22% of the deep fluids expelled might be traced back to a crustal origin. Further, the deep fluid circulation is supported by the anomalously high heat-flow values at the seafloor, when crossing the fault trace (73-122 mW/m<sup>2</sup>). These findings provide the first evidence of active fluid flow in the SWIM faults, indicating a crustal-scale fluid exchange spanning from the Horseshoe Abyssal Plain to the upper accretionary wedge.

## 5.2 Outlook

Fluid flow has been a prominent focus of research in various geological structures, including faults (e.g., Bense et al., 2013), mud volcanoes (e.g., Planke et al., 2003), pockmarks (e.g., Hovland et al., 2002), submarine hydrothermal vent systems (e.g., Lilley et al., 2003), as well as in diverse geological settings, such as sedimentary basins (e.g., Bjørlykke, 1993), accretionary prisms (e.g., Saffer and Tobin, 2011), and transform fault plate boundaries (e.g., Hensen et al., 2019). This Ph.D. dissertation focuses on fluid flow in mud volcanoes, pockmarks, and transform fault zones in the Gulf of Cadiz, providing insights into fluid sources, fluid-rock interactions, pathways, and related geological processes in the region. These findings have significant implications for future research and our understanding of the deep hydrologic cycle. Building upon the findings presented in this Ph.D. study, the following outlines potential future research directions:

1) Monitoring of fluid flow processes: The research has identified varying stages of activity among the MVs in the Gulf of Cadiz and shows different fluid pattern at different geomorphological parts and different stages. Future studies can focus on monitoring of these MVs to track changes in their fluid composition over time since recent developments in technology has enabled the long-term borehole monitoring (e.g., Kopf et al., 2017). Although research cruise M149 installed “MeBo CORKS” observatories on the Ginsburg MVs and active faults in the region (Hüpers et al., 2020), the retrieve during research cruise M167 was not successful (Menapace et al., 2021). Therefore, future research can involve installing more long-term monitoring devices at various geomorphological features of different MVs, where osmo-

samplers based on the design by Jannasch et al. (2003) may be promising since they do not require electronics and focus on geochemical variations over time. In addition to monitoring MVs, fluid flow along faults can also be monitored, which will provide valuable insights into fault activity and evolution.

2) Crustal-scale fluid exchange and its implications: While this Ph.D. study provides the first direct evidence of active fluid flow along the easternmost segments of the SWIM1 fault, consistent with the western compartment as suggested by previous research, both studies primarily rely on gravity and MeBo cores with limited length and are based on certain assumptions. Therefore, some uncertainties exist. To better characterize the crustal-scale fluid exchange and fault activity in the region, future research can involve deep ocean drilling, especially when considering the implications of the crustal-scale fluid exchange. The SWIM faults are located on the easternmost part of the Azores-Gibraltar Fracture Zone (AGFZ). The crustal-scale fluid exchange suggests an active tectonic state of the SWIM faults along their entire surficial expression, supporting the hypothesis that the SWIM faults could be one of the candidate sources for the 1755 Great Lisbon earthquake (Zitellini et al., 2009). The absence of recent significant seismicity reported in the SWIM faults might suggest that the seismogenic fault zone is locked (Gutscher, 2004). Therefore, it is worthwhile to re-evaluate the seismogenic and tsunamigenic potential of SWIM faults through deep ocean drilling, as they pose a major threat to the Southwestern European continental margin. Furthermore, the SWIM faults provide an opportunity to investigate the connection between fluid circulation and earthquakes.

3) Exploration beyond the Gulf of Cadiz: While this Ph.D. study primarily focuses on the Gulf of Cadiz, it is worth noting that similar geological features and processes may exist in other regions. Therefore, future research can expand to explore fluid flow in various parts of the world's geological structures and settings, contributing to a more comprehensive understanding of fluid flow in MVs and faults on a global scale. For instance, it is essential to verify the applicability of the model proposed in this Ph.D. dissertation accounting for different fluid patterns in various geomorphological regions of MVs. Furthermore, oceanic transform faults (TFs) have not received extensive study. Considering that oceanic TFs could serve as crucial settings for deep-sourced fluid flow circulation, their impact on global mass balances should be more accurately constrained and quantified by additional case studies. Comparative studies between continental and oceanic TFs also present a promising research direction, especially given that continental TFs, such as the San Andreas Fault, have been relatively well-studied.

## Acknowledgements

This doctoral dissertation was accomplished at the MARUM – Center for Marine Environmental Sciences, University of Bremen. I wish to express my profound appreciation to all who have supported me throughout this journey.

First and foremost, I would like to acknowledge my supervisors at the MARUM – Center for Marine Environmental Sciences, University of Bremen, Prof. Dr. A. Kopf and Dr. W. Menapace. Prof. Dr. A. Kopf not only granted me the autonomy to pursue the research topics of my interest but also recommended my participation in significant events such as the AGU Fall Meeting 2021, Meteor cruise M167, Sonne cruise SO292-2 and Maria S. Merian cruise MSM119, and generously covered all the expenses for the research cruises. Additionally, he provided irreplaceable guidance during manuscript composition and revision. Dr. W. Menapace, on the other hand, patiently instructed me in sample preparation and experiment operation, offered constant assistance in data interpretation and manuscript writing even after he moved to another institute, encouraged my active participation in conferences and research cruises, and funded my participation in research cruises together with Prof. Dr. A. Kopf. I am also grateful to Dr. A. Hüpers, who taught me to prepare samples and conduct experimental measurements, and offered me great help in data analysis and manuscript writing, especially during the first year of my Ph.D. study.

Furthermore, I extend my appreciation to the organizations that generously supported my doctoral studies: the China Scholarship Council (CSC), the MARUM – Center for Marine Environmental Sciences, and the Central Research Development Fund (CRDF) at the University of Bremen. The CSC funded my Ph.D. studies at the University of Bremen, while MARUM provided all the necessary facilities, and the CRDF funded my attendance at the AGU Fall Meeting 2021 online.

Moreover, my sincere thanks go to my co-authors and colleagues who provided indispensable scientific, technical, and administrative guidance and support throughout my doctoral studies. I also appreciate the contributions of all the individuals with whom I sailed during research cruises; their assistance was invaluable.

Lastly, I wish to convey my deepest gratitude to my parents and families. Their unwavering love, care, and trust have been my pillars of strength throughout this journey. Without their continuous support and understanding, I would not have reached this point in my life.

## References

- Abrams, M. A., 2005. Significance of hydrocarbon seepage relative to petroleum generation and entrapment. *Mar. Pet. Geol.* 22, 457-477.
- Akhmetzhanov, A. M., Ivanov, M. K., Kenyon, N. H., Mazzini, A., 2007. Deepwater cold seeps, sedimentary environments and ecosystems of the Black and Tyrrhenian Seas and Gulf of Cadiz. *IOC Tech. Ser.* 72, UNESCO.
- Aloisi, G., Drews, M., Wallmann, K., Bohrmann, G., 2004. Fluid expulsion from the Dvurechenskii mud volcano (Black Sea): Part I. Fluid sources and relevance to Li, B, Sr, I and dissolved inorganic nitrogen cycles. *Earth Planet. Sci. Lett.* 225, 347-363.
- Aloisi, G., Pierre, C., Rouchy, J. M., Foucher, J. P., Woodside, J., 2000. Methane-related authigenic carbonates of eastern Mediterranean Sea mud volcanoes and their possible relation to gas hydrate destabilisation. *Earth Planet. Sci. Lett.* 184, 321-338.
- Anthoni, J. F., 2006. The chemical composition of seawater. *Magnesium* 2701, 62-96.
- Banner, J. L., 2004. Radiogenic isotopes: systematics and applications to earth surface processes and chemical stratigraphy. *Earth Sci. Rev.* 65, 141-194.
- Baptista, M. A., Miranda, J. M., Batllo, J., Lisboa, F., Luis, J., Macia, R., 2016. New study on the 1941 Gloria Fault earthquake and tsunami. *Nat. Hazards Earth Syst. Sci.* 16, 1967-1977.
- Baraza, J., Ercilla, G., 1996. Gas-charged sediments and large pockmark-like features on the Gulf of Cadiz slope (SW Spain). *Mar. Pet. Geol.* 13, 253-261.
- Bartolome, R., Gràcia, E., Stich, D., Martinez-Lorient, S., Klaeschen, D., Mancilla, F. L., Lo Iacono, C., Dañoibeitia, J. J., Zitellini, N., 2012. Evidence for active strike-slip faulting along the Eurasia–Africa convergence zone: implications for seismic hazard in the SW Iberian margin. *Geology* 40, 495-498.
- Benito, R., López-Ruiz, J., Cebriá, J. M., Hertogen, J., Doblás, M., Oyarzun, R., Demaiffe, D., 1999. Sr and O isotope constraints on source and crustal contamination in the high-K calc-alkaline and shoshonitic Neogene volcanic rocks of SE Spain. *Lithos* 46, 773-802.
- Bense, V. F., Gleeson, T., Loveless, S. E., Bour, O., Scibek, J., 2013. Fault zone hydrogeology. *Earth Sci. Rev.* 127, 171-192.
- Berndt, C., 2005. Focused fluid flow in passive continental margins. *Phil. Trans. R. Soc. A* 363, 2855-71.
- Berner, R. A., 1980. Early Diagenesis: a theoretical approach. Princeton Univ. Press, Princeton, N. J.
- Berner, R. A., 1981. A new geochemical classification of sedimentary environments. *J. Sediment. Petrol.* 51, 259-365.
- Bird, P., 2003. An updated digital model of plate boundaries. *Geochem. Geophys. Geosyst.* 4, 1027.
- Bjørlykke, K., 1993. Fluid flow in sedimentary basins. *Sediment. Geol.* 86, 137-158.
- Blondel, S., Ford, J., Lockwood, A., Del Ben, A., Camerlenghi, A., 2023. Reprocessing 2-D airgun seismic reflection data SALTFLU (salt deformation and sub-salt fluid circulation in the Algero-Balearic abyssal plain) in the Balearic promontory and the Algerian basin. *Mar. Geophys. Res.* 44, 13.
- Boetius, A., Ravenschlag, K., Schubert, C. J., Rickert, D., Widdel, F., Gieseke, A., Amann, R., Jorgensen, B. B., Witte, U., Pfannkuche, O., 2000. A marine microbial consortium apparently mediating anaerobic oxidation of methane. *Nature* 407, 623-626.

- Bohrmann, G., Ivanov, M., Foucher, J. P., Spiess, V., Bialas, J., Greinert, J., Weinrebe, W., Abegg, F., Aloisi, G., Artemov, Y., Blinova, V., Drews, M., Heidersdorf, F., Krabbenhoft, A., Klaucke, I., Krastel, S., Leder, T., Polikarpov, I., Saburova, M., Schmale, O., Seifert, R., Volkonskaya, A., Zillmer, M., 2003. Mud volcanoes and gas hydrates in the Black Sea: new data from Dvurechenskii and Odessa mud volcanoes. *Geo-Mar. Lett.* 23, 239-249.
- Borowski, W. S., Paull, C. K., Ussler, W., 1996. Marine pore-water sulfate profiles indicate in situ methane flux from underlying gas hydrate. *Geology* 24, 655-658.
- Borowski, W. S., Paull, C. K., Ussler, W., 1999. Global and local variations of interstitial sulfate gradients in deep-water, continental margin sediments: sensitivity to underlying methane and gas hydrates. *Mar. Geol.* 159, 131-154.
- Boswell, R., Collett, T. S., Frye, M., Shedd, W., McConnell, D. R., Shelander, D., 2012. Subsurface gas hydrates in the northern Gulf of Mexico. *Mar. Pet. Geol.* 34, 4-30.
- Boudreau, B. P., 1996. The diffusive tortuosity of fine-grained unlithified sediments. *Geochim. Cosmochim. Acta* 60, 3139-3142.
- Boudreau, B. P., 1997. *Diagenetic models and their implementation: Modelling transport and reactions in aquatic sediments*. Berlin: Springer.
- Briggs, B. R., Pohlman, J. W., Torres, M., Riedel, M., Brodie, E. L., Colwell, F. S., 2011. Macroscopic biofilms in fracture-dominated sediment that anaerobically oxidize methane. *Appl. Environ. Microbiol.* 77, 6780-6787.
- Brown, K. M., 1990. The nature and hydrogeologic significance of mud diapirs and diatremes for accretionary systems. *J. Geophys. Res.* 95, 8969-8982.
- Brown, K. M., Saffer, D. M., Bekins, B. A., 2001. Smectite diagenesis, pore-water freshening, and fluid flow at the toe of the Nankai wedge. *Earth Planet. Sci. Lett.* 194, 97-109.
- Brumsack, H. J., Zuleger, E., 1992. Boron and boron isotopes in pore waters from ODP Leg 127, Sea of Japan. *Earth Planet Sci. Lett.* 113, 427-433.
- Camerlenghi, A., Cita, M. B., Vedova, B. D., Fusi, N., Mirabile, L., Pellis, G., 1995. Geophysical evidence of mud diapirism on the Mediterranean ridge accretionary complex. *Mar. Geophys. Res.* 17, 115-141.
- Camerlenghi, A., Corradin, C., Tinivella, U., Giustiniani, M., Bertoni, C., 2023. Subsurface heat and salts cause exceptionally limited methane hydrate stability in the Mediterranean Basin. *Geology* 51, 162-166.
- Cartwright, J., 2007. The impact of 3D seismic data on the understanding of compaction, fluid flow and diagenesis in sedimentary basins. *J. Geol. Soc.* 164, 881-893.
- Cartwright, J., Huuse, M., Aplin, A., 2007. Seal bypass systems. *AAPG Bull.* 91, 1141-1166.
- Cartwright, J., Kirkham, C., Espinoza, D. N., James, D., Hodgson, N., 2023. The evolution of depletion zones beneath mud volcanoes. *Mar. Pet. Geol.* 106351.
- Cartwright, J., Santamarina, C., 2015. Seismic characteristics of fluid escape pipes in sedimentary basins: Implications for pipe genesis. *Mar. Pet. Geol.* 65, 126-140.
- Cathles, L. M., Su, Z., Chen, D., 2010. The physics of gas chimney and pockmark formation, with implications for assessment of seafloor hazards and gas sequestration, *Mar. Pet. Geol.* 27, 82-91.
- Ceramicola, S., Dupré, S., Somoza, L., Woodside, J., 2018. Cold seep systems. In Micallef, A., Krastel, S., Savini, A. (Eds.), *Submarine Geomorphology*. Springer, pp. 367-387.

- Chan, L. H., Edmond, J. M., Thompson, G., Gillis, K., 1992. Lithium isotopic composition of submarine basalts: Implications for the lithium cycle in the oceans. *Earth Planet. Sci. Lett.* 108, 151-160.
- Chan, L. H., Gieskes, J. M., You, C. F., Edmond, J. M., 1994. Lithium isotope geochemistry of sediments and hydrothermal fluids of the Guaymas Basin, Gulf of California. *Geochim. Cosmochim. Acta* 58, 4443-4454.
- Chan, L. H., Kastner, M., 2000. Lithium isotopic compositions of pore fluids and sediments in the Costa Rica subduction zone: implications for fluid processes and sediment contribution to the arc volcanoes. *Earth Planet. Sci. Lett.* 183, 275-290.
- Chand, S., Thorsnes, T., Rise, L., Brunstad, H., Stoddart, D., Boe, R., Lagstad, P., Svolsbru, T., 2012. Multiple episode of fluid flow in the SW Barents Sea (Loppa High) evidenced by gas flares, pockmarks and gas hydrate accumulation. *Earth Planet. Sci. Lett.* 331, 305-314.
- Chao, H. C., You, C. F., Liu, H. C., Chung, C. H., 2013. The origin and migration of mud volcano fluids in Taiwan: Evidence from hydrogen, oxygen, and strontium isotopic compositions. *Geochim. Cosmochim. Acta* 114, 29-51.
- Chao, H. C., You, C. F., Lin, I. T., Liu, H. C., Chung, L. H., Huang, C. C., Chung, C. H., 2022. Two-end-member mixing in the fluids emitted from Mud Volcano Lei-Gong-Huo, Eastern Taiwan: Evidence from Sr isotopes. *Front. Earth Sci.* 9, 750436.
- Chaumillon, E., 1995. Structure de la Ride Méditerranéenne: apports de la sismique multitrace, (Doctoral thesis). Paris, France: Université Pierre-et-Marie-Curie.
- Chester, R., Jickells, T., 2012. *Marine geochemistry, 3rd ed.* London: Willey-Blackwell, 240pp.
- Chiodini, G., D'Alessandro, W., Parello, F., 1996. Geochemistry of gases and waters discharged by the mud volcanoes at Paterno, Mt. Etna (Italy), *Bull. Volcanol.* 58, 51-58.
- Clennell, M. B., Knipe, R. J., Fisher, Q. J., 1998. Fault zones as barriers to, or conduits for, fluid flow in argillaceous formations: a microstructural and petrophysical perspective. In *Fluid Flow Through Faults and Fractures in the Argillaceous Formations* (N.W. Group, ed.), pp. 125-139. Organisations for Economics Collaboration and Development, Paris.
- Cita, M. B., Camerlenghi, A., Erba, E., McCoy, F. W., Castradori, D., Cazzani, A., Guasti, G., Giambastiani, M., Lucchi, R., Nolli, V., Pezzi, G., Redaelli, M., Rizzi, E., Torricelli, S., Violanti, D., 1989. Discovery of mud diapirism on the Mediterranean Ridge: A preliminary report. *Boll. Soc. Geol. Ital.* 108, 537-543.
- Cita, M. B., Ivanov, M. K., Woodside, J. M., 1996. The Mediterranean Ridge diapiric belt. *Mar. Geol.* 132, 1-6.
- Colten-Bradley V. A., 1987. Role of pressure in smectite dehydration - effects on geopressure and smectite-to-illite transformation. *Am. Assoc. Pet. Geol. Bull.* 71, 1414-1427.
- Colwell, F., Matsumoto, R., Reed, D., 2004. A review of the gas hydrates, geology, and biology of the Nankai Trough. *Chem. Geol.* 205, 391-404.
- Craig, H., 1961. Isotopic variations in meteoric waters. *Science* 133, 1702-1703.
- Crutchley, G. J., Berndt, C., Klaeschen, D., Masson, D. G., 2011. Insights into active deformation in the Gulf of Cadiz from new 3-D seismic and high-resolution bathymetry data. *Geochem. Geophys. Geosyst.* 12, Q07016.

- Cunha, T. A., Matias, L. M., Terrinha, P., Negredo, A. M., Rosas, F., Fernandes, R. M. S., Pinheiro, L. M., 2012. Neotectonics of the SW Iberia margin, Gulf of Cadiz and Alboran Sea: a reassessment including recent structural, seismic and geodetic data. *Geophys. J. Int.* 188, 850-872.
- Dählmann, A., de Lange, G. J., 2003. Fluid-sediment interactions at Eastern Mediterranean mud volcanoes: a stable isotope study from ODP Leg 160. *Earth Planet. Sci. Lett.* 212, 377-391.
- Davies, R. J., Stewart, S. A., 2005. Emplacement of giant mud volcanoes in the South Caspian Basin: 3D seismic reflection imaging of their root zones. *J. Geol. Soc.* 162, 1-4.
- De Lange, G. J., Brumsack, H. J., 1998. Pore-water indications for the occurrence of gas hydrates in eastern Mediterranean mud dome structures. *Proceedings ODP. Scientific Results* 160, 569-574.
- Depreiter, D., Poort, J., Van Rensbergen, P., Henriot, J. P., 2005. Geophysical evidence of gas hydrates in shallow submarine mud volcanoes on the Moroccan margin. *J. Geophys. Res.* 110, B10103.
- Devey, C. W., Augustin, N., Brandt, A., Brenke, N., Köhler, J., Lins, L., Schmidt, C., Yeo, I. A., 2018. Habitat characterization of the Vema Fracture Zone and Puerto Rico Trench. *Deep Sea Res. Part II Top. Stud. Oceanogr.* 148, 7-20.
- Deville, E., Battani, A., Griboulard, R., Guerlais, S., Herbin, J. P., Houzay, J. P., Muller, C., Prinzhofer, A., 2003. The origin and processes of mud volcanism: new insights from Trinidad. In Van Rensbergen, P., Hillis, R. R., Maltman, A. J., Morley, C. K. (Eds.), *Subsurface Sediment Mobilization*. Geological Society, London, pp. 475-490. Special Publications 216.
- Deville, E., Guerlais, S. H., 2009. Cyclic activity of mud volcanoes: Evidences from Trinidad (SE Caribbean). *Mar. Pet. Geol.* 26, 1681-1691.
- Dewey, J. F., Helman, M. L., Turco, E., Hutton, D. H. W., Knott, S. D., 1989. Kinematics of the western Mediterranean. In Coward, M. P., Dietrich, D., Park, R. G. (Eds.), *Alpine Tectonics*. Geological Society, London, pp. 265-283. Special Publications 45.
- Deyhle, A., Kopf, A., 2001. Deep fluids and ancient pore waters at the backstop: Stable isotope systematics (B, C, O) of mud-volcano deposits on the Mediterranean Ridge accretionary wedge. *Geology* 29, 1031-1034.
- Deyhle, A., Kopf, A. J., Aloisi, G., 2003. Boron and boron isotopes as tracers for diagenetic reactions and depth of mobilization, using muds and authigenic carbonates from eastern Mediterranean mud volcanoes. In van Rensbergen, P., Hillis, R. R., Maltman, A. J., Morley, C. K. (Eds.), *Subsurface Sediment Mobilization*. Geological Society, London, pp. 491-503. Special Publications 216.
- Dia, A. N., Castrec, M., Boulègue, J., Boudou, J. P., 1995. Major and trace element and Sr isotope constraints on fluid circulations in the Barbados accretionary complex. Part 1: Fluid origin. *Earth Planet. Sci. Lett.* 134, 69-85.
- Diaz-del-Rio, V., Somoza, L., Martinez-Frias, J., Mata, M. P., Delgado, A., Hernandez-Molina, F. J., Lunar, R., Martin-Rubi, J. A., Maestro, A., Fernandez-Puga, M. C., Leon, R., Llave, E., Medialdea, T., Vazquez, J. T., 2003. Vast fields of hydrocarbon-derived carbonate chimneys related to the accretionary wedge/olistostrome of the Gulf of Cadiz. *Mar. Geol.* 195, 177-200.
- Dickens, G. R., Koelling, M., Smith, D. C., Schnieders, L., 2007. Rhizon sampling of pore waters on scientific drilling expeditions: an example from the IODP Expedition 302, Arctic Coring Expedition (ACEX). *Sci. Drill.* 4, 22-25.
- Dimitrov, L., Woodside, J., 2003. Deep sea pockmark environments in the eastern Mediterranean. *Mar. Geol.* 195, 263-276.

- Dimitrov, L. I., 2002. Mud volcanoes – the most important pathway for degassing deeply buried sediments. *Earth Sci. Rev.* 59, 49-76.
- Duarte, D., Roque, C., Ng, Z. L., Hernández-Molina, F. J., Magalhaes, V. H., Silva, S., Llave, E., 2022. Structural control and tectono-sedimentary evolution of the Gulf of Cadiz, SW Iberia since the late Miocene: Implications for contourite depositional system. *Mar. Geol.* 449, 106818.
- Dupuis, M., Imbert, P., Odonne, F., Vendeville, B., 2019. Mud volcanism by repeated roof collapse: 3D architecture and evolution of a mud volcano cluster offshore Nigeria. *Mar. Petrol. Geol.* 110, 368-387.
- Dymond, J., Suess, E., Lyle, M., 1992. Barium in deep-sea sediment: a geochemical proxy for paleoproductivity. *Paleoceanography* 7, 163-181.
- Elderfield, H., Gieskes, J. M., 1982. Sr isotopes in interstitial waters of marine sediments from Deep Sea Drilling Project cores. *Nature* 300, 493-497.
- Elderfield, H., Schultz, A., 1996. Mid-Ocean Ridge hydrothermal fluxes and the chemical composition of the ocean. *Ann. Rev. Earth Planet. Sci.* 24, 191-224.
- Emeis, K. C., Robertson, A. H. F., Richter, C., Shipboard Scientific Party ODP Leg 160, 1996. Proceedings of the Ocean Drilling Program, Initial reports, Volume 160: College Station, Texas, Ocean Drilling Program, 972 p.
- Etioppe, G., 2005. Mud volcanoes and microseepage: The forgotten geophysical components of atmospheric methane budget. *Ann. Geophys.* 48, 1-7.
- Etioppe, G., 2015. *Natural Gas Seepage: The Earth's Hydrocarbon Degassing*. Springer International Publishing, Switzerland, pp. 199.
- Etioppe, G., Caracausi, A., Favara, R., Italiano, F., Baciu, C., 2002. Methane emission from the mud volcanoes of Sicily (Italy). *Geophys. Res. Lett.* 29, 1215.
- Etioppe, G., Ciotoli, G., Schwietzke, S., Schoell, M., 2019. Gridded maps of geological methane emissions and their isotopic signature. *Earth Syst. Sci. Data* 11, 1-22.
- Etioppe, G., Martinelli, G., Caracausi, A., Italiano, F., 2007. Methane seeps and mud volcanoes in Italy: gas origin, fractionation and emission to the atmosphere. *Geophys. Res. Lett.* 34, L14303.
- Etioppe, G., Milkov, A. V., 2004. A new estimate of global methane flux from onshore and shallow submarine mud volcanoes to the atmosphere, *Environ. Geol.* 46, 997-1002.
- Etioppe, G., Nakada, R., Tanaka, K., Yoshida, N., 2011. Gas seepage from Tokamachi mud volcanoes, onshore Niigata Basin (Japan): origin, post-genetic alterations and CH<sub>4</sub>-CO<sub>2</sub> fluxes. *Appl. Geochem.* 26, 348-359.
- Etioppe, G., Schwietzke, S., 2019. Global geological methane emissions: an update of top-down and bottom-up estimates. *Elem. Sci. Anth.* 7, 47.
- Feseker, T., Brown, K. R., Blanchet, C., Scholz, F., Nuzzo, M., Reitz, A., Schmidt, M., Hensen, C., 2010. Active mud volcanoes on the upper slope of the western Nile deep-sea fan—first results from the P362/2 cruise of R/V Poseidon. *Geo-Mar. Lett.* 30, 169-186.
- Fisher, A. T., 2005. Marine hydrogeology: recent accomplishments and future opportunities. *Hydrogeol. J.* 13, 69-97.
- Fontes, J. C., Matray, J. M., 1993. Geochemistry and origin of formation brines from the Paris Basin, France: 1. Brines associated with Triassic salts. *Chem. Geol.* 109, 149-175.

- Foubert, A., Depreiter, D., Beck, T., Maignien, L., Pannemans, B., Frank, N., Blamart, D., Henriot, J. P., 2008. Carbonate mounds in a mud volcano province off north-west Morocco: key to processes and controls. *Mar. Geol.* 248, 74-96.
- Freed, R. L., Peacor, D. R., 1989. Variability in temperature of the smectite/illite reaction in Gulf Coast sediments. *Clay Miner.* 24, 171-180.
- Freudenthal, F., Wefer, G., 2007. Scientific drilling with the sea floor drill rig MeBo, *Sci. Drill.* 5, 63-66.
- Froelich, P. N., Klinkhammer, G. P., Bender, M. L., Luedtke, N. A., Heath, G. R., Cullen, D., Dauphin, P., Hammond, D., Hartman, B., Maynard, V., 1979. Early oxidation of organic matter in pelagic sediments of the eastern equatorial Atlantic: Suboxic diagenesis. *Geochim. Cosmochim. Acta* 43, 1075-1090.
- Fryer, P., Wheat, C. G., Williams, T., Kelley, C., Johnson, K., Ryan, J., Kurz, W., Shervais, J., Albers, E., Bekins, B., Debret, B., Deng, J., Dong, Y., Eickenbusch, P., Frery, E., Ichiyama, Y., Johnston, R., Kevorkian, R., Magalhaes, V., Mantovanelli, S., Menapace, W., Menzies, C., Michibayashi, K., Moyer, C., Mullane, K., Park, J., Price, R., Sissmann, O., Suzuki, S., Takai, K., Walter, B., Zhang, R., Amon, D., Glickson, D., Pomponi, S., 2020. Mariana serpentinite mud volcanism exhumes subducted seamount materials: Implications for the origin of life. *Philos. Trans. R. Soc. A Math. Phys. Eng. Sci.* 378, 20180425.
- Fujikura, K., Kojima, S., Tamaki, K., Maki, Y., Hunt, J., Okutani, T., 1999. The deepest chemosynthesis-based community yet discovered from the hadal zone, 7326 m deep, in the Japan Trench. *Mar. Ecol. Prog. Ser.* 190, 17-26.
- Gardner, J. M., 2001. Mud volcanoes revealed and sampled on the Western Moroccan continental margin. *Geophys. Res. Lett.* 28, 339-342.
- Gennari, G., Spezzaferri, S., Comas, M. C., eberg, A., Lopez-Rodriguez, C., Pinheiro, L. M., 2013. Sedimentary sources of the mud breccia and mud volcanic activity in the Western Alboran Basin. *Mar. Geol.* 339, 83-95.
- Gerya, T. V., 2016. Origin, evolution, seismicity, and models of oceanic and continental transform boundaries. In Duarte, J., Schellart, W. (Eds.), *Plate Boundaries and Natural Hazards*. Hoboken, N. J., AGU Geophys. Monograph Series 219, pp. 39-76.
- Gieskes, J. M., Mahn, C., 2007. Halide systematics in interstitial waters of ocean drilling sediment cores. *Appl. Geochem.* 22, 515-533.
- Gieskes, J., Mahn, C., Day, S., Martin, J. B., Greinert, J., Rathburn, T., McAdoo, B., 2005. A study of the chemistry of pore fluids and authigenic carbonates in methane seep environments: Kodiak Trench, Hydrate Ridge, Monterey Bay, and Eel River Basin. *Chem. Geol.* 220, 329-345.
- Gonzalez-Fernandez, A., Cordoba, D., Matias, L. M., Torne, M., 2001. Seismic crustal structure in the Gulf of Cadiz (SW Iberian Peninsula). *Mar. Geophys. Res.* 22, 207-223.
- Gràcia, E., Urgeles, R., Rothenbeck, M., Wenzlaff, E., Steinführer, A., Cruise Participants, 2018. ImagiNg large SeismogenIc and tsunamiGenic structures of the Gulf of Cadiz with ultra-High resolution Technologies (INSIGHT). Leg 1 survey cruise report. Barcelona: Institute of Marine Sciences (CSIC), 139 pp.
- Graue, K., 2000. Mud volcanoes in deepwater Nigeria. *Mar. Petrol. Geol.* 17, 959-974.
- Greinert, J., Artemov, Y., Egorov, V., De Batist, M., McGinnes, D., 2006. 1300-m-high rising bubbles from mud volcanoes at 2080 m in the Black Sea: Hydroacoustic characteristics and temporal variability, *Earth Planet. Sci. Lett.* 244, 1-15.
- Grevemeyer, I., Kaul, N., Kopf, A., 2009. Heat flow anomalies in the Gulf of Cadiz and off Cape San Vicente, Portugal. *Mar. Pet. Geol.* 26, 795-804.

Gründger, F., Carrier, V., Svenning, M. M., Panieri, G., Vonnahme, T. R., Klasek, S., Niemann, H., 2019. Methane-fuelled biofilms predominantly composed of methanotrophic ANME-1 in Arctic gas hydrate-related sediments. *Sci. Rep.* 9, 9725.

Gutscher, M. -A., 2004. What caused the Great Lisbon Earthquake? *Science* 305, 1247-1248.

Gutscher, M. -A., Dominguez, S., Westbrook, G. K., Gente, P., Babonneau, N., Mulder, T., Gonthier, E., Bartolome, R., Luis, J., Rosas, F., Terrinha, P., Delila and DelSis Scientific Teams, 2009. Tectonic shortening and gravitational spreading in the Gulf of Cadiz accretionary wedge: observations from multi-beam bathymetry and seismic profiling. *Mar. Pet. Geol.* 26, 647-659.

Gutscher, M. A., Malod, J., Rehault, J. P., Contrucci, I., Klingelhofer, F., Mendes-Victor, L., Spakman, W., 2002. Evidence for active subduction beneath Gibraltar. *Geology* 30, 1071-1074.

Haffert, L., Haeckel, M., Liebetrau, V., Berndt, C., Hensen, C., Nuzzo, M., Reitz, A., Scholz, F., Schonfeld, J., Perez-Garcia, C., Weise, S. M., 2013. Fluid evolution and authigenic mineral paragenesis related to salt diapirism—The Mercator mud volcano in the Gulf of Cadiz. *Geochim. Cosmochim. Acta* 106, 261-286.

Hedberg, H. D., 1974. Relation of methane generation to undercompacted shales, shale diapirs, and mud volcanoes. *AAPG Bull.* 58, 661-673.

Henkel, S., 2011. Pore water profiles and early diagenetic signals in marine sediments as indicators for (paleo-) environmental and depositional conditions, (Doctoral thesis). Bremen, Germany: Universität Bremen.

Hensen, C., Adao, H., Arn, S., Batista, L., Belosa, L., Cruise Participants, 2020. Exploring subsurface fluid flow and active dewatering along the oceanic plate boundary between Africa and Eurasia (Gloria Fault), Cruise No. M162, 06.03.2020 - 11.04.2020, Ponta Delgada (Portugal) - Emden (Germany), METEOR-Berichte, M162. Gutachterpanel Forschungsschiffe, Bonn, 189 pp.

Hensen, C., Duarte, J. C., Vannucchi, P., Mazzini, A., Lever, M. A., Terrinha, P., Géli, L., Henry, P., Villinger, H., Morgan, J., Schmidt, M., Gutscher M. A., Bartolome, R., Tomonaga, Y., Polonia, A., Gracia, E., Tinivella, U., Lupi, M., Çagatay, M. N., Elvert, M., Sakellariou, D., Matias, L., Kipfer, R., Karageorgis, A. P., Rufne, L., Liebetrau, V., Pierre, C., Schmidt, C., Batista, L., Gasperini, L., Burwicz, E., Neres, M., Nuzzo, M., 2019. Marine transform faults and fracture zones: a joint perspective integrating seismicity, fluid flow and life. *Front. Earth Sci.* 7, 39.

Hensen, C., Nuzzo, M., Hornibrook, E., Pinheiro, L. M., Bock, B., Magalhaes, V. H., Bruckmann, W., 2007. Sources of mud volcano fluids in the Gulf of Cadiz—indications for hydrothermal imprint. *Geochim. Cosmochim. Acta* 71, 1232-1248.

Hensen, C., Scholz, F., Liebetrau, V., Kaul, N., Nuzzo, M., Schmidt, M., Batista, L., Villinger, H., Terrinha, P., 2021. Oceanic strike-slip faults represent active fluid conduits in the abyssal sub-seafloor. *Geology* 50, 189-193.

Hensen, C., Scholz, F., Nuzzo, M., Valadares, V., Gracia, E., Terrinha, P., Liebetrau, V., Kaul, N., Silva, S., Martinez-Loriente, S., Bartolome, R., Pinero, E., Magalhaes, V. H., Schmidt, M., Weise, S. M., Cunha, M., Hilario, A., Perea, H., Rovelli, L., Lackschewitz, K., 2015. Strike-slip faults mediate the rise of crustal-derived fluids and mud volcanism in the deep sea. *Geology* 43, 339-342.

Hensen, C., Zabel, M., Pfeifer, K., Schwenk, T., Kasten, S., Riedinger, N., Schulz, H. D., Boettius, A., 2003. Control of sulfate pore-water profiles by sedimentary events and the significance of anaerobic oxidation of methane for the burial of sulfur in marine sediments. *Geochim. Cosmochim. Acta* 67, 2631-2647.

- Hesse, R., Harrison, W. E., 1981. Gas hydrates (clathrates) causing porewater freshening and oxygen isotope fractionation in deep-water sedimentary sections of terrigenous continental margins. *Earth Planet. Sci. Lett.* 55, 453-462.
- Hill, E. M., Yue, H., Barbot, S., Lay, T., Tapponnier, P., Hermawan, I., Hubbard, J., Banerjee, P., Feng, L., Natawidjaja, D., Sieh, K., 2015. The 2012 Mw 8.6 Wharton Basin sequence: a cascade of great earthquakes generated by near-orthogonal, young, oceanic mantle faults. *J. Geophys. Res. Solid Earth* 120, 3723-3747.
- Hinrichs, K. U., Boetius, A., 2002. The anaerobic oxidation of methane: new insights in microbial ecology and biogeochemistry. In Wefer, G., Billett, D., Hebbeln, D., Jørgensen, B. B., Schlüter, M., Van Weering, T., (Eds.), *Ocean Margin Systems*. Springer-Verlag Berlin Heidelberg, pp. 457-477.
- Hinrichs, K. U., Hayes, J. M., Sylva, S. P., Brewer, P. G., Delong, E. F., 1999. Methane-consuming archaeobacteria in marine sediments. *Nature* 398, 802-805.
- Holser, E. S., Saltzman, E. S., Brookins, D. G., 1983. Geochemistry and petrology of evaporites cored from a deepsea diapir at Site 546 offshore Morocco. In Hinz, K., Winterer E. L., (Eds.), *Init. Repts. DSDP*. Wash. U.S. Govt. Printing Office, pp. 509-540.
- Hong, W. L., Etiope, G., Yang, T. F., Chang, P. Y., 2013. Methane flux from miniseepage in mud volcanoes of SW Taiwan: comparison with the data from Italy, Romania, and Azerbaijan. *J. Asian Earth Sci.* 65, 3-12.
- Hooper, E., 1991. Fluid migration along growth faults in compacting sediments. *J. Petrol. Geol.* 14, 161-180.
- Hornbach, M. J., Ruppel, C., Van Dover, C. L., 2007. Three-dimensional structure of fluid conduits sustaining an active deep marine cold seep. *Geophys. Res. Lett.* 34, L05601.
- Hovland, M., 2002. On the self-sealing nature of marine seeps. *Cont. Shelf Res.* 22, 2387-2394.
- Hovland, M., Gardner, J. V., Judd, A. G., 2002. The significance of pockmarks to understanding fluid flow processes and geohazards. *Geofluids* 2, 127-136.
- Huguen, C., Mascle, J., Chaumillon, E., Kopf, A., Woodside, J., Zitter, T., 2004. Structural setting and tectonic control of mud volcanoes from the Central Mediterranean Ridge (Eastern Mediterranean). *Mar. Geol.* 209, 245-263.
- Hulme, S. M., Wheat, C. G., Fryer, P., Mottl, M. J., 2010. Pore water chemistry of the Mariana serpentinite mud volcanoes: A window to the seismogenic zone. *Geochem. Geophys. Geosyst.* 11.
- Hüpers, A., Kopf, A. J., 2012. Effect of smectite dehydration on pore water geochemistry in the shallow subduction zone: An experimental approach. *Geochem. Geophys. Geosyst.* 13.
- Hüpers, A., Menapace, W., Magalhaes, V., Freudenthal, T., Cruise Participants, 2020. Report and preliminary results of R/V METEOR cruise M149: shipboard and post-cruise analysis, recurrence of tsunamigenic hazards from MeBo drilling records and hazard mitigation using MeBo observatories, Las Palmas (Canary Islands) - Cadiz (Spain), 24.07.2018 - 24.08.2018. In *Berichte aus dem MARUM und dem Fachbereich Geowissenschaften der Universität Bremen* (No. 324). Bremen: Universität Bremen.
- Huuse, M., Jackson, C. A. L., Van Rensbergen, P., Davies, R. J., Flemings, P. B., Dixon, R. J., 2010. Subsurface sediment remobilization and fluid flow in sedimentary basins: an overview. *Basin Res.* 22, 342-360.
- Hyndman, R. D., Davis, E. E., Wright, J. A., 1979. The measurements of marine geothermal heat flow by a multipenetration probe with digital acoustic telemetry and insitu thermal conductivity. *Mar. Geophys. Res.* 4, 181-205.

- Ivanov, M. K., Kenyon, N., Nielsen, T., Wheeler, A., Monteiro, H., Gardner, J., Comas, M., Akhmanov, A., Akhmetzhanov, G., 2000. Goals and Principal Results of the TTR-9 Cruise. *IOC/UNESCO Worksh. Rep.* 168, 3-4.
- Ivanov, M. K., Limonov, A. F., Van Weering, T. C. E., 1996. Comparative characteristics of the Black Sea and Mediterranean Ridge mud volcanoes. *Mar. Geol.* 132, 253-271.
- Jannasch, H., Davis, E., Kastner, M., Morris, J., Pettigrew, T., Plant, J. N., Solomon, E., Villinger, H., Wheat, C. G., 2003. CORK-II: long-term monitoring of fluid chemistry, fluxes, and hydrology in instrumented boreholes at the Costa Rica subduction zone. In Morris, J. D., Villinger, H. W., Klaus, A., (Eds.), *Proceedings ODP, Initial Reports* 205, 1-36.
- Jones, A. T., Greinert, J., Bowden, D. A., Klaucke, I., Petersen, C. J., Netzeband, G. L., Weinrebe, W., 2010. Acoustic and visual characterisation of methane-rich seabed seeps at Omakere Ridge on the Hikurangi Margin, New Zealand. *Mar. Geol.* 272, 154-169.
- Jonk, R., 2010. Sand-rich injectites in the context of short-lived and long-lived fluid flow, *Basin Res.* 22, 603-621.
- Judd, A., Hovland, M., 2007. *Seabed fluid flow: the impact on geology, biology and the marine environment.* Cambridge Univ. Press. Cambridge.
- Kasten, S., Zabel, M., Heuer, V., Hensen, C., 2003. Processes and signals of nonsteady-state diagenesis in deep-sea sediments and their pore waters. In Wefer, G., Mulitza, S., Ratmeyer, V., (Eds.), *The South Atlantic in the Late Quaternary: Reconstruction of Material Budgets and Current Systems.* Springer-Verlag, Berlin, pp. 431-459.
- Kastner, M., Elderfield, H., Martin, J. B., 1991. Fluids in convergent margins: what do we know about their composition, origin, role in diagenesis and importance for oceanic chemical fluxes. *Phil. Trans. R. Soc. Lond. A* 335, 243-259.
- Kastner, M., Solomon, E. A., Harris, R. N., Torres, M. E., 2014. Fluid Origins, Thermal regimes, and fluid and solute fluxes in the forearc of subduction zones. In Stein, R., (Eds.), *Developments in marine geology* 7, 671-733.
- Kenyon, N. H., Ivanov, M. K., Akhmetzhanov, A. M., Akhmanov, G. G., 2000. Multidisciplinary study of geological processes on the north east Atlantic and Western Mediterranean Sea margins. *IOC Tech. Ser.* 56.
- Kharaka, Y. K., Mariner, R. H., 1989. Chemical geothermometers and their applications to formation waters from sedimentary basins. In Naeser N.D., McCulloh T.H., (Eds.), *Thermal History of Sedimentary Basins: Methods and Case Histories.* Springer-Verlag, New York, pp. 99-117.
- Khutorskoi, M. D., Polyak, B. G., 2017. Special features of heat flow in transform faults of the North Atlantic and Southeast Pacific. *Geotectonics* 51, 152-162.
- King, L. H., MacLean, B., 1970. Pockmarks on the Scotian Shelf. *Geol. Soc. Am. Bull.* 81, 3142-3148.
- Kirkham, C., Cartwright, J., Hermanrud, C., Jebsen, C., 2017. The spatial, temporal and volumetric analysis of a large mud volcano province within the Eastern Mediterranean. *Mar. Petrol. Geol.* 81, 1-16.
- Kirkham, C., Cartwright, J., Hermanrud, C., Jebsen, C., 2018. The genesis of mud volcano conduits through thick evaporite sequences. *Basin Res.* 30, 217-236.
- Kobayashi, K., 2002. Tectonic significance of the cold seepage zones in the eastern Nankai accretionary wedge – an outcome of the 15 years' KAIKO projects. *Mar. Geol.* 187, 3-30.
- Kopf, A. J., 2002. Significance of mud volcanism. *Rev. Geophys.* 40, 1-52.

- Kopf, A. J., 2003. Global methane emission through mud volcanoes and its past and present impact on the Earth's climate, *Int. J. Earth Sci.* 92, 806-816.
- Kopf, A., Behrmann, J. H., 2000. Extrusion dynamics of mud volcanoes on the Mediterranean Ridge accretionary complex. *Geol. Soc. Spec. Publ.* 174, 169-204.
- Kopf, A., Klaeschen, D., Mascle, J., 2001. Extreme efficiency of mud volcanism in dewatering accretionary prisms. *Earth. Planet. Sci. Lett.* 189, 295-313.
- Kopf, A., Robertson, A. H. F., Clennell, M. B., Flecker, R., 1998. Mechanism of mud extrusion on the Mediterranean Ridge Accretionary Complex, *Geo-Mar. Lett.* 18, 97-114.
- Kopf, A., Robertson, A. H. F., Volkmann, N., 2000. Origin of mud breccia from the Mediterranean Ridge accretionary complex based on evidence of the maturity of organic matter and related petrographic and regional tectonic evidence. *Mar. Geol.* 166, 65-82.
- Kopf, A., Saffer, D., Toczko, S., Araki, E., Carr, S., Kimura, T., Kinoshita, C., Kobayashi, R., Machida, Y., Rösner, A., Wallace, L. M., 2017. Expedition 365 summary. In Saffer, D., Kopf, A., Toczko, S., the Expedition 365 Scientists (Eds.), *NanTroSEIZE Stage 3: Shallow Megasplay Long-Term Borehole Monitoring System*. In *Proceedings of the International Ocean Discovery Program 365*. International Ocean Discovery Program, College Station, TX.
- Lachenbruch, A. H., Sass, J. H., 1980. Heat flow and energetics of the San Andreas fault zone. *J. Geophys. Res. Solid Earth* 85, 6185-6222.
- Lauer, R. M., Safer, D. M., Harris, R. N., 2017. Links between clay transformation and earthquakes along the Costa Rican subduction margin. *Geophys. Res. Lett.* 44, 7725-7732.
- León, R., Somoza, L., Medialdea, T., González, F. J., Díaz del Río, V., Fernández-Puga, M. C., Maestro, A., Mata, M. P., 2007. Sea-floor features related to hydrocarbon seeps in deepwater carbonate-mud mounds of the Gulf of Cádiz: from mud flows to carbonate precipitates. *Geo-Mar. Lett.* 27, 237-247.
- León, R., Somoza, L., Medialdea, T., Maestro, A., Diaz-del-Rio, V., Fernandez-Puga, M.C., 2006. Classification of sea-floor features associated with methane seeps along the Gulf of Cadiz continental margin. *Deep-Sea Res. II* 53, 1464-1481.
- León, R., Somoza, L., Medialdea, T., Vázquez, J. T., Gonzalez, F. J., Lopez-Gonzalez, N., Casas, D., Mata, M. P., Fernandez-Puga, M. C., Gimenez-Moreno, C. J., Diaz-del-Rio, V., 2012. New discoveries of mud volcanoes on the Moroccan Atlantic continental margin (Gulf of Cadiz): morpho-structural characterization. *Geo-Mar. Lett.* 32, 473-488.
- Levin, L., 2005. Ecology of cold seep sediments: Interactions of fauna with flow, chemistry and microbes. In Gibson, R. N., Atkinson, R. J. A., Gordon, J. D. M. (Eds.), *Oceanogr. Mar. Biol. Annu. Rev.* 43, 1-46.
- Levin, L. A., Baco, A. R., Bowden, D. A., Colaco, A., Cordes, E. E., Cunha, M. R., Demopoulos, A. W. J., Gobin, J., Grupe, B. M., Le, J., Metaxas, A., Netburn, A. N., Rouse, G., Thurber, A. R., Tunnicliffe, V., Van Dover, C. L., Vanreusel, A., Watling, L., 2016. Hydrothermal vents and methane seeps: rethinking the sphere of influence. *Front. Mar. Sci.* 3, 72.
- Lilley, M. D., Butterfield, D. A., Lupton, J. E., Olson, E. J., 2003. Magmatic events can produce rapid changes in hydrothermal vent chemistry. *Nature* 422, 878-881.
- Luff, R., Wallmann, K., 2003. Fluid flow, methane fluxes, carbonate precipitation and biogeochemical turnover in gas hydrate-bearing sediments at Hydrate Ridge, Cascadia Margin: numerical modeling and mass balances. *Geochim. Cosmochim. Acta* 67, 3403-3421.

- Lykousis, V., Alexandra, S., Woodside, J., Nomikou, P., Perissoratis, C., Sakellariou, D., De Lange, G., Dählmann, A., Casas, D., Rousakis, G., Ballas, D., Ioakim, C., 2004. New evidence of extensive active mud volcanism in the Anaximander mountains (Eastern Mediterranean): the “ATHINA” mud volcano. *Environ. Geol.* 46, 1030-1037.
- Maestro, A., Somoza, L., Medialdea, T., Talbot, C. J., Lowrie, A., Vazquez, J. T., Diaz-del-Rio, V., 2003. Large-scale slope failure involving Triassic and Middle Miocene salt and shale in the Gulf of Cadiz (Atlantic Iberian Margin). *Terra Nova* 15, 380-391.
- Maldonado, A., Somoza, L., Pallares, L., 1999. The Betic orogen and the Iberian–African boundary in the Gulf of Cadiz: geological evolution (central North Atlantic). *Mar. Geol.* 155, 9-43.
- Maltman, A. J., Bolton, A., 2003. How sediments become mobilized. In Van Rensbergen, P., Hillis, R. R., Maltman, A. J., Morley, C. K. (Eds.), *Subsurface Sediment Mobilization*, Geological Society, London, pp. 9-20. Special Publications 216.
- Manning, C. E., Ingebritsen, S., 1999. Permeability of the continental crust: implications of geothermal data and metamorphic systems. *Rev. Geophys.* 37, 127-150.
- Martin, J. B., Gieskes, J. M., Torres, M., Kastner, M., 1993. Bromine and iodine in Peru margin sediments and pore fluids: implications for fluid origins. *Geochim. Cosmochim. Acta* 57, 4377-4389.
- Martín-Puertas, C., Mata, M. P., Fernández-Puga, M. C., Díaz del Río, V., Vázquez, J. T., Somoza, L., 2007. A comparative mineralogical study of gas-related sediments of the Gulf of Cádiz. *Geo-Mar. Lett.* 27, 223-235.
- Martínez-Loriente, S., Gracia, E., Bartolome, R., Sallares, V., Connors, C., Perea, H., Lo Iacono, C., Klaeschen, D., Terrinha, P., Danobeitia, J. J., Zitellini, N., 2013. Active deformation in old oceanic lithosphere and significance for earthquake hazard: Seismic imaging of the Coral Patch Ridge area and neighboring abyssal plains (SW Iberian Margin). *Geochem. Geophys. Geosyst.* 14, 2206-2231.
- Martínez-Loriente, S., Sallarès, V., Gràcia, E., Bartolome, R., Dañobeitia, J. J., Zitellini, N., 2014. Seismic and gravity constraints on the nature of the basement in the Africa-Eurasia plate boundary: New insights for the geodynamic evolution of the SW Iberian margin. *J. Geophys. Res. Solid Earth* 119, 127-149.
- Martos-Villa, R., Mata, M. P., Williams, L. B., Nieto, F., Rey, X. A., Sainz-Diaz, C. I., 2020. Evidence of hydrocarbon-rich fluid interaction with clays: Clay mineralogy and boron isotope data from Gulf of Cádiz mud volcano sediments. *Minerals* 10, 651.
- Masclé, J., Mary, F., Praeg, D., Brosolo, L., Camera, L., Ceramicola, S., Dupré, S., 2014. Distribution and geological control of mud volcanoes and other fluid/free gas seepage features in the Mediterranean Sea and nearby Gulf of Cadiz. *Geo-Mar. Lett.* 34, 89-110.
- Mazurenko, L. L., Soloviev, V. A., 2003. Worldwide distribution of deep-water fluid venting and potential occurrences of gas hydrate accumulations. *Geo-Mar. Lett.* 23, 162-176.
- Mazurenko, L. L., Soloviev, V. A., Gardner, J. M., Ivanov, M. K., 2003. Gas hydrates in the Ginsburg and Yuma mud volcano sediments (Moroccan Margin): results of chemical and isotopic studies of pore water. *Mar. Geol.* 195, 201-210.
- Mazzini, A., Etiope, G., 2017. Mud volcanism: an updated review. *Earth Sci. Rev.* 168, 81-112.
- Mazzini, A., Svensen, H., Planke, S., Guliyev, I., Akhmanov, G. G., Fallik, T., Banks, D., 2009. When mud volcanoes sleep: Insight from seep geochemistry at the Dashgil mud volcano, Azerbaijan. *Mar. Pet. Geol.* 26, 1704-1715.

- McArthur, J. M., Mutterlose, J., Price, G. D., Rawson, P. F., Ruffell, A., Thirlwall, M. F., 2004. Belemnites of Valanginian, Hauterivian and Barremian age: Sr-isotope stratigraphy, composition ( $^{87}\text{Sr}/^{86}\text{Sr}$ ,  $\delta^{13}\text{C}$ ,  $\delta^{18}\text{O}$ , Na, Sr, Mg), and palaeo-oceanography. *Palaeogeogr. Palaeoclimatol. Palaeoecol.* 202, 253-272.
- McCaffrey, M. A., Lazar, B., Holland, H. D., 1987. The evaporation path of seawater and the coprecipitation of  $\text{Br}^-$  and  $\text{K}^+$  with halite. *J. Sediment. Petrol.* 57, 928-937.
- Medialdea, T., Somoza, L., Pinheiro, L. M., Fernandez-Puga, M. C., Vazquez, J. T., Leon, R., Ivanov, M. K., Magalhaes, V., Diaz-del-Rio, V., Vegas, R., 2009. Tectonics and mud volcano development in the Gulf of Cadiz. *Mar. Geol.* 261, 48-63.
- Medialdea, T., Vegas, R., Somoza, L., Vazquez, J. T., Maldonado, A., Diaz-del-Rio, V., Maestro, A., Cordoba, D., Fernandez-Puga, M.C., 2004. Structure and evolution of the "Olistostrome" complex of the Gibraltar Arc in the Gulf of Cadiz (eastern Central Atlantic): evidence from two long seismic cross-sections. *Mar. Geol.* 209, 173-198.
- Meissner, F. F., 1978. Petroleum geology of the Bakken Formation, Williston Basin, North Dakota and Montana. In Rehrig, D., (Eds.), *Williston Basin Symposium Guidebook: Montana Geological Society*. Mont. Geol. Soc., Billings, Mont. pp. 207-227.
- Menapace, W., Chahid, D., Duarte, D., Fleischmann, T., Heitmann-Bacza, C., Cruise Participants, 2021. Long-term monitoring of fluid and solid emissions at the African-Eurasian tectonic boundary in the ALBORAN Sea and the Gulf of CADIZ, Cruise No. M167, 11.10.2020 - 05.11.2020, Emden (Germany) - Emden (Germany), ALBOCA II. In *METEOR-Berichte, M167* (pp. 96). Bonn: Gutachterpanel Forschungsschiffe.
- Menapace, W., Kopf, A., Zabel, M., de Beer, D., 2017a. Mud volcanoes as dynamic sedimentary phenomena that host marine ecosystems. In Kallmeyer, J., (Eds.), *Life in Extreme Environments - Life at vents and seeps*. Berlin, Boston: De Gruyter, pp. 53-84.
- Menapace, W., Tanguan, D., Maas, M., Williams, T., Kopf, A., 2019. Rheology and biostratigraphy of the Mariana Serpentine Muds Unravel Mud Volcano evolution. *J. Geophys. Res., Solid Earth* 124, 10752-10777.
- Menapace, W., Völker, D., Kaul, N., Tryon, M. D., Kopf, A. J., 2017b. The role of mud volcanism and deep-seated dewatering processes in the Nankai Trough accretionary prism and Kumano Basin, Japan. *Geochem. Geophys. Geosyst.* 18, 2486-2509.
- Menapace, W., Völker, D., Sahling, H., Zoellner, C., dos Santos Ferreira, C., Bohrmann, G., Kopf, A., 2017c. Long-term in situ observations at the Athina mud volcano, Eastern Mediterranean: Taking the pulse of mud volcanism. *Tectonophysics* 721, 12-27.
- Merey, S., Longinos, S. N., 2018. Does the Mediterranean Sea have potential for producing gas hydrates? *J. Nat. Gas Sci. Eng.* 55, 113-134.
- Milkov, A. V., 2000. Worldwide distribution of submarine mud volcanoes and associated gas hydrates. *Mar. Geol.* 167, 29-42.
- Milkov, A. V., 2005. Global distribution of mud volcanoes and their significance in petroleum exploration as a source of methane in the atmosphere and hydrosphere and as a geohazard. In Martinelli, G., Panahi, B., (Eds.), *Mud Volcanoes, Geodynamics and Seismicity*. Springer Netherlands, pp. 29-34.
- Milkov, A. V., Sassen, R., Apanasovich, T. V., Dadashev F. G., 2003. Global gas flux from mud volcanoes: a significant source of fossil methane in the atmosphere and the ocean. *Geophys. Res. Lett.* 30, 1037.
- Minshull, T. A., Marín-Moreno, H., Betlem, P., Bialas, J., Bünz, S., Burwicz, E., Cameselle, A. L., Cifci, G., Giustiniani, M., Hillman, J. I. T., Holz, S., Hopper, J. R., Ion, G., Leon, R., Magalhaes, V., Makovsky,

- Y., Mata, M., Max, M. D., Nielsen, T., Okay, S., Ostrovsky, I., O'Neil, N., Pinheiro, L. M., Plaza-Faverola, A. A., Rey, D., Roy, S., Schwalenberg, K., Senger, K., Vadakkepuliambatta, S., Vasilev, A., Vazquez, J. T., 2020. Hydrate occurrence in Europe: a review of available evidence. *Mar. Pet. Geol.* 111, 735-764.
- Moore, J. C., Vrolijk, P., 1992. Fluids in accretionary prisms. *Rev. Geophys.* 30, 113-135.
- Niemann, H., Duarte, J., Hensen, C., Omoregie, E., Magalhaes, V. H., Elvert, M., Pinheiro, L. M., Kopf, A., Boetius, A., 2006a. Microbial methane turnover at mud volcanoes of the Gulf of Cadiz. *Geochim. Cosmochim. Acta* 70, 5336-5355.
- Niemann, H., Losekann, T., de Beer, D., Elvert, M., Nadelig, T., Knittel, K., Amann, R., Sauter, E. J., Schluter, M., Klager, M., Foucher, J-P., Boetius, A., 2006b. Novel microbial communities of the Hakon Mosby mud volcano and their role as a methane sink. *Nature* 443, 854-858.
- Noda, H., Lapusta, N., 2013. Stable creeping fault segments can become destructive as a result of dynamic weakening. *Nature* 493, 518-521.
- Nuzzo, M., Hornibrook, E. R. C., Gill, F., Hensen, C., Pancost, R. D., Haeckel, M., Reitz, A., Scholz, F., Magalhaes, V. H., Bruckmann, W., Pinheiro, L. M., 2009. Origin of light volatile hydrocarbon gases in mud volcano fluids, Gulf of Cadiz—Evidence for multiple sources and transport mechanisms in active sedimentary wedges. *Chem. Geol.* 266, 350-363.
- Nuzzo, M., Tomonaga, Y., Schmidt, M., Valadares, V., Faber, E., Pintero, E., Reitz, A., Haeckel, M., Tyroller, L., Godinho, E., Kipfer, R., Terrinha, P. G., Hensen, C., 2019. Formation and migration of hydrocarbons in deeply buried sediments of the Gulf of Cadiz convergent plate boundary—Insights from the hydrocarbon and helium isotope geochemistry of mud volcano fluids. *Mar. Geol.* 410, 56-69.
- Oppo, D., Evans, S., Iacopini, D., Kabir, S. M., Maselli, V., Jackson, C. A. L., 2021. Leaky salt: Pipe trails record the history of cross-evaporite fluid escape in the northern Levant Basin, Eastern Mediterranean. *Basin Res.* 33, 1798-1819.
- Orange, D. L., Teas, P. A., Decker, J., Baillie, P., Johnstone, T., 2009. Using SeaSeep Surveys to Identify and Sample Natural Hydrocarbon Seeps in Offshore Frontier Basins. *Proceedings of The Annual Convention - Indonesian Petroleum Association* 33, 363-384.
- Orphan, V. J., House, C. H., Hinrichs, K. U., Mckeegan, K. D., Delong, E. F., 2001. Methane-consuming archaea revealed by directly coupled isotopic and phylogenetic analysis. *Science* 293, 484-487.
- Ortí, F., Pérez-López, A., García-Veigas, J., Rosell, L., Cendón, D. I., Pérez-Valera, F., 2014. Sulfate isotope compositions ( $\delta^{34}\text{S}$ ,  $\delta^{18}\text{O}$ ) and strontium isotopic ratios ( $^{87}\text{Sr}/^{86}\text{Sr}$ ) of Triassic evaporites in the Betic Cordillera (SE Spain). *Revista Sociedad Geológica España* 27, 79-89.
- Osborne, M. J., Swarbrick, R. E., 1997. Mechanisms for generating overpressure in sedimentary basins: a reevaluation. *AAPG Bull.* 81, 1023-1041.
- Ovsyannikov, D. O., Sadekov, A. Y., Kozlova, E. V., 2003. Rock fragments from mud volcanic deposits of the Gulf of Cadiz: an insight into the Eocene–Pliocene sedimentary succession of the basin. *Mar. Geol.* 195, 211-221.
- Palomino, D., Lopez-Gonzalez, N., Vazquez, J. T., Fernandez-Salas, L. M., Rueda, J. L., Sanchez-Leal, R., Diaz-del-Rio, V., 2016. Multidisciplinary study of mud volcanoes and diapirs and their relationship to seepages and bottom currents in the Gulf of Cadiz continental slope (northeastern sector). *Mar. Geol.* 378, 196-212.

- Panagiotopoulos, I. P., Paraschos, F., Rousakis, G., Hatzianestis, I., Parinos, C., Morfis, I., Gogou, A., 2020. Assessment of the eruptive activity and identification of the mud breccia's source in the Olimpi mud volcano field, Eastern Mediterranean. *Deep Sea Res. Part II Top. Stud. Oceanogr.* 171, 104701.
- Perez-Garcia, C., Berndt, C., Klaeschen, D., Mienert, J., Haffert, L., Depreiter, D., Haeckel, M., 2011. Linked halokinesis and mud volcanism at the Mercator mud volcano, Gulf of Cadiz. *J. Geophys. Res. Solid Earth* 116, B05101.
- Pickering, K. T., Agar, S. M., Ogawa, Y., 1988. Genesis and deformation of mud injections containing chaotic basalt-limestone-chert associations: examples from the southwest Japan forearc. *Geology* 16, 881-885.
- Pilcher, R., Argent, J., 2007. Mega-pockmarks and linear pockmark trains on the west African continental margin. *Mar Geol.* 244, 15-32.
- Pinheiro, L. M., Ivanov, M., Kenyon, N., Magalhaes, V., Somoza, L., Gardner, J., Kopf, A., Van Rensbergen, P., Monteiro, J.H., the Euromargins-MVSEIS Team, 2005. Structural control of mud volcanism and hydrocarbon-rich gas seepage in the Gulf of Cadiz: results from the TTR-15 and other previous cruises. *CIESM Workshop Monogr.* 29, 53-58.
- Pinheiro L. M., Ivanov M. K., Sautkin A., Akhmanov G., Magalhaes V. H., Volkonskaya A., Monteiro J. H., Somoza L., Gardner J., Hamouni N., Cunha M. R., 2003. Mud volcanism in the Gulf of Cadiz: results from the TTR-10 cruise. *Mar. Geol.* 195, 131-151.
- Planke, S., Svensen, H., Hovland, M., Banks, D. A., Jamtveit, B., 2003. Mud and fluid migration in active mud volcanoes in Azerbaijan. *Geo-Mar. Lett.* 23, 258-268.
- Praeg, D., Ceramicola, S., Barbieri, R., Unnithan, V., Wardell, N., 2009. Tectonically-driven mud volcanism since the late Pliocene on the Calabrian accretionary prism, central Mediterranean Sea. *Mar. Petrol. Geol.* 26, 1849-1865.
- Prigent, C., Warren, J. M., Kohli, A. H., Teyssier, C., 2020. Fracture-mediated deep seawater flow and mantle hydration on oceanic transform faults. *Earth Planet. Sci. Lett.* 532, 115988.
- Prouty, N. G., Brothers, D. S., Kluesner, J. W., Vaughn Barrie, J., Andrews, B. D., Lauer, R. M., Greene, H. G., 2020. Focused fluid flow and methane venting along the Queen Charlotte fault, offshore Alaska (USA) and British Columbia (Canada). *Geosphere* 16, 1336-1357.
- Pryce, E., Kirkham, C., Cartwright, J., 2023. Crater formation during the onset of mud volcanism. *Geology* 51, 252-256.
- Rafferty, P., Shiao, S. Y., Binz, C. M., Meyer, R. E., 1981. Adsorption of Sr(II) on clay minerals: Effects of salt concentration, loading, and pH. *J. Inorg. Nucl. Chem.* 43, 797-805.
- Ranero, C. R., Grevemeyer, I., Sahling, H., Barckhausen, U., Hensen, C., Wallmann, K., Weinrebe, W., Vannucchi, P., von Huene, R., McIntosh, K., 2008. Hydrogeological system of erosional convergent margins and its influence on tectonics and interplate seismogenesis. *Geochemistry, Geophys. Geosystems* 9, Q03S04.
- Reeburgh, W. S., 2007. Oceanic methane biogeochemistry. *Chem. Rev.* 107, 486-513.
- Revil, A., 2002. Genesis of mud volcanoes in sedimentary basins: a solitary wave-based mechanism. *Geophys. Res. Lett.* 29, 2002.
- Ritger, S., Carson, B., Suess, E., 1987. Methane-derived authigenic carbonates formed by subduction-induced pore-water expulsion along the Oregon/Washington margin. *Geol. Soc. Am. Bull.* 98, 147-156.

- Roberts, H. H., Carney, R. S., 1997. Evidence of episodic fluid, gas, and sediment venting on the northern Gulf of Mexico continental slope. *Econ. Geol.* 92, 863-879.
- Robertson, A. H. F., Kopf, A., 1998. Tectonic setting and processes of mud volcanism on the Mediterranean Ridge accretionary complex: Evidence from Leg 160. In A. H. F. Robertson, K. -C. Emeis, C. Richter, A. Camerlenghi, (Eds.), *Proceedings of the Ocean Drilling Program, Scientific Results 160*. College Station, Tex: Ocean Drill Program. pp. 665-680.
- Rosenbaum, G., Lister, G. S., Duboz, C., 2002. Relative motions of Africa, Iberia and Europe during Alpine orogeny. *Tectonophysics* 359, 117-129.
- Saffer, D. M., Bekins, B. A., 1998. Episodic fluid flow in the Nankai accretionary complex: Timescale, geochemistry, flow rates, and fluid budget. *J. Geophys. Res. Solid Earth* 103, 30351-30370.
- Saffer, D. M., Tobin, H. J., 2011. Hydrogeology and mechanics of subduction zone forearcs: Fluid flow and pore pressure. *Annu. Rev. Earth. Planet. Sci.* 39, 157-186.
- Sahling, H., Masson, D. G., Ranero, C. R., Hühnerbach, V., Weinrebe, W., Klaucke, I., Bürk, D., Brückmann, W., Suess, E., 2008. Fluid seepage at the continental margin offshore Costa Rica and southern Nicaragua. *Geochem. Geophys. Geosyst.* 9, Q05S05.
- Schlesinger, W. M., Bernhardt, E. S., 2013. *Biogeochemistry: An analysis of global change, 3rd ed.* New York, NY: Academic Press.
- Schmidt, C., Burwicz, E., Hensen, C., Wallmann, K., Martinez-Loriente, S., Gracia, E., 2018. Genesis of mud volcano fluids in the Gulf of Cadiz using a novel basin-scale model approach. *Geochim. Cosmochim. Acta* 243, 186-204.
- Scholz, F., 2010. Pore water expulsion at submarine cold seeps: geochemical evidence for short-cuts between crust, sediments and ocean, (Doctoral thesis). Kiel, Germany: Christian-Albrechts-Universität.
- Scholz, F., Hensen, C., de Lange, G. J., Haeckel, M., Liebetrau, V., Meixner, A., Reitz, A., Romer, R. L., 2010a. Lithium isotope geochemistry of marine pore waters—insights from cold seep fluids. *Geochim. Cosmochim. Acta* 74, 3457-3459.
- Scholz, F., Hensen, C., Lu, Z., Fehn, U., 2010b. Controls on the  $^{129}\text{I}/\text{I}$  ratio of deep-seated marine interstitial fluids: ‘Old’ organic versus fissiogenic  $^{129}\text{I}$ -iodine. *Earth Planet. Sci. Lett.* 294, 27-36.
- Scholz, F., Hensen, C., Reitz, A., Romer, R. L., Liebetrau, V., Meixner, A., Weise, S. M., Haeckel, M., 2009. Isotopic evidence ( $^{87}\text{Sr}/^{86}\text{Sr}$ ,  $\delta^7\text{Li}$ ) for alteration of the oceanic crust at deep-rooted mud volcanoes in the Gulf of Cadiz, NE Atlantic Ocean. *Geochim. Cosmochim. Acta* 73, 5444-5459.
- Schoonen, M. A. A., 2004. Mechanisms of sedimentary pyrite formation. In Amend, J. P., Edward, J. K., Lyons, T. W., (Eds.), *Sulfur biogeochemistry - Past and present*. Geol. Soc. Am. Spec. Pap. 379, Boulder, Colorado, pp. 117-134.
- Schulz, H. M., Emeis, K. C., Volkmann, N., 1997. Organic carbon provenance and maturity in the mud breccia from the Napoli mud volcano: Indicators of origin and burial depth, *Earth Planet. Sci. Lett.* 147, 141-151.
- Shakirov, R., Obzhairov, A., Suess, E., Salyuk, A., Biebow, N., 2004. Mud volcanoes and gas vents in the Okhotsk Sea area. *Geo-Mar. Lett.* 24, 140.
- Sheppard, D. S., Truesdell, A. H., Janik, C. J., 1992. Geothermal gas compositions in Yellowstone National Park, U.S.A. *J. Volcanol. Geotherm. Res.* 51, 79-93.
- Sheppard, S. M. F., Gilg, H. A., 1996. Stable isotope geochemistry of clay minerals. *Clay Miner.* 31, 1-24.

- Sibson, R., 1995. Selective fault reactivation during basin inversion: potential for fluid redistribution through fault-valve action. *Geol. Soc. Lond., Spec. Publ.* 88, 3-19.
- Sibson, R. H., 1996. Structural permeability of fluid-driven fault-fracture meshes. *J. Struct. Geol.* 18, 1031-1042.
- Sibson, R. H., 1988. High angle reverse faults, fluid pressure cycling, and meso-thermal gold quartz deposits. *Geology* 16, 151-155.
- Sibuet, M., Olu, K., 1998. Biogeography, biodiversity and fluid dependence of deep-sea cold-seep communities at active and passive margins. *Deep Sea Res. II* 45, 517-567.
- Silva, S., Terrinha, P., Matias, L., Duarte, J. C., Roque, C., Ranero, C. R., Geissler, W. H., Zitellini, N., 2017. Micro-seismicity in the Gulf of Cadiz: is there a link between micro-seismicity, high magnitude earthquakes and active faults? *Tectonophysics* 717, 226-241.
- Smith, D. A., 1980. Sealing and nonsealing faults in Louisiana Gulf Coast salt basin. *AAPG Bull.* 64, 145-172.
- Somoza, L., Diaz-del-Rio, V., Leon, R., Ivanov, M., Fernandez-Puga, M. C., Gardner, J. M., Hernandez-Molina, F. J., Pinheiro, L. M., Rodero, J., Lobato, A., Maestro, A., Vazquez, J. T., Medialdea, T., Fernandez-Salas, L. M., 2003. Seabed morphology and hydrocarbon seepage in the Gulf of Cadiz mud volcano area: acoustic imagery, multibeam and ultra-high resolution seismic data. *Mar. Geol.* 195, 153-176.
- Somoza, L., Medialdea, T., León, R., Ercilla, G., Vázquez, J. T., Farran, M. L., Hernandez-Molina, J., Gonzalez, J., Juan, C., Fernandez-Puga, M. C., 2012. Structure of mud volcano systems and pockmarks in the region of the ceuta contourite depositional system (western Alboran sea). *Mar. Geol.* 332, 4-26.
- Somoza, L., Medialdea, T., Terrinha, P., Ramos, A., Vázquez, J-T., 2021a. Submarine active faults and morpho-tectonics around the Iberian Margins: Seismic and tsunamis hazards. *Front. Earth Sci.* 9, 653639.
- Somoza, L., Rueda, J. L., González, F. J., Rincon-Tomas, B., Medialdea, T., Sánchez-Guillamón, O., Hoppert, M., Vázquez, J. T., Madureira, P., Santofimia, E., López-Pamo, E., Palomino, D., Ortiz, J. E., Blanco, L., Fernández-Puga, M. C., Fernández-Salas, L. M., Reitner, J., 2021b. A relict oasis of living deep-sea mussels *Bathymodiolus* and microbial-mediated seep carbonates at newly-discovered active cold seeps in the Gulf of Cádiz, NE Atlantic Ocean. *PalZ* 95, 793-807.
- Spinelli, G. A., Giambalvo, E. R., Fisher, A. T., 2004. Sediment permeability, distribution and influence on fluxes in oceanic basement. In Davis, E. E., Elderfield, H., (Eds.), *Hydrology of the Oceanic Lithosphere*. Cambridge: Cambridge University Press, pp. 151-188.
- Spulber, L., Etiope, G., Baciuc, C., Malos, C., Vlad, S. N., 2010. Methane emission from natural gas seeps and mud volcanoes in Transylvania (Romania). *Geofluids* 10, 463-475.
- Srodon, J., 1999. Nature of mixed-layer clays and mechanisms of their formation and alteration. *Ann. Rev. Earth Planet. Sci.* 27, 19-53.
- Stadnitskaia, A., Ivanov, M. K., Blinova, V., Kreulen, R., Van Weering, T. C. E., 2006. Molecular and carbon isotopic variability of hydrocarbon gases from mud volcanoes in the Gulf of Cadiz, NE Atlantic. *Mar. Petrol. Geol.* 23, 281-296.
- Stadnitskaia, A., Ivanov, M. K., Damsté, J. S., 2008. Application of lipid biomarkers to detect sources of organic matter in mud volcano deposits and post-eruptional methanotrophic processes in the Gulf of Cadiz, NE Atlantic. *Mar. Geol.* 255, 1-14.
- Staffini, F., Spezzaferri, S., Aghib, F., 1993. Mud diapirs of the Mediterranean Ridge: sedimentological and micropaleontological study of the mud breccia. *Riv. Ital. Paleontol. Strat.* 99, 225-254.

- Stakes, D. S., Trehu, A. M., Goffredi, S. K., Naehr, T. H., Duncan, R. A., 2002. Mass wasting, methane venting, and biological communities on the Mendocino transform fault. *Geology* 30, 407-410.
- Stern, R. J., 2002. Subduction zones. *Rev. Geophys.* 40, 1012.
- Stewart, S. A., Davies, R. J., 2006. Structure and emplacement of mud volcano systems in the South Caspian Basin. *AAPG Bull.* 90, 771-786.
- Strasser, M., Dugan, B., Kanagawa, K., Moore, G. F., Toczko, S., Maeda, L., the Expedition 338 Scientists, 2014. *Proceedings of the Integrated Ocean Drilling Program Volume 338*. Yokohama: Integrated Ocean Drilling Program.
- Suess, E., 2014. Marine cold seeps and their manifestations: geological control, biogeochemical criteria and environmental conditions. *Int. J. Earth Sci.* 103, 1889-1916.
- Talukder, A. R., 2012. Review of submarine cold seep plumbing systems: leakage to seepage and venting. *Terra Nova* 24, 255-272.
- Tari, G., Molnar, J., Ashton, P., 2003. Examples of salt tectonics from West Africa: a comparative approach. In Arthur, T. J., MacGregor, D. S., Cameron, N. R., (Eds.), *Petroleum Geology of Africa: New Themes and Developing Technologies*, Geological Society, London, pp. 85-104. Special Publications 207.
- Tatsumi, Y., 2005. The subduction factory: how it operates in the evolving Earth. *GSA Today* 15, 4-10.
- Thiebot, E., Gutscher, M. A., 2006. The Gibraltar Arc seismogenic zone (part 1): constraints on a shallow east dipping fault plane source for the 1755 Lisbon earthquake provided by seismic data, gravity and thermal modeling. *Tectonophysics* 426, 135-152.
- Tobin, H. J., Moore, J. C., Mackay, M. E., Orange, D. L., Kulm, L. D., 1993. Fluid flow along a strike-slip fault at the toe of the Oregon accretionary prism: Implications for the geometry of frontal accretion. *Geol. Soc. Am. Bull.* 105, 569-582.
- Torelli, L., Sartori, R., Zitellini, N., 1997. The giant chaotic body in the Atlantic Ocean off Gibraltar: new results from a deep seismic reflection survey. *Mar. Pet. Geol.* 14, 125-138.
- Toyos, M. H., Medialdea, T., Leon, R., Somoza, L., Gonzalez, F. J., Melendez, N., 2016. Evidence of episodic long-lived eruptions in the Yuma, Ginsburg, Jesus Baraza and Tasyo mud volcanoes, Gulf of Cadiz. *Geo-Mar. Lett.* 36, 197-214.
- Treude, T., Krüger, M., Boetius, A., Jørgensen, B. B., 2005. Environmental control on anaerobic oxidation of methane in gassy marine sediments of Eckernförde Bay (German Baltic). *Limnol. Oceanogr.* 50, 1771-1786.
- Truffert, C., Chamot-Rooke, N., Lallemand, S., De Voogd, B., Huchon, P., Le Pichon X., 1993. The crust of the western Mediterranean ridge from deep seismic data and gravity modelling. *Geophys. J. Int.* 114, 360-372.
- Urgeles, R., INSIGHT Leg 2 Cruise Shipboard Participants, 2019. *ImagiNg large SeismogenIc and tsunamiGenic structures of the gulf of cadiz with ultra-High resolution Technologies (INSIGHT). Leg 2 survey cruise report*. Barcelona: Institute of Marine Sciences (CSIC), 128 pp.
- Uzdowski, E., 1973. Geochemical properties of strontium during genesis of Ca-carbonates and Ca-sulfates (in German). *Contrib. Mineral. Petrol.* 38, 177-195.
- Ussler, W., Paull, C. K., 1995. Effects of ion exclusion and isotopic fractionation on pore water geochemistry during gas hydrate formation and decomposition. *Geo-Mar. Lett.* 15, 37-44.

- Van de Kamp, P. C., 2008. Smectite-illite-muscovite transformations, quartz dissolution, and silica release in shales. *Clay Clay Miner.* 56, 66-81.
- Van Rensbergen, P., Depreiter, D., Pannemans, B., Moerkerke, G., Van Rooij, D., Marsset, B., Akhmanov, G., Blinova, V., Ivanov, M., Rachidi, M., Magalhaes, V., Pinheiro, L., Cunha, M., Henriët, J. P., 2005. The El Arraiche mud volcano field at the Moroccan Atlantic slope, Gulf of Cadiz. *Mar. Geol.* 219, 1-17.
- Vandorpe, T., Martins, I., Vitorino, J., Hebbelnc, D., Garcia, M., Van Rooij, D., 2016. Bottom currents and their influence on the sedimentation pattern in the El Arraiche mud volcano province, southern Gulf of Cadiz. *Mar. Geol.* 378, 114-126.
- Vanneste, H., Kelly-Gerrey, B. A., Connelly, D. P., James, R. H., Haeckel, M., Fisher, R. E., Heeschen, K., Mills, R. A., 2011. Spatial variation in fluid flow and geochemical fluxes across the sediment-seawater interface at the Carlos Ribeiro mud volcano (Gulf of Cadiz). *Geochim. Cosmochim. Acta* 75, 1124-1144.
- Vogt, C., Lauterjung, J., Fischer, R. X., 2002. Investigation of the clay fraction (<2 µm) of the clay mineral society reference clays. *Clay Clay Miner.* 50, 388-400.
- Vogt, P. R., Cherkashev, G., Ginsburg, G., Ivanov, G., Milkov, A., Crane, K., Lein, A., Sundvor, E., Pimenov, N., Egorov, A., 1997. Håkon Mosby mud volcano provides unusual example of venting. *EOS Trans. Am. Geophys. Union* 78, 549-557.
- von Huene, R., Scholl, D. W., 1991. Observations at convergent margins concerning sediment subduction, subduction erosion, and the growth of continental crust. *Rev. Geophys.* 29, 279-316.
- Wang, C., Zheng, M., Zhang, X., Xing, E., Zhang, J., Ren, J., Ling, Y., 2020. O, H, and Sr isotope evidence for origin and mixing processes of the Gudui geothermal system, Himalayas, China. *Geosci. Front.* 11, 1175-1187.
- Werne, J. P., Haese, R. R., Zitter, T., Aloisi, G., Bouloubassi, L., Heijs, S., Fiala-Medioni, A., Pancost, R. D., Damste, J. S. S., De Lange, G., Forney, L. J., Gottschal, J. C., Foucher, J. P., Mascle, J., Woodside, J., 2004. Life at cold seeps: a synthesis of biogeochemical and ecological data from Kazan mud volcano, eastern Mediterranean Sea. *Chem. Geol.* 205, 367-390.
- Wheat, C. G., Seewald, J. S., Takai, K., 2020. Fluid transport and reaction processes within a serpentinite mud volcano: South Chamorro Seamount. *Geochim. Cosmochim. Acta* 269, 413-428.
- Wienberg, C., Hebbeln, D., Fink, H. G., Mienis, F., Dorschel, B., Vertino, A., Lopez Correa, M., Freiwald, A., 2009. Scleractinian cold-water corals in the Gulf of Cadiz—first clues about their spatial and temporal distribution. *Deep-Sea Res. I* 56, 1873-1893.
- Xu, S., Menapace, W., Hüpers, A., Kopf, A., 2021. Mud volcanoes in the Gulf of Cadiz as a manifestation of tectonic processes and deep-seated fluid mobilization. *Mar. Pet. Geol.* 132, 105188.
- Yamano, M., Foucher, J. P., Kinoshita, M., Fisher, A., Hyndman, R. D., 1992. Heat flow and fluid flow regime in the western Nankai accretionary prism. *Earth Planet. Sci. Lett.* 109, 451-462.
- Yardley, B. W., 2013. The chemical composition of metasomatic fluids in the crust. In Harlov, D.E., Austrheim, H., (Eds.), *Metasomatism and the chemical transformation of rock*. Springer-Verlag, Berlin, Heidelberg, pp. 17-51.
- Yassir, N. A., 1989. Mud volcanoes and the behaviour of overpressured clays and silts, (Doctoral thesis). London, UK: University College London.
- You, C. F., Gieskes, J. M., 2001. Hydrothermal alteration of hemi-pelagic sediments: experimental evaluation of geochemical processes in shallow subduction zones. *Appl. Geochem.* 16, 1055-1066.

You, C. F., Spivack, A. J., Gieskes, J. M., Rosenbauer, R., Bischoff, J. L., 1995. Experimental study of boron geochemistry: Implications for fluid processes in subduction zones. *Geochim. Cosmochim. Acta* 59, 2435-2442.

Yusifov, M., Rabinowitz, P. D., 2004. Classification of mud volcanoes in the South Caspian Basin, offshore Azerbaijan. *Mar. Pet. Geol.* 21, 965-975.

Zitellini, N., Gracia, E., Matias, L., Terrinha, P., Abreu, M. A., DeAlteriis, G., Henriot, J.P., Danobeitia, J.J., Masson, D.G., Mulder, T., Ramella, R., Somoza, L., Diez, S., 2009. The quest for the Africa-Eurasia plate boundary west of the Strait of Gibraltar. *Earth Planet. Sci. Lett.* 280, 13-50.

Zitter, T. A. C., Huguen, C., Woodside, J. M., 2005. Geology of mud volcanoes in the eastern Mediterranean from combined sidescan sonar and submersible surveys. *Deep-Sea Res. I Oceanogr. Res. Pap.* 52, 457-475.